Dielektrophorese basierte Integration von Nanostrukturen und ihre sensorische Anwendung

Dissertation

zur Erlangung des akademischen Grades
doctor rerum naturalium (Dr. rer. nat)
vorgelegt dem Rat der Chemisch-Geowissenschaftlichen
Fakultät der Friedrich-Schiller-Universität von

Dipl.-Biochemiker Christian Leiterer
Geboren am 23.01.1984 in Jena.

Gutachter:

1. …….

2. …….

Tag der öffentlichen Verteidigung: ……

Abstract / Kurzfassung

The presented work deals with the integration and characterization of nanostructures, such as Desoxiribonucleoic acid (DNA), gold nanoparticle (AuNP) or semiconducting nanowire (NW) for sensory applications. Here, the technique called dielectrophoresis (DEP) is used to position and apply contact to bottom-up nanostructures, in order to subsequently use them as key elements for chemo resistive and optoelectronic sensing. In this context the optical properties of silicon (SiNW) and gallium arsenide nanowires (GaAsNW) were also investigated, along with the ability for the chemical and biological modification of similar NW. Overall the work should contribute to pave the way for the application of those nanostructures in chemical and biological sensing.

Die dargelegte Arbeit beschäftigt sich mit der Integration und Charakterisierung von Nanostrukturen z.B. Desoxyribonukleinsäure (DNA), Goldnanopartikeln (AuNP) oder Halbleiternanodrähten (NW) für sensorische Anwendungen. Dabei wird die Technik der Dielektrophorese (DEP) eingesetzt, um Nanostrukturen submikrometergenau zu positionieren, elektrisch zu kontaktieren und diese anschließend als Sensorelemente für optoelektronische oder chemoresistive Analytik einzusetzen. In diesem Kontext beschäftigt sich die vorliegende Arbeit auch mit den optischen Eigenschaften von Silizium- (SiNW) und Galliumarsenid-Nanodrähten (GaAsNW), und der chemischen Modifikation vergleichbarer NW. Insgesamt soll ein Beitrag geleistet werden den Weg für die zukünftige Anwendung dieser Nanostrukturen in der chemischen und biochemischen Sensorik zu ebenen.

Keywords: nanowire, nanoparticle, DNA, dielectrophoresis, Mie-resonance

Schlüsselworte: Nanodrähte, Nanopartikel, DNA, Dielektrophorese, Mie-Resonanz

Inhaltsverzeichnis

Preface / Vorwort

“There is a plenty of room at the bottom” was the topic of a lecture given by the famous Nobel Prize winner Richard Feynman in 1959 at the Californian Institute of Technology. In this talk he described the opportunities and challenges when working “on a small scale” today known as nanotechnology. He proposed that having control on a small scale meant faster computers and more efficient machines while also considering the challenges which have to be faced there. Nevertheless, in his talk he did not consider the new unique physical (e.g. optical and electrical) properties of the materials generated in this size, which are also leading to new opportunities and challenges in this field. This work will deal with some of the challenges Feynman mentioned especially in relation to handling and connecting nanoobjects to our macroscopic world, with the goal to use their unique optical or electrical properties to find new ways to more sensitive and cost efficient sensing. One focus hereby will be on a dielectrophoresis based integration technique for manipulation of nano- and microsized objects in an alternating electrical field. This technique not only allows the arrangement of nano objects with submicron precision but also to apply contact to them for electrical or optoelectronical characterization. The final goal is to show that it is possible to fabricate a sensor device which uses a nanostructure as key element for a basic sensing principle. The focus lies hereby in using the unique properties of those objects conditioned by their quantum confinement and work out new sensing principles for future sensing devices.

“There is a plenty of room at the bottom” ist das Thema eines Vortrages des bekannten Nobelpreisträgers Richard Feynman. In diesem Vortrag im Jahr 1959 am Californian Institute of Technology adressierte er die Chancen und Herausforderungen der Technologie im Nanometerbreich („on a small scale“). In seinem Vortrag prognostiziert er, dass mit den Erkenntnissen und der Kontrolle über Prozesse in dieser Größenskala der Weg für effizientere Maschinen und schnellere Computer geebnet wird. Genauso sprach er aber auch über neue Hürden, die beim Arbeiten in diesem Größenbereich überwunden werden müssen. Dennoch gab es auch Dinge die Feynman in seinem Vortrag noch nicht berücksichtigte, wie zum Beispiel die sich ergebenden, neuen Materialeigenschaften im Bereich der Elektronik und Optik.

Die vorliegende Arbeit beschäftigt sich mit einigen der o. g. Herausforderungen, besonders im Zusammenhang mit der Manipulation und Integration von Nanoobjekten, mit dem Ziel, ihre einzigartigen optischen und elektronischen Eigenschaften praktisch nutzbar zu machen und dabei Grundlagen für neue Wege zur Entwicklung sensitiverer und kosteneffizienterer Sensorik zu schaffen. Ein besonderer Fokus wird dabei auf die Die-

lektrophorese (DEP) basierende Integration gelegt, welche es ermöglicht, Objekte im Mikro- und Nanometerbereich mit Hilfe eines elektrischen Wechselfeldes zu manipulieren. Mit Hilfe dieser Technik gelang nicht nur die Positionierung von Objekten mit Submikrometergenauigkeit, sondern auch ihre elektrische Kontaktierung. Das letztendliche Ziel besteht darin zu zeigen, dass mit dieser Technik gezielt Sensoren hergestellt werden können, welche eine Nanostruktur als zentrales Element besitzen. Damit soll ein Beitrag zur Nutzung der einzigartigen Eigenschaften von Nanoobjekten, für die Entwicklung neuer sensorischer Prinzipien und damit zukünftiger noch leistungsfähigerer chemischer und biochemischer Sensoren geleistet werden.

1 Overview / Übersicht

This work deals with utilization of bottom-up nanostructures in the field of optical basic research, optoelectronic and chemoresistiv sensing and their microintegration using AC electrical fields. It will focus on three types of nanostructured materials in particular: DNA/DNA-superstructures, gold nanoparticle and semiconducting nanowire e.g. silicon, gallium arsenide, zinc oxide.

The basic research part deals with optical properties of silicon and gallium arsenide nanowires. Based on the Mie solution to *Maxwell's Equation* for infinite long cylinders the scattering and absorption properties of these nanostructures were calculated in respect to their diameter, angle of incident and polarization of the illuminating light. The results were correlated to spectral measurements of single nanowires in respect to their diameter and polarization of the illuminated light. Based on the results a procedure was proposed for determining nanowire diameters by optical measurements using a spectral fitting method.

The applied part of the research deals with the micro integration of DNA, AuNP and SiNW using an AC electrical field (dielectrophoresis). The focus of DNA micro integration lies hereby in determining conditions allowing the handling of single DNA molecules on a microelectrode substrate in a stretched conformation, which enables subsequent investigation and experimenting on single DNA molecules in an organized and ordered fashion.

The micro integration based on dielectrophoresis of AuNP and SiNW focuses on applying contact to these nanostructures in order to use them as optoelectronic or chemo resistive sensors. In order to achieve this, a micro integration process was developed to apply contact to SiNW and AuNP as basis for their sensory application. The contacted nanostructures were characterized electrically to optimize the integration procedure to acquire best possible sensing capabilities. Silicon nanowires were demonstrated to work as wavelength sensitive optical sensors and gold nanoparticle as chemo resistive sensor.

Furthermore, a DNA modification technique for SiNW and ZnONW was developed providing the basis for future DNA sensors with electrical read-out. The modified NW have been proven to work for the detection of selective DNA hybridization via fluorescence, similar to the classical microarray approach. Overall the work should contribute to pave the way for the application of those nanostructures in chemical and biological sensing.

Diese Arbeit beschäftigt sich mit der Nutzung von bottom-up Nanostrukturen in den Bereichen der optischen Grundlagenforschung, sowie der optoelektronischen und der chemoresistiven Sensorik. Einen Schwerpunkt bildet dabei die Mikrointegration dieser Nanostrukturen mittels Dielektrophorese. Die Forschungen konzentrieren sich auf drei verschieden Typen von Nanostrukturen: DNA / DNA-Überstrukturen, Goldnanopartikel und halbleitenden Nanodrähte aus Silizium, Galliumarsenid sowie Zinkoxid.

Im Bereich der optischen Grundlagenforschung konzentrieren sich die Untersuchungen auf die Charakterisierung der optischen Eigenschaften einzelner SiNW und GaAsNW. Basierend auf der Lösung der Maxwell-Gleichungen nach Mie für unendlich lange Zylinder lassen sich die Streu- und Absorptionseigenschaften dieser Nanostrukturen in Abhängigkeit von Durchmesser und Einfallswinkel / Polarisation des eingestrahlten Lichts berechnen. Die Verifizierung der Ergebnisse erfolgte durch die Korrelation mit spektralen Messungen an einzelnen NW in Abhängigkeit des Durchmessers und der Polarisation. Basierend auf diesen Ergebnissen wird eine Methode vorgeschlagen, welche es ermöglicht, durch einen spektralen Fit den Durchmesser von NW anhand von optischen Messungen zu bestimmen.

Der anwandte Teil der Arbeit beschäftigt sich mit der Mikrointegration von DNA, AuNP und SiNW mittels elektrischem Wechselfeld (Dielektrophorese). Der Fokus der DNA-Mikrointegration liegt hierbei in der Bestimmung der Parameter, welche die Manipulation von DNA-Einzelmolekülen auf einem Mikroelektrodensubstrat in einer gestreckten Konformation ermöglichen. Einen weiteren wesentlichen Schwerpunkt der Untersuchungen bildete die Entwicklung eines Mikrointegrationsverfahrens zur Kontaktierung von AuNP und SiNW, als Voraussetzung für einen Einsatz als optoelektronische oder chemoresistive Sensoren. Die kontaktierten Nanostrukturen wurden elektrisch charakterisiert und der Integrationsprozess optimiert um damit die bestmögliche Sensorleistung zu erreichen. Es gelang experimentell nachzuweisen, dass einzelne SiNW als wellenlängenabhängige optoelektronische und AuNP als chemoresistive Sensoren genutzt werden können.

Des Weiteren wurde ein DNA-Modifikationverfahren für SiNW und ZnONW entwickelt, welches die Basis für eine elektrisch auslesbare DNA-Sensorik darstellt. Die modifizierten NW erwiesen sich als geeignete Plattform für die Detektion selektiver DNA-Hybridisierung mittels Fluoreszenz, vergleichbar zu klassischen Ansätzen in der etablierten Mikroarraytechnologie. Hiermit konnte ein erster Schritt für die zukünftige Anwendung von halbleitenden NW in der Biosensorik getan werden.

2 Motivation

Considering DNA as a chemical polymer rather than carrier of genetic information, DNA can be a very useful tool in nanotechnology. For example by conjoining single stranded DNA with nanostructures (e.g. AuNP, carbon nanotubes (CNT), NW and quantum dots) they can be directed to specific locations which are labelled with the complementary DNA using the DNA's native self-assembly process called "DNA-hybridization". In contrast to most chemical polymers, coding DNA does not consist of repetitive monomers. Due to the coding background, its sequence is highly individual which enables addressing specific loci, if they are marked by DNA accordingly. So due to DNA-DNA interactions, positioning of DNA-conjoint nanostructures can be done with nanometer precision just by self-assembly processes. Through modern molecular biological methods DNA can be synthesized, sequenced or chemically modified easily, therefore large quantities of DNA with all possible sequences are available at low cost, which not only allows developing DNA based systems on an experimental laboratory scale but also utilize developed DNA technology on an industrial scale. DNA can be used as a nano breadboard to align DNA-conjoint nano objects in a two or three dimensional manner, for example[1–7]. This not only gives the opportunity to study interaction of specific single nano objects in close vicinity to each other, but allows gaining control over chemical or physical interaction on a molecular level and enables the fabrication of new sensing principles or even nano sized machines[8]. But also micron DNA-superstructures or nanostructure systems have to be aligned with at least micro-precision in order to handle them easily in our macroscopic world. Therefore one part of this work deals with the alignment of DNA using strong AC electrical fields (DEP) on microelectrode substrates. It will be shown that single DNA molecules can be aligned fully stretched between two microelectrodes. This makes the electrode substrates work as a "work bench" to study single molecule interaction on a DNA molecule in a specific location, which can be easily found and tracked in an experimental process.

Hence this technique is not limited to charged objects like DNA, also other micro/nano sized objects can be manipulated. Especially the fact that the objects are aligned directly in a microelectrode gap having contact to both electrodes, the technique allows subsequent electrical or optoelectronic characterization of single nano objects. So another part focuses on the optical and electrical characterization of single SiNW and GaAsNW. Furthermore, the integration and characterization of AuNP using DEP will be addressed to develop a chemoresistive sensor.

Betrachtet man DNA als chemisches Polymer und nicht als Träger von genetischen Informationen, kann sie ein sehr nützliches Werkzeug für die Nanotechnologie darstellen. Beispielsweise kann einzelsträngige DNA in Verbindung mit Nanostrukturen wie AuNP, NW, Kohlenstoffnanoröhren (CNT) und Quantenpunkten (QD) genutzt werden, um diese zu spezifischen Positionen zu führen, welche vorher mit der komplementären DNA markiert wurden. Hierbei wird der native Selbstassemblierungsprozess (Hybridisierung) der DNA genutzt. Im Vergleich zu den meisten chemischen Polymeren besteht codierende DNA nicht aus repetetiven Monomeren. Infolge der Codierungsfunktion der DNA ist die Sequenz der Monomere hoch individuell. Damit ist es möglich auch spezifische Positionen zu adressieren, wenn diese mit der entsprechenden DNA modifiziert wurden. Auf diese Weise können durch DNA-DNA-Wechselwirkungen Nanostrukturen mit Nanometerpräzision durch Selbstassemblierungsprozesse positioniert werden.

Durch moderne molekularbiologische Methoden kann DNA einfach synthetisiert, sequenziert oder auch chemisch modifiziert werden. Daher steht DNA in großen Mengen mit allen möglichen Sequenzen und geringem Kostenaufwand zur Verfügung. Dies ermöglicht die Entwicklung von DNA basierenden Systemen nicht nur im Labormaßstab, sondern auch für industrielle Anwendungen. Basierend auf diesen Gegebenheiten und ihrer enormen Flexibilität kann DNA als Nanobaukasten dienen, um DNA modifizierte Nanostrukturen in zwei und drei Dimensionen anzuordnen [1–7]. Das bietet nicht nur die Gelegenheit, Interaktionen von einzelnen Nanoobjekten miteinander zu untersuchen, sondern es ermöglicht auch die Kontrolle über chemische und physikalische Interaktionen auf Einzelmolekülebene zu erlangen. Ebenso ist es möglich neue sensorische Prinzipien zu etablieren oder gar nanometergroße Maschinen zu assemblieren. Aber auch mikrometergroße DNA-Überstrukturen oder Systeme bestehend aus Nanostrukturen müssen mit einer Mindestpräzision im Mikrometerbereich positioniert und ausgerichtet werden können, damit sie praktisch zu handhaben sind. Daher beschäftigt sich ein Teil der Arbeit mit der Ausrichtung und Positionierung von DNA auf Mikroelektrodensubstraten unter Verwendung von starken elektrischen Wechselfeldern. Es soll gezeigt werden, dass einzelne DNA-Moleküle zwischen zwei Elektroden gestreckt und positioniert werden können. Hierbei werden die Elektrodensubstrate zu einer „Werkbank“ um Interaktionen an einem DNA-Molekül, an einer spezifischen Position zu untersuchen. Mittels dieser gezielten Fixierung wird das Untersuchungsobjekt einfach wiederauffindbar und während des gesamten experimentellen Prozesses verfolgbar.

Da die DEP nicht auf geladene Moleküle wie DNA begrenzt ist, können auch andere Mikro- und Nanostrukturen mit dieser Methode manipuliert werden. Insbesondere die direkte Positionierung der Nanoobjekte auf den Mikroelektroden ermöglicht eine anschließende elektrische oder optoelektronische Charakterisierung von einzelnen Nanostrukturen. So beschäftigt sich ein weiterer Teil der Arbeit mit der elektrischen und optischen Charakterisierung von einzelnen SiNW und GaAsNW. Des Weiteren werden

auch AuNP mittels DEP integriert, welche anschließend der Entwicklung eines chemoresistiven Sensors dienen.

3 Stand der Technik

Die Charakterisierung und Anwendung von Bottom-up Nanostrukturen wie beispielsweise metallische Nanopartikel, QD, leitende oder halbleitende NW oder auch CNT sind ein vielversprechender Forschungsschwerpunkt seit einigen Jahrzehnten. Man erwartet, dass die darauf aufbauende Nanotechnologie die Medizin, Informationstechnologie, Luft- und Raumfahrt, Transport und Verkehr sowie Energietechnologie revolutioniert[9,10]. Wenn man sich jedoch einen Überblick über industriell gefertigte Produkte auf der Basis von bottom-up Nanostrukturen verschafft, fällt auf, dass es sich bei den meisten Produkten lediglich um Beschichtungen (antiseptisch, hydrophob, e.g.) oder Nahrungsergänzungsmittel (Farbstoffe, Konservierungsmittel, e.g.) handelt, während moderne Hochtechnologieprodukte nach wie vor durch klassische top-down Technologien gefertigt werden. Ein entscheidender Grund für die mangelnde Einsatzfähigkeit von bottom-up Nanostrukturen in Hochtechnologieprodukten ist die Schwierigkeit ihrer Integration in mikro- und makroskopische Umgebung. Die Anordnung und Positionierung sowie Kontaktierung dieser Strukturen sind schwierig und meist nur sehr kostenaufwendig zu realisieren, da die meisten Techniken hierfür nur seriell arbeiten und Präzisionsgeräte und -ausrüstungen benötigen (z.B. Elektronenstrahllithographie, Extreme-UV-Lithographie). Eine alternative Technik ohne diese Nachteile ist die DEP. Sie ermöglicht Nanostrukturen kontaktlos (ohne das Objekt zu berühren) entlang eines elektrischen Feldgradienten zu bewegen und zu positionieren. Das elektrische Feld wird hierbei von zwei oder mehr Elektroden durch eine Wechselspannung (AC) erzeugt. Es polarisiert Objekte entsprechend seiner Feldstärke in der unmittelbaren oder entfernten Umgebung. Da diese Polarisation leicht verzögert zum äußeren elektrischen Feld erfolgt, ergibt sich eine Phasenverschiebung zwischen dem inhärenten Feld des polarisierten Objekts und dem äußeren Feld. Dies führt dazu, dass auf diese Objekte entsprechend der Phasenverschiebung eine Kraft (F_{DEP}) wirkt und sie damit eine Bewegung erfahren. Ändert man diese Phasenverschiebung in dem man beispielsweise die Frequenz des äußeren Feldes erhöht oder erniedrigt, ist es möglich Objekte sowohl auf die Elektroden zu oder von ihnen weg zu bewegen. Die folgende Gleichung beschreibt diese Kraft:

$$F_{DEP} = 2\pi l r^2 \varepsilon_m Re\left\{\frac{\varepsilon_p^* - \varepsilon_m^*}{\varepsilon_m^*}\right\} \nabla \left|\vec{E}\right|^2$$

Die dielektrophoretische Kraft F_{DEP} wird dabei von der Geometrie des Objektes (Ellipsoid; r: Länge, Radius), dem elektrischen Feldgradienten $\nabla\left|\vec{E}\right|^2$ und dem Realteil des Clausius-Mossotti-Faktors $Re\left\{\frac{\varepsilon_p^*-\varepsilon_m^*}{\varepsilon_m^*}\right\}$ bestimmt. Letzterer enthält die komplexen Dielektrizitätskonstanten ε_m, ε_p des Mediums und des Partikels.

Die Präzision der Bewegung / Positionierung wird dabei ausschließlich von der Form des elektrischen Feld bestimmt und damit im Wesentlichen durch die Elektrodenform beeinflusst. Mittels photolithographisch hergestellter Elektrodensubstrate ist es daher bereits möglich, Nanostrukturen mit Submikrometergenauigkeit zu bewegen und zu positionieren.

Diese Form der Manipulation von Nanometer und Mikrometer großen Objekten mittels Wechselspannung wurde erstmals 1951 von Herbert Pohl anhand von Milchsuspensionen und Hefezellen beschrieben[11–13]. Von ihm wurde ebenso der Begriff Dielektrophorese geprägt, da er zunächst davon ausging, dass diese Form der Manipulation ausschließlich für dielektrische Objekte in Frage kommt. Erst Jahrzehnte später wurde diese Technik für die Manipulation von leitenden (e.g. Au-NP[14–16], CNTs[17–19]), halbleitenden (e.g. ZnONW[20,21], SiNW[22] InAsNW[23]) und dielektrischen Nanostrukturen (e. g. DNA[24,25], Proteine[25,26] Mikrosphären[27,28]) wiederentdeckt. Im Allgemeinen gibt es zwei Anwendungsgebiete für die Nutzung der DEP in der Wissenschaft. Zum einen die Integration oder Konzentration von Mikro- und Nanostrukturen, zum anderen die Sortierung der selbigen aufgrund ihrer Permittivitätsunterschiede. Dabei ist die Sortierung von Zellen ein populäreres Anwendungsgebiet der DEP[29]. Im Rahmen der Mikrointegration ist DEP meist eine Technik, um Nano- und Mikrostrukturen auf Elektrodenstrukturen zu positionieren. Zumeist fehlte es jedoch in der Vergangenheit an Präzision, um Untersuchungen an Einzelstrukturen durchführen zu können. Ebenso ist der hohe Kontaktwiderstand, der nach dem Einfangen und Ablegen der Strukturen entsteht, ein Problem. Zur Absenkung des Kontaktwiderstandes wird oft eine zusätzliche Metallabscheidung oder ein „thermal annealing“ eingesetzt[21,30]. Die vorliegende Arbeit beschäftigt sich unter anderem mit der Untersuchung und Lösung dieser Probleme, um damit neue Wege zu eröffnen, einfach und kostengünstig Nanostrukturen submikrometergenau zu positionieren und zu kontaktieren. In den eigenen Arbeiten wird gezeigt, dass es mittels DEP möglich ist, Nanostrukturen hochpräzise zu positionieren, zu kontaktieren und diese sowohl für die Sensorik als auch die Charakterisierung von Nanostrukturen einzusetzen [CL3, CL4, CL5].

Im Bereich der Sensorik ist insbesondere die chemische und biochemische Sensorik von Interesse. Diese wird nicht mehr nur für die Sicherheitstechnik, sondern auch immer mehr für die Prozesssteuerung von chemischen und biologischen Reaktion, bis hin zum Energiemanagement (z.B. Lüftungsanlagen) eingesetzt. Ein besonders hohes Potential haben dabei die Chemoresistoren, welche eine leitfähige Sensorschicht besitzen, die gegenüber der Anbindung von Analyten spezifisch ist. Hier ist es möglich das Sensorsignal direkt - in Form einer Widerstandsänderung - elektrisch auszulesen. Solche Sensorschichten bestehen meist aus leitenden oder halbleitenden Materialen, die entweder intrinsisch spezifisch für bestimmte Moleküle oder Molekülgruppen sind oder molekülspezifische Rezeptoren enthalten. Im Allgemeinen zeichnen sie sich durch ihre kostengünstige Herstellung und die Möglichkeit zur Miniaturisierung aus. Der Einsatz von Nanostrukturen als leitfähige Sensorschichten steht hierbei besonders im Fokus der Forschung, da die Empfindlichkeit durch den Einsatz von Nanostrukturen um ein Vielfaches gesteigert werden kann und damit eine markerfreie Analytik ermöglicht. Außerdem erlaubt die Verwendung von Nanostrukturen eine weitere Miniaturisierung sowie "multiplexing" und somit das Erfassen komplexer Informationen. Aktuelle nanoskalige Chemoresistoren basieren meist auf CNTs, Graphen, leitenden oder halbleitenden NW sowie Partikelketten oder Partikelschichten[31]. Der chemoresistive Effekt wird hierbei hauptsächlich für die Detektion von Gasen, Lösungsmitteln und Biomolekülen (DNA, Proteine) eingesetzt.

Im Rahmen dieser Arbeit wurde die Anbindung von DNA-Sonden an SiNW und ZnONW und deren Hybridisierung mit Ziel-DNA untersucht, welche als Vorarbeit zur Etablierung eines chemoresistiven DNA-Sensors dienen soll [CL6]. Chemoresistive Sensoren auf Basis halbleitender NW sind sowohl für bottom-up, als auch top-down Nanostrukturen beschrieben. Im Bereich der Bioanalytik an top-down strukturierten NW war in den letzten Jahren die Gruppe um G. Zhang besonders erfolgreich. Strukturierte NW-Arrays werden genutzt, um sowohl DNA als auch Proteine elektrische zu detektieren[32–36]. Erst kürzlich wurde ein integriertes System zur Detektion von Biomarkern vorgestellt, welche in Zusammenhang mit Myokardinfarkten gebracht werden[33]. Vergleichbare Systeme, welche sich ebenfalls mit der markerfreien elektrischen Detektion von Proteinen[37–41] oder DNA[42–45] beschäftigen, zeigen ebenso vielversprechende Ergebnisse. Mindestens genauso populäre Nanostrukturen für die markerfreie elektrisch auslesbare Bioanalytik stellen CNTs dar. Sie zeichnen sich durch ihren noch geringeren Durchmesser und damit ein noch höheres Oberflächen/Volumenverhältnis aus. 2002

gelang mit Hilfe von Peptid-Nukleinsäure (peptid nucleic acid - PNA)-Sonden erstmals die Detektion von DNA durch spezifische Hybridisierung an CNTs[46]. Der Nachweis wurde jedoch ausschließlich per Rasterkraftmikroskopie (atomic force microscopy – AFM) und nicht elektrisch erbracht. Ein Jahr später erfolgte der erste elektrische Nachweis einer Ligand-Rezeptor-Interaktion anhand von Streptavidin und DNA-Hybridisierung an CNTs durch Nanomix Inc.[47,48] . Die Funktionsweise eines solchen Sensors ähnelt der eines Feldeffekttransistors (FET). Der von zwei Elektroden (source, drain) kontaktierte halbleitende NW wird hierbei durch die Anbindung von DNA in seiner Leitfähigkeit durch das inhärente elektrische Feld des Biomoleküls (negativ geladen) beeinflusst. Auf diese Weise schalten angebundene Moleküle den Stromfluss zwischen „source“ und „drain“ genauso wie eine Gate-Elektrode bei einem FET. Die Differenz im Stromfluss kann quantitativ als Sensorsignal ausgelesen werden. Zur Aufklärung des FET-Effekts werden vier mögliche Mechanismen diskutiert: electrostatic gating[49–51], Schottky-barrier-effekt[52–54], capacitance modulation[55] und carrier mobility change[56,57]. Ähnliche Effekte werden auch für die chemoresistive Detektion an Goldnanopartikelketten postuliert[58–60]. Im Vergleich zu NW oder CNT basierenden Sensoren sind diese jedoch weitaus weniger verbreitet. Zumeist werden die verwendeten Ketten mittels „self-assembly“-Techniken aufgebaut[61]. Sie bestehen daher aus einem oder multiplen Partikelschichten (2D und 3D), welche sich durch eine große Oberfläche für die Anbindung von Analyten auszeichnen. In solchen Systemen wird beispielsweise die Transition vom Leiter zum Isolator als Detektionssignal eingesetzt, wenn sich der Abstand zwischen den Nanopartikeln vergrößert[62–65]. Die Veränderungen im Ladungstransport innerhalb dieser beweglichen Nanopartikelketten kann auch optisch durch eine Rotverschiebung, sowie eine Verbreiterung des Plasmonpeaks detektiert werden[62,64,66–68]. Eine weitere Möglichkeit, den Widerstand in Nanopartikelkonstrukten zu beeinflussen, ist die Verbindung mit einer organischen Matrix, welche dann durch Einbetten des Analyten eine Veränderung der Dielektrizitätskonstanten bewirkt[69–77]. Reversible Sensoren mit einer hohen Sensitivität und schnellen Reaktionszeiten auf Basis von 3D-Nanopartikelkonstrukten wurden für die Detektion von Tetrachlorethylen und Toluol (Octanethiolmatrix)[71], Hydrochinon und Adrenalin (Bis-bipyridinium-cylclophane-Matrix)[78] und H_2O_2 (Mikroperoxydase-11)[79] gezeigt. Aus wenigen perlenschnurartigen Ketten bestehende Goldnanopartikelketten (1D) sind eher selten das Sensorelement chemoresistiver Analytik. Ein gut funktionierendes System für die chemoresistive Detektion auf der Grundlage von 1D-Nanopartikelketten ist die Detektion von H_2 basie-

rend auf Pd-Nanopartikelketten[80,81]. Hierbei wird die Fähigkeit von Palladium genutzt, H_2-Atome in sein Kristallgitter aufzunehmen. Diese Inkorporation führt zur Bildung von Pd-Hydrid und damit zur Expansion des Kristallgitters, womit sich die Abstände der Pd-Nanopartikel in der Kette verkleinern und damit der Elektronentransport entlang der Kette verbessert wird. Eine Entfernung des Wasserstoffs vergrößert wiederum die Abstände der Nanopartikel, was den Widerstand erhöht. Diese Nanopartikelketten bilden damit einen reversiblen elektrochemischen Sensor mit Reaktionszeiten im Millisekundenbereich. Analog zu diesem Sensor wurden auch Hybridstrukturen bestehend aus Pd-Nanopartikel konjugierten NW oder CNT als Sensor publiziert[82–87].

In den eigenen Arbeiten wurden Untersuchungen zur chemoresistiven Detektion an dielektrophoretisch integrierten Nanopartikelketten durchgeführt, welche die Echtzeitdetektion von Thiolen in Flüssigkeit erlauben [CL4]. Ein weiterer Teil der Arbeit beschäftigt sich mit der optischen Charakterisierung von einzelnen NW [CL1, CL2]. Besonders im Fokus stehen hierbei die Mie-Resonanzen der NW, welche die Absorptions- und Streueigenschaften im Wesentlichen beeinflussen. Die Mie-Theorie beschreibt die Interaktion von Licht in Form einer ebenen Welle mit einem sphärischen oder zylindrischen Objekt. Insbesondere für Objekte in der Größenordnung des interagierenden elektromagnetischen Feldes beschreibt die Mie-Theorie den Einfluss der Größe des Objekts auf diese Interaktion besser als der allgemein bekannte Rayleigh-Ansatz. Basierend auf diesem Modell wurde die Absorption und Streuung von einzelnen NW in Abhängigkeit ihres Durchmessers und Materials (Si / GaAs) sowie des Einfallswinkels und der Polarisation des eingestrahlten Lichts berechnet. Die Berechnungen wurden experimentell durch spektrale Messungen an einzelnen NW, sowie durch AFM und Rasterelektronenmikroskopie (REM) verifiziert und dienten als Basis für die optische Bestimmung von NW-Durchmessern. Die verwendeten NW wurden mittels VLS (vapour-liquid-solid)-Technik hergestellt[88]. Das VLS-Verfahren ermöglicht das Kristallisieren von halbleitenden Materialien aus der Gasphase als Einzelkristalle. Die Kristallisation erfolgt in nanometergroßen Tropfen aus einem eutektischen Gemisch aus Halbleiter und Metall (meist Au oder auch Pt, Pd, Cu, Ag oder Ni) welche sich auf der Oberfläche eines Substrats befinden. Im Zuge der Kristallisation bilden sich aus jedem Tropfen „zylindrische“ Einkristalle welche an ihrer Spitze eine Kappe aus dem eutektischen Gemisch besitzen. Dieses Verfahren wurde erstmals von Wagner und Ellis 1964 für Silizium publiziert und wird bis heute für die Herstellung von NW aus verschiedensten Halbleitermaterialien eingesetzt[89]. Die optischen Eigenschaften von einzelnen NW wurden

erstmalig von Wang et al. 2001 untersucht[90]. Er beschreibt eine Polarisationsanisotropie der Photoluminiszenz für einzelnen NW. Die Messungen erfolgt hierbei für transversal elektrisch (TE) und transversal magnetisch (TM) polarisiertes Licht bei 500 nm an Indiumphosphid (InP)-NW mit einem Durchmesser von 10 – 50 nm. 2006 beschrieb Cao et al. unter Verwendung der Mie-Theorie das Raman-Spektrum von einzelnen NW. Die NW für diese Experimente waren kegelförmig und hatten Durchmesser im Mikrometerbereich. Es wurden Raman-Verstärkungen festgestellt, jedoch keine einzelnen Mie-Resonanzen. Mie-Resonanzen von einzelnen halbleitenden NW wurden besonders in den letzten Jahren thematisiert[91–104], e.g. insbesondere von der Gruppe um Prof. Brongersma[94,95,97–100,104]. Hierbei waren die optischen Eigenschaften von Si- und GeNW von Interesse. Bei beiden Materialien handelt es sich um indirekte Halbleiter, daher werden Mie-Resonanzen für Wellenlänger kleiner ~400 nm unterdrückt. Die Absorptionseigenschaften von einzelnen Si- und GeNW wurden von der Gruppe um Prof. Brongersma experimentell bestimmt. Dabei erfolgte die Bestimmung der Absorption indirekt, durch die Messung der Photoleitfähigkeit bei verschiedenen Wellenlängen. Dieses Vorgehen basiert auf der Annahme, dass sich die Photoleitfähigkeit proportional zur Absorptionseffizienz verhält. Die zugehörigen Spektren wurden mittels Mie-Theorie modelliert. Die Publikation von Cao et al.[99] unterstreicht im Speziellen das Potential von SiNW für Solarzellen und untersucht vor allem die optischen Eigenschaften innerhalb des sichtbaren Lichts. Unter Annahme einer Quanteneffizienz $n_i = 1$ wird ein Kurzschlussstromdichte in Abhängigkeit vom Lichteinfallswinkel und Durchmesser der NW berechnet. Die Untersuchungsergebnisse von Cao et al.[98] bestätigen die gleichzeitig zur Publikation eingereichten eigenen Forschungsergebnisse [CL1]. Bei Cao et al. werden die Streuspektren von einzelnen NW in Abhängigkeit von Polarisation und Beleuchtungswinkel gezeigt und mit berechneten Streueffizienzen verglichen. Anders als bei den eigenen Untersuchungen [CL1], basieren die Experimente jedoch auf lithographisch hergestellten SiNW. Ebenso wird gezeigt, dass auf Basis dieser lithographischen SiNW farbige Bilder im Mikrometermaßstab erzeugt werden können. Außerdem wird der Einfluss von Metallschichten (Gold) auf die NW diskutiert. Die präsentierten Spektren zeigen nicht nur eine Peak-Verschiebung, sondern auch eine Veränderung des gesamten Spektrums bezüglich Form und Streuintensität. Xu et al.[105] berechnen die optischen Absorptionseigenschaften von SiNW unter Berücksichtigung des Substrates. Der Einfluss des Substrats ist hierbei relativ gering. Zur Verifizierung der Ergebnisse werden ebenso numerische Methoden verwendet. Diese ermöglichen die Erweiterung der Berechnungen auf

Matten aus parallel liegenden NW. Auch hier zeigen Photoleitfähigkeitsmessungen und berechnete Absorptionen eine gute Übereinstimmung. Ebenso wurde die gegenseitige Beeinflussung zweier parallel liegender NW untersucht. Der Abstand beider NW muss hierbei deutlich kleiner als die Wellenlänge sein, um einen signifikanten Effekt zu erzielen. Lopez et al. nutzen sich verjüngende NW zur Charakterisierung des Einflusses der NW-Form auf die optischen Eigenschaften[106]. Es wird herausgestellt, dass die Farbänderungen auf deren Durchmesseränderung beruhen. Das gezeigte Bild ähnelt dem in Publikation [CL2, Fig. 9] welches die Durchmesserabhängigkeit für GaAsNW untersucht. GaAs besitzt eine besondere Bedeutung als technologisch nutzbarer, direkter Halbleiter (1.42 eV = 870 nm). Die Mie-Streuung sowie die Mie-Resonanzen in halbleitenden NW sind im Vergleich zu Silizium kaum untersucht. Eine Veröffentlichung von Lysov et al. untersucht die Absorptionseffizienz an einem GaAsNW mit axialem p-n Übergang, welcher auf einem Substrat kontaktiert wurde[93]. Hier wurde mittels Mie-Theorie die Absorptionseffizienz eines NW mit dem Durchmesser von ~100 nm und damit die Effizienz dieser Diode als Solarzelle bestimmt. Die elektrische Charakterisierung der Diode erfolgt bei 532 nm und damit nahe ihrer Mie-Resonanz. Montazeri et al. beschäftigt sich mit der Polarisationsanisotropie von GaAs- und InPNW[102]. Hierbei wird ein durchstimmbarer Laser zur Induzierung der Photoluminszenz eingesetzt. Die Experimente erfolgten in einer Hellfeldkonfiguration, wodurch die Mie-Resonanzen in den erhalten Spektren nur relativ schwach zu sehen sind. Der Fokus dieser Publikation liegt jedoch auf der Photomodulation der Bandstruktur durch einen weiteren Pump-Laser. Die resultierende Änderung im Brechungsindex wird in Abhängigkeit der Polarisation und des NW-Durchmessers untersucht. Das stete Interesse an der Mie-resonanten Absorption von SiNW zeigt sich ebenso in der erst kürzlich erschienen Publikation von Solaniki et al.[96]. Hier wurden SiNW mittels Photolithographie elektrisch kontaktiert und anschließend mit 200 nm SiO_2 beschichtet. Anschließend wurden Elektrodenstrahl-induzierte Strommessungen (EBIC) zur Abschätzung der Ladungsträgerdiffusionslänge und der wellenlängenabhängigen Absorptionseffizienz durchgeführt. Die Messungen erfolgten indirekt über die Photoleitfähigkeit analog zu den Veröffentlichungen[94,105]. Außerdem wurde der Durchmesser der NW durch Korrelation der gemessen Absorptionseffizienz mit der berechnete Absorptionseffizienz bestimmt. Die erhaltenen Durchmesser stimmten mit den rasterelektronenmikroskopischen Messungen der Durchmesser überein. Im Gegensatz zu eigenen Publikation [CL1] wurden hierfür Absorptionseffizienzen und nicht Streueffizienzen verwendet. Dennoch bekräftigen diese Ergebnisse die

in Publikation [CL1] aufgestellte These, dass Mie-Resonanzen zur Bestimmung der Durchmesser verschiedenster NW genutzt werden können. Des Weiteren wurde der Einfluss von Gold-[107] und Silbernanopartikeln[108] auf die optischen Eigenschaften von SiNW untersucht. Es ist bekannt, dass aufgrund der Plasmonresonanz der NP-Feldverstärkungen in der unmittelbaren Umgebung auftreten[109]. Diese Feldverstärkung kann die resonante Absorption von NW beeinflussen. Es wurde gezeigt, dass das elektromagnetische Feld des Partikels von einem NW absorbiert werden kann, wenn sich dieser nur wenige Nanometer entfernt befindet. Hierbei findet eine verstärkte Lichtabsorption des NW im spektralen Bereich der Plasmonresonanz des NPs statt[107,108].

4 Eigene Arbeiten

4.1 Optische Eigenschaften von Si- und GaAsNW [CL1, CL2]

Si- und GaAsNW werden seit Jahren als Schlüsselelemente für optische Detektoren, chemische Sensoren, Transistoren oder Solarzellen gehandelt. Jedoch gibt es bisher kein kommerziell erhältliches Gerät welches NW als zentrales Sensorelement nutzt. Ein Grund hierfür ist, dass es bisher noch nicht möglich war die optischen und elektrischen Eigenschaften der NW exakt einzustellen. In den Arbeiten CL1 und CL2 wird ein Beitrag geleistet die optischen Eigenschaften von Silizium- und GaAsNW exakt bestimmen zu können.

Alle verwendeten NW wurden nach dem VLS-Prinzip mittels CVD-Verfahren (chemical vapour deposition) hergestellt. In diesem Prozess werden Substrate entweder mit dünnen Goldschichten oder mit chemisch angebundenen Goldnanopartikeln in einer definierten Gasatmosphäre der Halbleitersubstanz (Silan / GaAs) bis zur Schmelze erhitzt. Während dieses Prozesses diffundiert das gasförmige Halbleitermaterial in die Goldpartikel und bildet mit diesen eine eutektische Schmelze mit einem deutlich niedrigeren Schmelzpunkt als die Einzelkomponenten, welche sich nach und nach mit dem Halbleitermaterial übersättigt. Der Überschuss an Halbleitermaterial scheidet sich daraufhin an der Tropfenunterseite in kristalliner Form ab. Auf diese Weise entsteht ein NW mit etwa dem Durchmesser des Goldpartikels, aus dem er wächst. Die erhaltenen NW sind fest mit dem Substrat (Silizium / Glas) verbunden und besitzen an ihrer Spitze einen Partikel, welcher aus dem eutektischen Gemisch besteht. Anschließend können die NW von dem Substrat abgelöst und für die optische Charakterisierung flach auf ein Glassubstrat positioniert werden. Die optische Charakterisierung und die Aufnahme der Streuspektren von einzelnen NW erfolgt im Durchlicht-Dunkelfeld. Hierbei wird die Probe in einem flachen Winkel beleuchtet, sodass das direkte Licht am Objektiv vorbeigeführt wird. Diese mikroskopische Methode ermöglicht nicht nur Objekte im Nanometerbereich sichtbar zu machen, sondern auch die selektive Aufnahme von Streulichtspektren dieser Objekte bei minimalem Hintergrund. Um einzelne NW spektral untersuchen zu können, wurde eine Lochblende (100 µm) in die Zwischenbildebene des Objektivs (50x) eingesetzt und durch eine Multimodefaser in ein Spektrometer eingekoppelt. Hierdurch wird in der Zwischenbildebene ein reales Bild mit einer Auflösung von 2 µm erzeugt, welches mit Hilfe des eingekoppelten Spektrometers optisch charakterisiert werden kann. Für die Messung werde Glassubstrate mit einer rasterartige Einteilung genutzt, welche das Lokalisieren von ein und demselben Nanoobjekt für sowohl optische als auch AFM- und REM-Aufnahmen erleichtert. Die optische Charakterisie-

rung und die Aufzeichnung der Streuspektren erfolgte polarisationsabhängig (T_M / T_E / unpolarisiert), indem zusätzlich ein linearer Polarisator in den Strahlengang eingesetzt wurde. Der gesamte Strahlengang ergibt sich wie folgt: Das Objekt wird mittels Dunkelfeldkondensor im Durchlicht beleuchtet, dass gestreute Licht wird durch das Objektiv (typisch 50x) vergrößert und anschließend durch ein in der realen Zwischenebene befindliches, koplanares Pinhole (100 µm) geführt. Dieses Pinhole blockt das „unerwünschte“ Licht und führt das nicht geblockte über eine Multimode-Faser in das Spektrometer. Die spektrale Ortsauflösung ergibt sich dabei aus dem Quotienten Pinhole-Durchmesser dividiert durch die Vergrößerung des Objektivs (100 µm / 50 = 2 µm). Durch die inverse Verwendung dieses Aufbaus (Einkoppeln einer Lichtquelle in die Multimode-Faser), kann ein Lichtpunkt auf der Probe erzeugt werden, welcher die räumliche Justierung des Systems ermöglicht. Unter Verwendung dieses Systems wurden Streuspektren von NW verschiedenster Durchmesser aufgenommen und mit berechneten Streuspektren korreliert. Die Berechnung basiert hierbei auf der Mie-Theorie, welche nach Lösung der Maxwell-Gleichungen die optischen Eigenschaften von kugelförmigen Objekten im Nanometerbereich beschreibt. In den Publikationen [CL1 und CL2] wurden Streueffizienzen ($Q(l)_{sca}$) berechnet, welche sich aus dem Quotienten Streuquerschnitt ($C(l)_{sca}$) dividiert durch die Projektionsfläche des Objekts ergeben. Für die Korrelation der berechneten Steueffizienzen mit den gemessen Steuintensitäten wird davon ausgegangen, dass $I(l)_{sca} \sim C(l)_{sca} \sim Q(l)_{sca}$ ist. Da jedoch die Streuintensitäten nicht nur abhängig von den Streueffizienzen, sondern auch von der Lichtquelle sind, wurden die gemessen Streuintensitäten normalisiert und vom Hintergrundsignal bereinigt:

$$I(\lambda)_{norm} = \frac{I(\lambda)_{NW,DF} - I(\lambda)_{BG,DF}}{I(\lambda)_{BG,BF}}$$

Die normierte Streuintensität $I(\lambda)_{norm}$ berechnet sich nach der o. g. Gleichung aus der gemessenen Streuintensität im Dunkelfeld $I(\lambda)_{NW,\,DF,}$ dem Hintergrund im Dunkelfeld $I(\lambda)_{BG,DF}$ und dem Lampenspektrum bzw. dem Hintergrund im Hellfeld $I(\lambda)_{BG,HF}$.

Unter Berücksichtigung dieser Randbedingungen wurden einzelne NW mit unterschiedlichem Durchmesser (70 – 180 nm) in Dunkelfeldkonfiguration spektral charakterisiert, ihr Durchmesser mittels AFM exakt bestimmt und anschließend mit den Berechnungen korreliert. Hierbei ergibt sich eine erstaunlich gute Übereinstimmung zwischen gemessenen und berechneten Werten, besonders wenn man berücksichtigt, dass bei den Berechnungen der Einfluss der Substratoberfläche vernachlässigt wurde. Des Weiteren wurden ebenso die Absorptionseffizienz und Streueffizienz in Abhängigkeit des Beleuchtungswinkels berechnet und publiziert. Im Falle der GaAsNW [CL2] gelang durch das Fitten von gemessen und berechneten Streuspektren zusätzlich eine sehr genaue

Bestimmung des Durchmessers der NW. Entsprechende Ergebnisse wurden auch hier mittels AFM-Aufnahmen verifiziert. Zusätzlich können mit dem entwickelten Verfahren ebenso nicht-zylindrische NW charakterisiert werden. Es wird gezeigt, dass Irregularitäten, wie kleinste Änderungen des NW-Durchmessers (> 5 nm) optisch detektiert, quantifiziert und die für zylindrische NW verwendeten Berechnungsalgorithmen ebenso für kegelförmige NW angewendet werden können (Abb. 1).

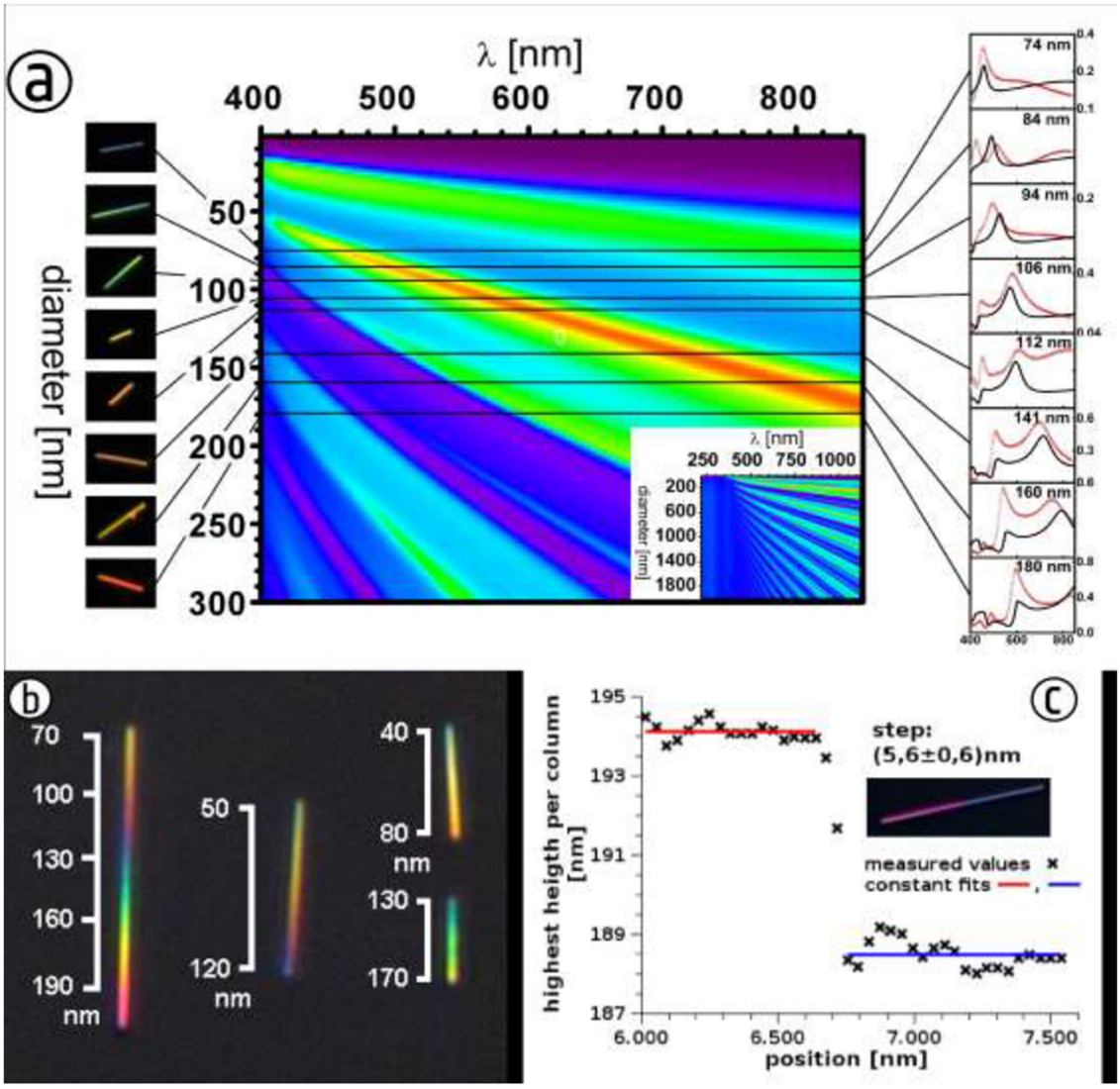

Abb. 1: Optische Eigenschaften von Si- und GaAsNW. (a) Streueffizienzen von SiNW in Abhängigkeit der Wellenlänge und des Durchmessers. Die Spektren (rechts) zeigen die Korrelation von berechneten (schwarz) und gemessenen (rot) Streueffizienzen. (b) Verjüngte NW (GaAs) zeigen eine Farbänderung durch das gesamte Spektrum entsprechend ihrer durchmesserabhängigen Streueffizienzen. Die Balken neben den NW zeigen den Durchmesser des NW in der entsprechenden Position. (c) Anhand des Streuspektrums wurde der Durchmesser eines NW bestimmt. Der NW besteht aus zwei unterschiedlich dicken Abschnitten (194.0 nm / 188.5 nm).

Zusammenfassend kann gesagt werden, dass Anhand dieser Publikationen erstmals eine umfassende Charakterisierung der Streueigenschaften von SiNW und GaAsNW erfolgte. Die theoretischen Berechnungen basieren hierbei auf der Lösung der Maxwell-Gleichungen nach Mie für unendlich lange Zylinder, während die experimentelle Cha-

rakterisierung durch spektroskopische Messungen an einzelnen NW erfolgte. Anhand dieser Ergebnisse ist es möglich den Durchmesser von SiNW und GaAsNW entsprechend ihrer Farbe / spektraler Information mit einer Genauigkeit von wenigen Nanometern zu bestimmen.

4.2 Dielektrophoretische Integration von DNA, AuNP und Si/ZnONW im Mikroelektrodenspalt [CL3, CL4, CL5]

In unserer „makroskopischen Welt“ sind Tätigkeiten wie Aufnehmen, Festhalten oder Loslassen von einzelnen Objekten simple Aufgaben. Wirft man jedoch einen Blick auf die mikro- oder nanoskopische Welt sieht das ganz anders aus. Hier dominieren Kohäsion und Adhäsionskräfte basierend auf Van-der-Waals Interaktionen, während z.B. die Gravitationskraft nur eine untergeordnete Rolle spielt. Daher werden obengenannte Manipulationen auf der Einzelmolekülebene, selbst wenn es sich um Makromoleküle wie DNA handelt, schwierige Aufgaben. So erfordert die gezielte Handhabung von nanoskaligen Objekten meist sehr kostspielige Geräte und Methoden, was wiederum den wirtschaftlichen Einsatz von einzelnen Nanostrukturen trotz ihres hohen Potentials behindert. Besonders in komplexen miniaturisierten Systemen, wie sie in Lab-on-a-Chip-Systemen im Bereich der Diagnostik und Analytik immer mehr Anwendung finden, ist die Handhabung von wenigen oder auch einzelnen Molekülen von Interesse. In Publikation [CL3] wird eine auf DEP basierende Technik vorgestellt, welche die Manipulation von DNA-Einzelmolekülen in einem Mikrometerelektrodenspalt ermöglicht. Als Neuerung im Vergleich zu vergleichbaren Publikationen konnten nicht-modifizierte DNA-Einzelmoleküle über Distanzen von bis zu 10 µm zwischen zwei Elektroden gestreckt werden und als Einzelmoleküle mittels AFM nachgewiesen werden. Als Basisplattform wurden Chipsubstrate photolithographisch über einen Standard-Lift-off-Prozess hergestellt. Die Elektrodenstrukturen zur Etablierung des elektrischen Feldes bestehen aus Gold (100 nm). Es werden Elektroden mit spitzt zulaufender oder flacher Geometrie mit einem Elektrodenspalt von 2 µm (spitz) oder 10 µm (flach) verwendet. Durch Variation der Spannung bei einer konstanten Frequenz von 100 kHz war es möglich, verschiedene Konzentrationen an DNA-Molekülen im Elektrodenspalt einzustellen. Durch Senken der Spannung auf 0.5 V_{pp} gelang es, einzelne DNA-Moleküle im Elektrodenspalt einzufangen und zu befestigen. Es konnte gezeigt werden, dass es mittels DEP möglich ist, DNA-Moleküle zwischen zwei Elektroden zu positionieren und über Distanzen von 2 - 10 µm zu strecken (Abb. 2). Entsprechende Ergebnisse wurden sowohl mit Fluoreszenzmikroskopie als auch AFM bestätigt. Des Weiteren konnte mittel Fluoreszenz-Echtzeit-Detektion der Assemblierungsvorgang verfolgt und das Ausrichten der gestreckten DNA-Moleküle entlang der Feldlinien demonstriert werden.

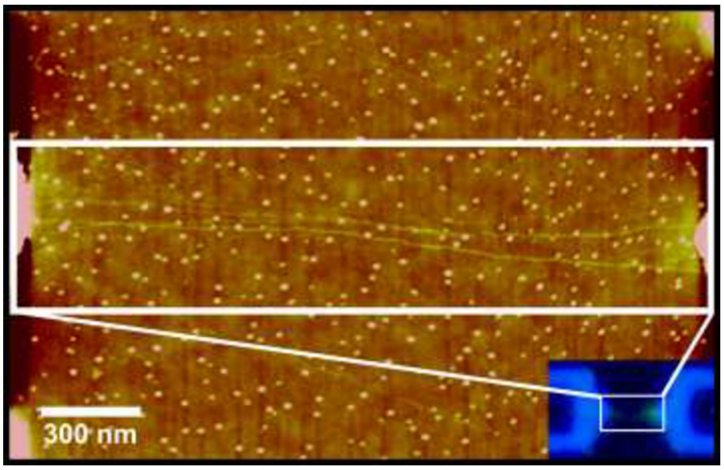

Abb. 2: AFM-Aufnahme von mehreren
„aufgespannten“ einzelnen DNA-Molekülen [CL3]

Das gleiche Prinzip, welches bereits für die Integration von DNA in Mikroelektrodenspalten genutzt wurde, kann auch für nicht-biologische Nanostrukturen wie halbleitende NW [CL5] oder AuNP [CL4] genutzt werden. Die Mikroelektrodensubstrate sind für die Integration dieser Nanoobjekte nicht mehr nur Werkzeug für die Handhabung sondern gleichzeitig Kontakte für die elektrische Charakterisierung und Sensorik. Daher kommt, neben der bloßen Handhabung (Einfangen und Ablegen), die elektrische Kontaktierung als wichtiger Aspekt der Integration hinzu. Die zur DEP-Integration verwendeten NW wurden unter den analogen, in Publikation [CL1] bereits beschrieben Bedingungen nach dem VLS-Prinzip hergestellt. Zur elektrischen Charakterisierung der Kontakte wurden für die Aufzeichnung von U-I-Kennlinien n-dotierte SiNW verwendet. Die Synthese erfolgte durch Zugabe des Dotiergases Phosphin unter vergleichbaren Bedingungen wie bei den nicht-dotierten SiNW. Schmid et al. beschrieben SiNW welche unter analogen Bedingungen hergestellt wurden[110]. Sie besitzen eine Dotierungsdichte von 10^{19} bis 10^{20} Atome / cm³. Es wird daher davon ausgegangen, dass der Dotierungsgrad der verwendeten SiNW in der gleichen Größenordnung liegt. Die Integration der SiNW erfolgte mit der Zielstellung, optoelektronische Sensorik an einzelnen SiNW durchzuführen. Daher wurde ein Chiplayout entworfen, welches speziell das Einfangen, Ausrichten und Integrieren von einzelnen NW (e.g. SiNW) ermöglicht. Sich verjüngende Elektroden erzeugen hierbei einen Feldgradienten mit einem Maximum im Zentrum des Chips. Dies ermöglicht das Dirigieren der SiNW von den Elektrodenrandbereichen zum Elektrodenspalt im Zentrum. Damit gelingt es einzelne SiNW mittels DEP entlang der Elektroden zum Elektrodenspalt zu führen. Entsprechend der Elektrodengeometrie richtet sich dann der SiNW aus und kann mit kurzen AC-Pulsen auf den Elektroden befestigt werden. Im besonderen Fokus stand bei dieser experimentellen Arbeit die Minimierung des Kontaktwiderstands zwischen Halbleiter und Metallelektroden. Um die Schottky-Barrieren zwischen Halbleiter und Metall so gering wie möglich zu halten, wurden die Elektroden aus Titan strukturiert. Die Austrittsarbeit von Titan ist hierbei deutlich

näher an der Bandlücke von Silizium als andere häufig verwendete Elektrodenmaterialien (e.g. Gold, Nickel-Chrom, Platin). Damit konnte eine Methode entwickelt werden, die es ermöglicht, einzelne halbleitende NW optisch kontrolliert zu kontaktieren, ohne kostenaufwendige Reinraumtechnologien verwenden zu müssen (e.g. E-Beam-Lithographie, UV-Lithographie). Die Analyse der Qualität der Kontakte erfolgte mittels Aufnahme der U-I-Kennlinien.

Während SiNW einzeln integriert werden konnten, war dies für AuNP auf Grund ihrer Größe nur in Form von Partikelketten oder Partikelteppichen (multiple Partikelketten) möglich. Die Verfahren zur DEP basierenden Integration beider Nanostrukturen unterscheiden sich grundlegend voneinander. AuNP-Ketten assemblieren sowohl bei Frequenzen im kHz- als auch im MHz-Bereich. Es konnte herausgefunden werden, dass Partikelketten im kHz-Bereich bei der Assemblierung in Form eines „Nanodrahts“ miteinander verschmelzen, während im MHz-Bereich assemblierte Partikelketten im allgemeinen nicht miteinander verschmelzen [CL4]. Die Unterscheidung von verschmolzenen (nanodrahtartig) und nicht-verschmolzenen (perlenschnurartig) Ketten kann leicht anhand des elektrischen Widerstands erfolgen. Nanodrahtartige Ketten zeigen Widerstände im kΩ-Bereich, während perlenschnurartige Ketten Widerstände im MΩ-Bereich besitzen. Des Weiteren konnte in [CL4] gezeigt werden, wie durch Anpassung entsprechender Parameter eine Assemblierung von AuNP-Ketten unterschiedlicher Dichte mit AuNP verschiedenster Größe (5 – 60 nm) möglich ist. Ebenso gelang die Parallelisierung der Integration sowie die Integration mit Nanoelektroden. Hierbei ist es möglich in Abhängigkeit des Elektrodenabstands wenige AuNP oder auch einzelne AuNP zu integrieren. Die entsprechenden Ergebnisse wurden mittels REM charakterisiert und verifiziert. Die Kontrolle des Integrationsprozesses erfolgte meist optisch mittels Durchlichtmikroskopie. Hierbei wurde die starke Absorption der Partikel genutzt, um die Kettenbildung mittels Immersionsobjektiv in Lösung in Echtzeit zu verfolgen. Des Weiteren gelang erstmals eine elektrische Echtzeitdetektion der Partikelkettenformation. Hierbei wurde während der Assemblierung der Realteil der Impedanz gemessen. Eine sukzessive Verringerung des Widerstandes zeigte die Integration von Partikeln in den Elektrodenspalt. Dies ermöglicht sowohl das Kettenwachstum zu detektieren als auch den Zeitpunkt des „Kurzschlusses“ exakt zu bestimmen. Speziell der Zeitpunkt des Kurzschlusses ist für die Assemblierung von entscheidender Bedeutung, da ein andauernder Kurzschlussstrom die Partikelketten direkt nach der Assemblierung beschädigt oder auch zerstört. Es wird davon ausgegangen, dass die Echtzeiterfassung der komplexen Impedanz ebenfalls hilfreich für die Integration anderer optisch nicht auflösbarer Nanostrukturen (e.g. CNT) sein kann. Entsprechende Arbeiten sind Inhalt aktueller Forschung.

Zusammenfassend kann festgestellt werden, dass mit den o. g. Arbeiten [CL3, CL4 und CL5] neue Verfahren zur submikrometergenauen Positionierung von Nanostrukturen (AuNP / NW) oder gar Makromolekülen (DNA) mittels DEP entwickelt, optimiert und

experimentell charakterisiert werden konnten. Hieraus ergeben sich weitreichende Anwendungsgebiete für diese Technik im Lab-on-a-Chip-Bereich oder auch im Bereich der elektrischen Sensorik. Zum jetzigen Zeitpunkt existieren keine vergleichbaren Selbstassemblierungstechniken die es ermöglichen einzelne bottom-up Nanostrukturen auf Chipsubstraten geordnet zu assemblieren und zu kontaktieren.

4.3 Resistive Sensorik und Biomodifikation von AuNP-Ketten und Si/ZnONW [CL4, CL5, CL6]

Ein weiterer Teil der Arbeiten beschäftigt sich mit der Untersuchung grundlegender Mechanismen zum Einsatz DEP-assemblierter AuNP-Ketten als chemische bzw. biochemische Sensoren. Hierfür wurden sowohl experimentelle Verfahren für eine Widerstandsmessung der AuNP-Ketten in Form von Endpunktmessungen als auch in Echtzeit entwickelt und entsprechende Messungen durchgeführt [CL4]. Die Anbindung eines Modellanalyten (1-Mecaptohexanol) erhöht hierbei den Widerstand der AuNP-Ketten welcher als elektrisches Signal ausgelesen werden kann (Abb. 3).

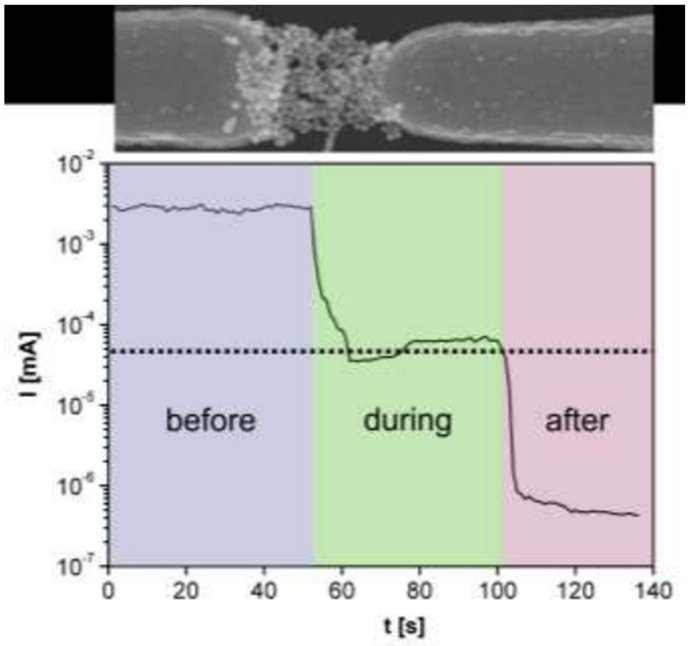

Abb. 3: Echtzeitmessung des Widerstands bei Anbindung eines Modellanalyten (6-Mercaptohexanol) an die dargestellte Goldnanopartikelkette. Die REM-Aufnahme zeigt eine mittels DEP hergestellte Nanopartikelkette zwischen zwei Mikroelektroden, welche aus 30 nm großen Goldnanopartikeln besteht [CL4].

Es wird davon ausgegangen, dass der sensorische Mechanismus dabei auf einer Änderung der Tunnelwiderstände zwischen den AuNP im Leitungsprozess beruht. Die Tatsache, dass nanodrahtartige AuNP-Ketten im Vergleich zu perlenschnurartigen AuNP-Ketten kaum eine Widerstandsänderung zeigen, unterstützt diese Vermutung. Perlenschnurartige AuNP-Ketten können hierbei als seriell geschalten Kapazitäten gesehen

werden, die auf Grund des Tunnelstroms von AuNP zu AuNP zusätzlich einen resistiven Widerstand (Tunnelwiderstand) besitzen. Es wird vermutet, dass durch die Anbindung von „isolierenden“ Molekülen der resistive Widerstand erhöht wird und somit als Signal zur elektrischen Auslesung dienen kann. Entsprechende Mechanismen werden auch in [58–60] diskutiert.

DEP kontaktierte SiNW wurden für die optoelektronische Sensorik genutzt. Für die entsprechenden Versuche wurden einzelne SiNW kontaktiert und ihre photosensitive Leitfähigkeit genutzt. Hierbei werden durch das absorbierte Licht Elektronen-Lochpaare kreiert welche die Leitfähigkeit des NW erhöhen. Basierend auf diesem Effekt wurden Reaktionszeitmessungen und wellenlängenabhängige Messungen der Photoleitfähigkeit durchgeführt [CL5]. Die Belichtung erfolgte mit Hilfe einer fokussierten 100 W Halogenlampe in Verbindung mit Metallinterferenzfiltern. Die Verwendung von Hochintensitätslichtquellen ist nicht notwendig. Es zeigte sich das NW eine wellenlängenabhängige Photoleitfähigkeit entsprechend ihrer Mie-Resonanz aufweisen. Entsprechend der Berechnungen in [CL1] zeigt ein SiNW mit einem Durchmesser von 130 nm eine verstärkte Absorption bei 475 nm (Abb. 4, rote Linie). Die Messungen weisen einen erhöhten Photostrom in diesem Wellenlängenbereich nach. Damit kann gezeigt werden, dass DEP kontaktierte NW entsprechend ihres Durchmessers (Mie-Resonanz) als wellenlängenabhängige und somit spektral aufgelöste, nanoskalige Photosensoren eingesetzt werden können (Abb. 4).

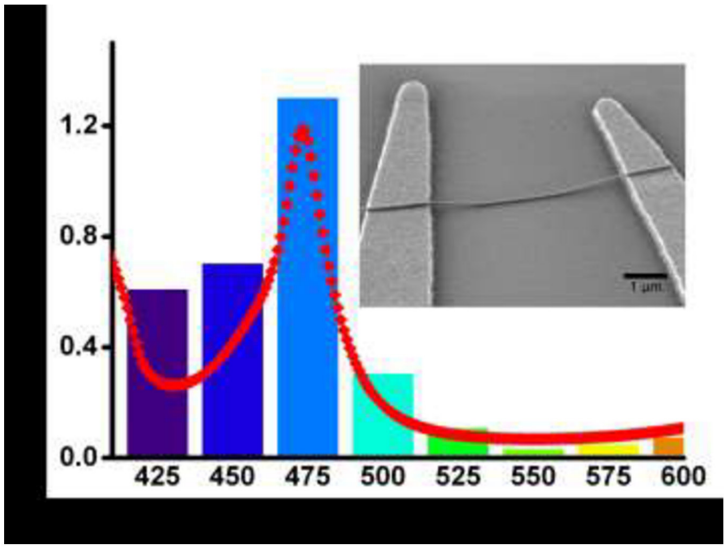

Abb. 4: Mittels DEP kontaktierter SiNW, auf einem Mikroelektrodensubstrat. Die Grafik zeigt die Korrelation zwischen Mie-resonanter Absorption (rot) und dem gemessen Photostroms bei der entsprechenden Wellenlänge (Balken) [CL5].

Ein weiteres Ziel ist DEP integrierte SiNW sowie ZnONW auch für die biologische Sensorik einzusetzen [CL6]. Hierbei soll die Hybridisierung von DNA oder die Bindung zwischen Antikörper und Antigen für die notwendige Spezifität sorgen, wobei das Bindungsereignis markerfrei elektrisch ausgelesen wird. Damit das bewerkstelligt werden

kann, muss ein kontaktierter NW ähnlich wie ein Metalloxidfeldeffekttransistor arbeiten. Das Schalten des Transistors erfolgt nicht durch eine Gateelektrode sondern durch die native Ladung der Biomoleküle. Hierfür müssen zunächst „Fängermoleküle“ (e.g. DNA-Sonden) auf oder in unmittelbare Nähe des NW gebunden werden. Bindet nun ein passendes Molekül an die Sonde, ändert sich das lokale elektrische Feld in dem sich der SiNW befindet, was zur Verarmung oder Anreicherung von Ladungsträgern im NW führt und als Widerstandsänderung detektiert werden kann. Damit dieses Fernziel erreicht werden kann, wurde an der chemischen Modifikation der NW gearbeitet. Hierfür wurden DNA-Sonden für die spezifische Hybridisierung angebunden. Im ersten Schritt wurden die NW nach Aktivierung durch Sauerstoffplasmaätzen direkt auf dem Wachstumssubstrat mit 3-Glycidoxypropyltriethoxysilan silanisiert. Dieses Silan dient als Linkermolekül und vermittelt so eine kovalente Bindung zwischen der DNA-Sonde und der NW-Oberfläche. Durch diesen Linker können amino-modifizierte DNA-Sonden durch eine Additionsreaktion an den Linker gebunden werden. Der Nachweis der erfolgreiche Anbindung erfolgte durch Verwendung einer direkt fluoreszenzmarkierten DNA-Sonde (CY3-5‘-AGA ATC AAG GAG CAC ATG CTG AAA AAA-3‘-NH2). Anschließend erfolgte die Modifizierung mit nicht-markierten Sonden. Ein NW-Substrat wurde dabei mit einer zu Ziel-DNA komplementären Sonden-DNA modifiziert (5‘-TTT TTT CAG CAT GTG CTC CTT GAT TCT ATG - NH2 - 3‘), während ein zweites NW-Substrat mit einer zur Ziel-DNA nicht-komplementärer Sonde (5‘-ACT GAC TGA CTG ACT GAC TGA CTG GGC GGC GAC CT - NH2 - 3‘) versehen wurde. Anschließend erfolgte die Hybridisierung beider Substrate mit der Ziel-DNA (5‘-CAT AGA ATC AAG GAG CAC ATG CTG AAA AAA-3‘-Cy3). Als Ergebnis zeigt sich, dass komplementäre DNA wie erwartet spezifisch an die NW bindet, während nicht-komplementäre DNA kein Signal zeigt. Anhand der Korrelation der optischen Dunkelfeld-Aufnahmen (Darstellung aller NW unabhängig von ihrer DNA-Modifikation) mit den Fluoreszenzaufnahmen konnte nachgewiesen werden, dass die Hybridisierung mit einer hohen Effizienz bei geringem Hintergrund erfolgt. Die experimentellen Ergebnisse belegen die Möglichkeit, SiNW vergleichbar zu planaren Substraten in der Mikroarraytechnologie biologisch zu modifizieren. Sie eignen sich somit auch als Substrate für die DNA-Chiptechnologie (Abb. 5).

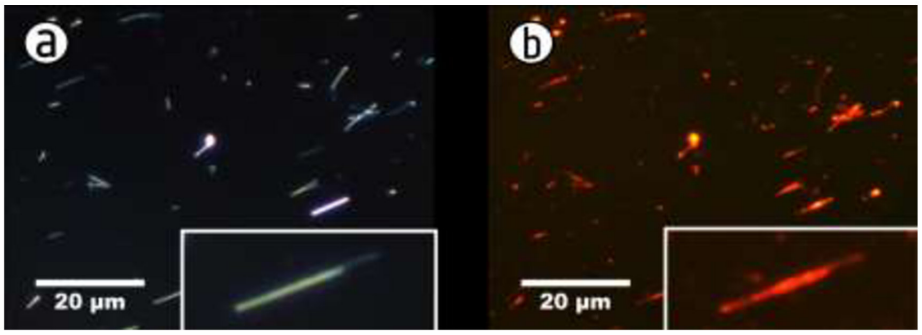

Abb. 5: DNA-modifizierte SiNW (DNA-Sonde), welche mit komplementärer, fluoreszenzmarkierter DNA hybridisiert wurden. Aufnahme (a) zeigt die SiNW im optischen Dunkelfeld unabhängig ihrer Fluoreszenz. Aufnahme (b) zeigt mittels Fluoreszenz die Hybridisierungspositionen der DNA.

Für die Arbeiten [CL4, CL5, CL6] kann zusammenfassend festgestellt werden, dass sowohl AuNP-Ketten, als auch NW mittels DEP integriert und als Sensoren eingesetzt werden können. AuNP-Ketten eignen sich als chemoresistive Sensoren für die Anbindung von Thiolen, während SiNW für die photoresistive Sensorik genutzt wurden. Vergleichbar zur chemoresitiven Sensorik an AuNP-Ketten wären genauso SiNW oder ZnONW als chemoresistive Sensoren denkbar. Für die zukünftige Etablierung eines DNA-Microarrays wurden NW mit DNA-modifiziert und für die spezifische Detektion von DNA nach Hybridisierung und Fluoreszenzmarkierung eingesetzt.

5 Zusammenfassung und Ausblick

Die dargelegte Arbeit zeigt das hohe Potential von bottom-up Nanostrukturen für die Analytik. Sie umfasst alle grundliegenden Schritte für die Demonstration eines Sensors auf der Basis von chemisch synthetisierten Nanostrukturen (AuNP, SiNW, ZnONW). Beginnend bei der optischen und elektrischen Charakterisierung der Nanostrukturen, über die elektrische Integration als wohl anspruchsvollstem Schritt, bis hin zur Demonstration eines optoelekronischen und chemoresistiven Sensors wurden all diese multidisziplinäre Ziele realisiert.

Die optische Charakterisierung konzentrierte sich auf SiNW und GaAsNW. Es wurde gezeigt, dass die optischen Eigenschaften dieser Halbleiternanodrähte, in Abhängigkeit von Durchmesser und Polarisation, im gesamten Bereich des sichtbaren Lichtes einstellbar sind. Diese Ergebnisse wurden durch Berechnungen basierend auf Mie-Resonanzen bestätigt. Basierend auf diesen Resultaten wurde eine Methode vorgeschlagen, die Durchmesser dieser NW anhand ihrer spektralen Information zu bestimmen. Die elektrische Charakterisierung der Nanostrukturen erfolgte nach der Integration mittels DEP. Kontaktierte SiNW konnten als wellenlängenabhängige und damit spektral aufgelöste Photosensoren demonstriert werden, während AuNP in Form von Ketten als chemoresistive Sensoren für Thiolverbindungen eingesetzt wurden. Ebenso war auch die Integration von DNA-Einzelmolekülen möglich. Des Weiteren wurde ein Verfahren entwickelt, welches die Modifikation von SiNW und ZnONW mit DNA-Sonden ermöglicht. Entsprechend modifizierte NW haben das Potential für einen Einsatz im Bereich der resistiven DNA-Analytik.

Im Allgemeinen können die hergestellten Sensoren im Bereich der kostengünstigen Sensoren eingeordnet werden, da die verwendeten bottom-up Nanostrukturen in großen Mengen einfach herstellbar sind. Die elektrische Integration dieser Strukturen durch eine Parallelschaltung [CL4] lässt sich einfach und kostengünstig realisieren. Die zusätzliche Aufbringung von selektiven Sensorschichten wie z.B. DNA-Sonden oder Antikörpern für die Bioanalytik kann ebenso im Hochdurchsatz effizient mittels Piezo-Drucker erfolgen. Entsprechende Techniken sind bereits im Bereich der Microarray-Technologie etabliert. Das Sensorsignal selbst wird bei allen vorgestellten Sensorprinzipien in Form eine Widerstandsänderung ausgelesen und erfordert somit keine aufwendige Ausrüstung.

Insgesamt konnte mit dieser Arbeit ein Beitrag geleistet werden, das große Potential von bottom-up Nanostrukturen im Bereich resistiven Sensorik zu demonstrieren. Zusätzlich wurden experimentelle Untersuchungsergebnisse gewonnen, die zur Erweiterung der

Kenntnisse über grundlegende optische Eigenschaften von halbleitenden Nanodrähten beitragen. Basierend auf diesen Erkenntnissen wurde ein Verfahren entwickelt, welches die optische Bestimmung von Nanodrahtdurchmessern (Si / GaAs) ermöglicht. Des Weiteren konnte ein optoelektronischer, wellenlängenselektiver Sensor demonstriert werden, welcher auf der Mie-Resonanzabhängigen Leitfähigkeit von Silizium Nanodrähten basiert. Die weitere Optimierung solcher Systeme bis zur Anwendungsreife ist ein vielversprechendes Ziel für weitere Forschung und Technologieentwicklung. Hierbei wären das Vorantreiben der Parallelisierung der Integration sowie die Etablierung günstiger Chipsubstrate sinnvoll. Entsprechende Inhalte sind Thema aktueller Forschungsarbeiten.

6 Thesis Publikationen

[CL1] Optical properties of individual silicon nanowires for photonic devices. Gerald Brönstrup, Norbert Jahr, Christian Leiterer, Andrea Csaki, Wolfgang Fritzsche, Silke Christiansen. ACS Nano 4 (2010) 7113–7122.

[CL2] A precise optical determination of nanoscale diameters of semiconductor nanowires. Gerald Brönstrup, Christian Leiterer, Norbert Jahr, Christoph Gutsche, Andrej Lysov, Ingo Regolin, Werner Prost, Franz-Joseph Tegude, Wolfgang Fritzsche, Silke Christiansen. Nanotechnology 22 (2011) 385201.

[CL3] Dielectrophoretic manipulation of DNA in microelectrode gaps for single-molecule constructs. Andreas Wolff, Christian Leiterer, Andrea Csaki, Wolfgang Fritzsche, Frontiers in Bioscience 13 (2008) 6834–6840

[CL4] Assembling gold nanoparticle chains using an AC electrical field: Electrical detection of organic thiols. Christian Leiterer, Steffen Berg, Antti-Pekka Eskelinen, Andrea Csaki, Matthias Urban, Päivi Törmä, Wolfgang Fritzsche. Sensors and Actuators B 176 (2013) 368-373.

[CL5] Applying contact to individual silicon nanowires using a dielectrophoresis (DEP) based technique. Christian Leiterer, Gerald Brönstrup, Norbert Jahr, Matthias Urban, Cornelia Arnold, Silke Christiansen, Wolfgang Fritzsche. Journal of Nanoparticle Research 15 (2012), 5, 1-7**.**

[CL6] DNA hybridization assay at individual, biofunctionalized zinc oxide nanowires. Christian Leiterer, Barbara Seise, Irma Slowik, Gerald Brönstrup, Raphael Niepelt, Karina Weber, Carsten Ronning, Silke Christiansen, Wolfgang Fritzsche. Journal of Biophotonics 16 (2013), 6, No. 2, 143–147.

6.1.1 Optical Properties of Individual Silicon Nanowires for Photonic Devices [CL1]

Gerald, Brönstrup:	Konzeptentwicklung Berechnungen und Evaluierung der Daten Diskussion des Konzepts und der Ergebnisse Diskussion und Korrektur des Manuskripts
Norbert, Jahr:	Messungen und Evaluierung der Daten Diskussion des Konzepts und der Ergebnisse Diskussion und Korrektur des Manuskripts
Christian, Leiterer:	Messungen und Evaluierung der Daten Diskussion des Konzepts und der Ergebnisse Diskussion und Korrektur des Manuskripts
Andrea, Csaki:	Messungen und Evaluierung der Daten Diskussion und Korrektur des Manuskripts
Wolfgang, Fritzsche:	Diskussion und Korrektur des Manuskripts
Silke, Christiansen:	Diskussion und Korrektur des Manuskripts

ACS Nano, **2010**, 4, 12, 7113–7122

ARTICLE

Optical Properties of Individual Silicon Nanowires for Photonic Devices

Gerald Brönstrup,[†,*] Norbert Jahr,[†] Christian Leiterer,[†] Andrea Csáki,[†] Wolfgang Fritzsche,[†] and Silke Christiansen[†,‡]

[†]Institute of Photonic Technology Jena, 07745 Jena, Germany, and [‡]Max Planck Institute for the Science of Light, 91058 Erlangen, Germany

ABSTRACT Silicon is a high refractive index material. Consequently, silicon nanowires (SiNWs) with diameters on the order of the wavelengths of visible light show strong resonant field enhancement of the incident light, so this type of nanomaterial is a good candidate for all kinds of photonic devices. Surprisingly enough, a thorough experimental and theoretical analysis of both the polarization dependence of the absorption and the scattering behavior of individual SiNWs under defined illumination has not been presented yet. Here, the present paper will contribute by showing optical properties such as scattering and absorption of individual SiNWs experimentally in an optical microscope using bright- and dark-field illumination modes as well as in analytical Mie calculations. Experimental and calculation results are in good agreement, and both reveal a strong correlation of the optical properties of individual SiNWs to their diameters. This finding supports the notion that SiNWs can be used in photonic applications such as for photovoltaics or optical sensors.

KEYWORDS: silicon · nanowire · optics · individual spectra · scattering · absorption · Mie

Silicon nanowires (SiNWs) in ensembles, usually on large area substrates such as wafers or glass sheets, have attracted much attention in the past few years to potentially serve as future building blocks in sensors,[1] transistors,[2] solar cells,[3−7] and photodetectors.[8,9] A prerequisite for using SiNWs in the aforementioned devices is that the electrical and optical properties are understood and can be controlled. So far, neither the understanding nor the control is satisfying. The present paper tries to support an enhanced understanding of the optical properties of individual SiNWs.

Many papers have been published dealing with the optical properties of nanowire (NW) ensembles.[10−15] A major part of the analysis of the measured data therein is based on the scattering properties of individual NWs in the Rayleigh limit, which is valid for diameters $d \ll \lambda/(\pi n)$.[16] Furthermore, non-Rayleigh-type resonances for these systems have been reported.[13] The knowledge of the values of optical cross sections is fundamental for other quantitative analyses; for example, a calculated value of the absorption cross section for CdSe NWs has been used to estimate the quantum yield of their photoluminescence.[17] Consequently, absolute values of the absorption cross sections of both CdTe and CdSe NWs in a solution have been reported[18] for a couple of wavelengths. Furthermore, the polarization anisotropy of CdSe and CdSe/CdS core/shell NWs has been analyzed for two different wavelengths,[19] and even experimental polarization-dependent absolute values of the absorption cross section of CdSe NWs for one wavelength have been published.[20] These experimentally obtained absolute values are in good agreement with those obtained by Mie theory. So far, a profound analysis of the optical properties of individual NWs is available for germanium.[21] In comparison to Ge, Si has a smaller extinction coefficient k for the whole visible spectrum, that is, for wavelengths larger than ~340 nm.[22] This should, in principle, result in even stronger resonances. The same line of thought applies for the direct semiconductors[22] since they have, depending on the wavelength, either very high extinction coefficients k or extinction coefficients close to zero. The latter, of course, would rule out strong absorption, and thus, even strong resonant enhancement would still result in very low absorption efficiencies. Very recently, some optical properties, such as light absorption of NWs of different materials including silicon, have been published[23] and the basic physical principles are described that are responsible for the generality of resonances in one-dimensional nanostructures and that indicate which resonances are mostly suited for absorption and how absorption depends

*Address correspondence to gerald.broenstrup@gmail.com.

Received for review May 9, 2010 and accepted November 04, 2010.

Published online November 16, 2010. 10.1021/nn101076t

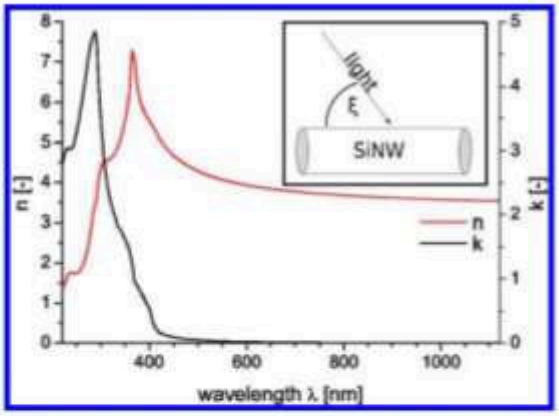

Figure 1. Complex refractive index $\hat{n} = n + ik$ of silicon given by the refractive index n and the extinction coefficient k taken from ref 24. Inset: Schematics of SiNW position with respect to the incident illuminating light: definition of the angle of light incidence ξ.

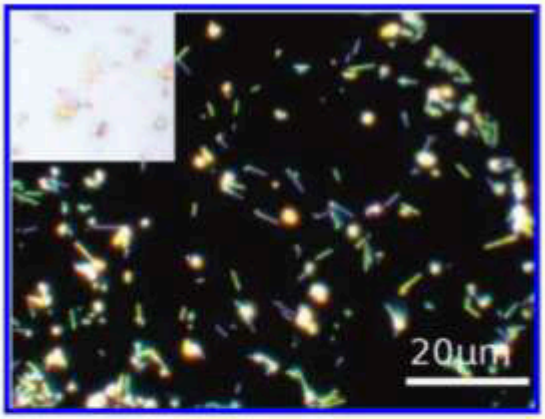

Figure 2. Optical micrograph of SiNWs on a glass substrate using a dark-field illumination configuration. Thus, only the scattered light is visible. The different colors of the SiNWs indicate that SiNWs of different diameters scatter the light differently. Inset: bright-field image of SiNWs on a glass substrate; in this case, only the transmitted light is visible. SiNWs are visible with an optical microscope because they scatter light efficiently despite their nanometer scale.

on the geometrical cross section of the SiNWs. Moreover, this paper describes how several rectangular NWs of amorphous Si lying in parallel can enhance the light absorption compared to a thin film.

However, both a detailed analysis of the scattering behavior of SiNWs and an analysis of the polarization dependence of the optical properties of SiNWs are still missing. Here, the present paper will contribute new experimental data of polarization and illumination controlled bright- and dark-field optical analyses together with analytical Mie calculations, contributing the polarization-dependent absorption efficiencies Q_{abs} of individual SiNWs. The dependence of scattering and absorption on the diameter d of SiNWs, on the wavelength λ of the illuminating light, on its angle of incidence ξ and on the polarization is discussed. The angle of incidence ξ is the angle between the illuminating light and the long axis of the SiNW, as schematically shown in the inset of Figure 1. Our findings show that absorption and scattering efficiencies are strongly dependent on the wavelength λ of the illuminating light, its polarization, and the diameters d of the SiNWs. These findings indicate that SiNWs are ideal candidates for a sensitive tuning of photonic devices by varying certain parameters of the SiNWs, such as the diameter and orientation with respect to the incident light.

To calculate scattering and absorption efficiencies Q_{sca} and Q_{abs}, the well-known Mie theory[16] is used. The efficiencies Q_{sca} and Q_{abs} are dimensionless and defined by the ratio of the particular cross section C_{sca} or C_{abs} and the geometrical area A of the object, $Q_{sca/abs} = C_{sca/abs}/A$. The cross section is defined as an imagined area around the illuminated object. As soon as an illuminating beam hits this area, interaction will occur. Within the limits of geometrical optics, this means the absorption cross section C_{abs} of a hypothetical, perfectly absorbing black body is always equal to the geometrical area A of the object and thus the absorption efficiency Q_{abs} always equals 1—independently of the geometrical shape. For a body that is an imperfect absorber, the absorption efficiency Q_{abs} resides between 0 and 1. Furthermore, within the limits of geometrical optics, the efficiencies Q are, in general, limited to values between 0 and 1. Leaving these limits of geometrical optics, as occurs when structures smaller than the illuminating wavelength λ are illuminated, such as the SiNWs in our experiments, different findings concerning the cross sections can occur (*e.g.*, absorption efficiencies Q_{abs} much bigger than 1). This means that absorption cross sections, C_{abs}, are bigger than the geometrical area A of the object; that is, the SiNW can thus collect light from an area much bigger than its geometrical area A (*i.e.*, the area covered by the SiNW itself). A similar effect has been calculated for an array consisting of SiNWs with a diameter d = 200 nm and a length of 2000 nm embedded in a polymer matrix for one wavelength λ = 350 nm.[8] In analogy to the absorption efficiencies Q_{abs} bigger than 1 outside of the framework of geometrical optics, scattering efficiencies Q_{sca} bigger than 1 can occur, which means in this case that light is scattered from an area bigger than the geometrical area A of the SiNW. In our examples, the calculated scattering efficiencies Q_{sca} reach values up to 901% and the absorption efficiencies Q_{abs} reach values of up to 449%. This shows that SiNWs have the potential to harvest and scatter light very effectively.

RESULTS

Optical Microscopy. SiNWs lying flat on a glass substrate show a broad spectrum of different colors (*cf.* Figure 2) as presented in optical micrographs in both dark-field and bright-field geometry. Each straight SiNW shows only one color, except the end points or when other particles are lying very close to the SiNW. The investigated SiNWs are several times longer than the wavelength of the illuminating light in vacuum. The ef-

fective wavelength of the light in the SiNWs is about 3.5 times smaller. Therefore, we do not consider the length of the SiNWs important for resonances, which could lead to different colors. These resonances would be considerably damped over such distances in Si. Hence, we assume that different colors point to different SiNW diameters.

To further analyze the cause of these different colors of individual SiNWs, the diameters of some of these SiNWs are measured using a scanning electron microscope (SEM) (*cf.* insets in Figure 3). The relation to the optical dark-field measurements that show the different colors is maintained by making use of markers that can be identified in the SEM as well as in the optical microscope. The color of the SiNWs in the optical microscope images is clearly correlated to the diameters *d* of the SiNWs (*cf.* insets in Figure 3). SiNWs with colors ranging all over the visible spectrum can be found. The correlation of SiNW diameter measurements and the color analysis with an optical microscope shows that a change in SiNW diameter *d* from 77 to 118 nm is responsible for a color change of blue to orange in dark field. This finding suggests that the SiNW scattering or absorption can be tuned very sensitively by slightly varying the SiNW diameter. The aforementioned experimental findings are supported by analytical Mie calculations[16] of the scattering efficiencies Q_{sca}.

Scattering Efficiencies Q_{sca} Based on Mie Theory. The colors of individual SiNWs in dark field and their diameters *d* as obtained by SEM measurements can be related to the scattering efficiencies Q_{sca} from Mie calculations (Figure 3). The colors of SiNWs vary with their diameters *d* since the intensity of the scattered light is proportional to the product of the intensity of the illuminating light and the scattering efficiencies Q_{sca}. Q_{sca} is dependent not only on the wavelength of the incident light but also on the diameter *d* of the SiNWs. As shown in Figure 3, the colors of individual SiNWs obtained from optical dark-field microscopy very well coincide with the colors that are expected from the Mie theory calculations. For example, SiNWs with a diameter of d = 77 nm show big scattering efficiencies Q_{sca} for blue light and thus appear blue in the corresponding optical dark-field image, or SiNWs with a diameter of d = 107 nm appear yellow in optical dark-field microscopy according to a scattering efficiency peak at a wavelength of yellow light.

Scattering Spectra. To quantitatively analyze the scattering behavior of the SiNWs, including the dependence on the polarization, scattering spectra with polarized, transmitted (*i.e.*, the SiNWs are illuminated through the glass substrate) light are taken in dark-field configuration. The positions of the peaks in the measured spectra are in accordance with the corresponding Mie calculations (*cf.* Figure 4, Figure 5, and Figure 6), and the spectra show pronounced polarization dependence.

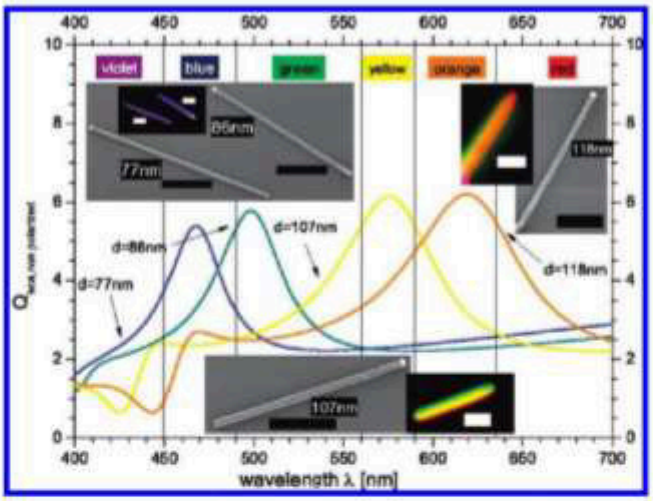

Figure 3. Scattering efficiencies Q_{sca} depending on SiNW diameters *d* calculated using Mie theory for perpendicular illumination (ξ = 90°) with nonpolarized light. Insets: SEM images and corresponding dark-field light optical micrographs of individual SiNWs lying flat on a glass substrate; all scale bars represent 1 μm; the SiNW diameters *d* are labeled in the SEM micrographs; the error for these values ranges from 5 to 8 nm, for the 77 and 118 nm diameter, respectively. The optical dark-field images superimposed with the calculated scattering efficiency Q_{sca} show a very good agreement.

Any illuminating electromagnetic field can be split into two independent polarizations. For the so-called transversal electric (TE) polarization, the vector of the magnetic $\vec{H}$-field is parallel to the SiNW's long axis, and for the so-called transversal magnetic (TM) polarization, the vector of the electric $\vec{E}$-field is parallel to the SiNW's long axis. The ratio of the intensities of the spectra measured with TE and TM polarized light, however, shows differences with respect to the ratio of the calculated scattering cross sections $Q_{sca,TE}/Q_{sca,TM}$ (*cf.* Figure 5 and Figure 6). In particular, the TE polarized light is scattered much stronger compared to the TM polarized light than predicted by the Mie calculations. This may be interpreted as an influence of the substrate, given that the substrate is not considered in the Mie calculations of the scattering efficiencies Q_{sca}. Though the background of the scattered light from the substrate does not show any pronounced peaks, the interaction between a SiNW and the substrate could lead to new patterns in the scattering spectrum. Spectra taken without polarizer show these differences between experimental measurements and Mie calculations, as well (*cf.* Figure 4).

Calculations of Scattering and Absorption Efficiencies of Individual SiNWs Based on Mie Theory. ***Scattering Efficiencies for Perpendicular Illumination ξ = 90°.*** As shown in Figure 4, Figure 5, and Figure 6, the scattering cross sections Q_{sca} do strongly depend on the wavelength λ of the illuminating light and its polarization, thus permitting to tune light scattering in SiNWs for device applications, though if the SiNWs are not embedded in a homogeneous medium the effects of the close (*i.e.*, distances comparable to a few times the wavelength λ) surrounding have to be considered.

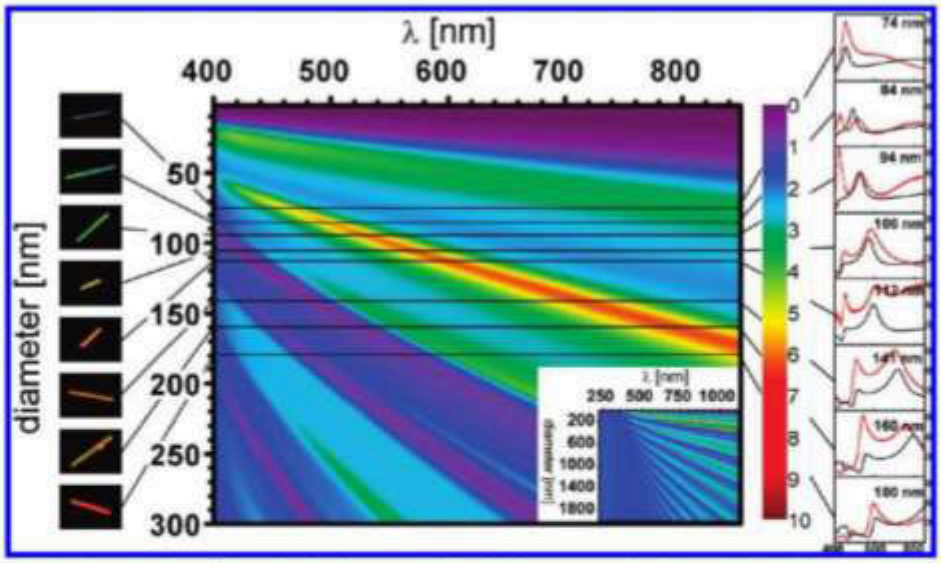

Figure 4. Calculated scattering efficiencies Q_{sca} for nonpolarized light at normal incidence ($\xi = 90°$) for $d = 2$ and 300 nm and $\lambda = 400$ and 850 nm. Solid black lines indicate the positions of the measured spectra. On the right-hand side, normalized measured scattering spectra are shown (red lines), and the black lines in these graphs are the corresponding calculated scattering efficiencies Q_{sca}. The measured and normalized (following eq 10) scattering intensities are scaled with a constant factor for each SiNW to match the calculated scattering efficiencies Q_{sca}. Thess factors are the same for every polarization shown in Figure 4, Figure 5, and Figure 6. The diameters of the SiNW shown in the graphs are measured using an AFM. The scale on the right-hand side shows the scattering efficiencies. On the left side, optical dark-field micrographs of the corresponding SiNWs are shown. Inset: Q_{sca} for $d = 2$ and 2000 nm and $\lambda = 220$ and 1120 nm.

For illumination with wavelengths smaller than ~360 nm, such as for ultraviolet light, the scattering efficiencies Q_{sca} do not show a strong dependence on the diameters of the SiNWs (*cf.* insets in Figure 4, Figure 5, and Figure 6). This is in line with the direct band gap of Si,[25] which resides at 3.4 eV ($\lambda = 365$ nm). In consequence of this, Si has a very high extinction coefficient k below wavelengths smaller than ~360 nm (*cf.* Figure 1). This results in a mean free path of light in Si of only a few nanometers for these wavelengths effectively suppressing resonant enhancement effects.

For wavelengths larger than ~400 nm, Q_{sca} shows a branched structure for both TE and TM polarization. The branches of high Q_{sca} are nearly straight lines in the plotted (λ, d)-plane (*cf.* Figure 4, Figure 5, and Figure 6). The slope of the branches is decreasing with increasing diameters d and decreasing wavelengths λ. The number of these branches for a given diameter d is increasing with increasing diameter d. This branched structure accounts for effective scattering of only one optically active SiNW at different incident wavelengths. The occurrence of such a branched structure can be ex-

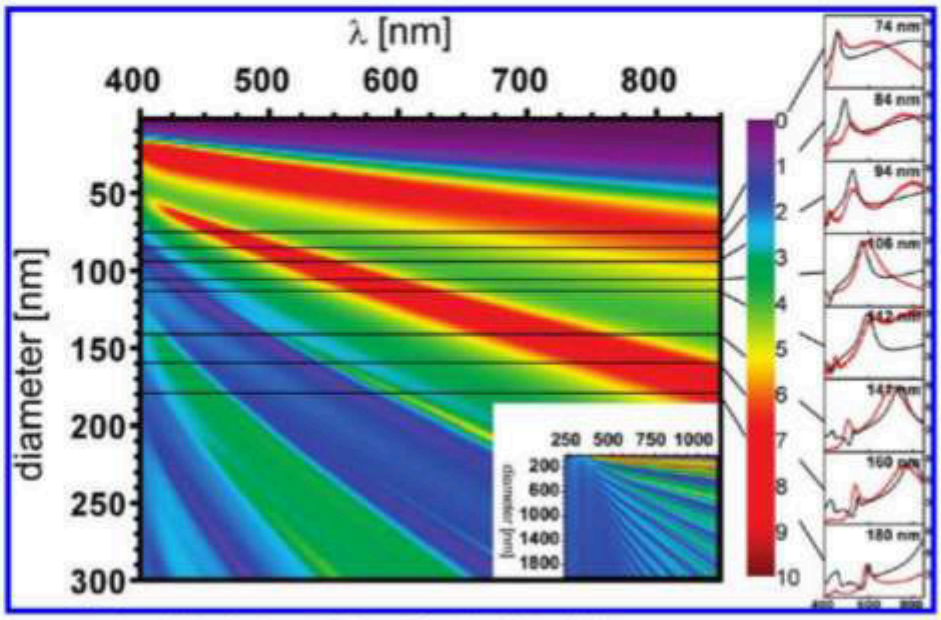

Figure 5. Same scattering efficiencies Q_{sca} as in Figure 4 for TM polarized light.

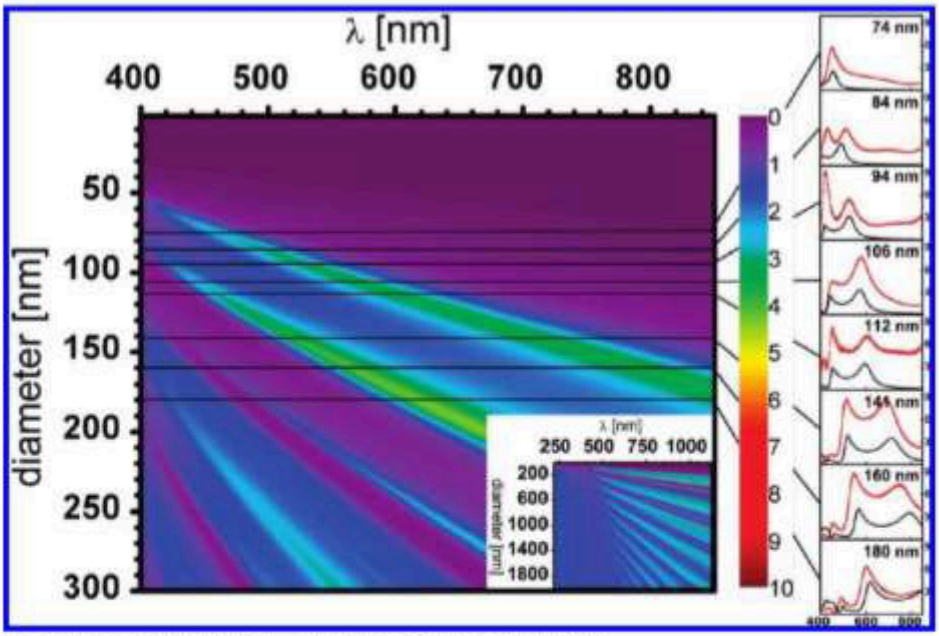

Figure 6. Same scattering efficiencies Q_{sca} as in Figure 4 for TE polarized light.

plained based on the analytical expressions for $Q_{sca}(\xi = 90°)$ as given by:[16]

$$a_i = \frac{\tilde{n}J_i(\tilde{n}x)J_i'(x) - J_i'(\tilde{n}x)J_i(x)}{\tilde{n}J_i(\tilde{n}x)H_i^{(1)\prime}(x) - J_i'(\tilde{n}x)H_i^{(1)}(x)} \quad (1)$$

$$b_i = \frac{J_i(\tilde{n}x)J_i'(x) - \tilde{n}J_i'(\tilde{n}x)J_i(x)}{J_i(\tilde{n}x)H_i^{(1)\prime}(x) - \tilde{n}J_i'(\tilde{n}x)H_i^{(1)}(x)} \quad (2)$$

$$x = \frac{2\pi d}{\lambda\ 2} \quad (3)$$

$$\tilde{n} = n + ik \quad (4)$$

$$Q_{sca,TM} = \frac{2}{x}\left[|b_0|^2 + 2\sum_{i=1}^{\infty}|b_i|^2\right] \quad (5)$$

$$Q_{sca,TE} = \frac{2}{x}\left[|a_0|^2 + 2\sum_{i=1}^{\infty}|a_i|^2\right] \quad (6)$$

Here $\tilde{n} = n + ik$ is the already mentioned complex refractive index, J_i is the Bessel functions of first kind of order i, and $H^{(1)}$ is the Hankel functions of first kind of order i. The scattering efficiencies Q_{sca} for perpendicular illumination $\xi = 90°$ are only dependent on terms like $x = d\pi/\lambda$ and $x\tilde{n}$. Since the complex refractive index $\tilde{n} = n + ik$ of silicon shows only a weak dependence on the wavelength λ for $\lambda > 500$ nm (*cf.* Figure 1), these terms are nearly proportional to d/λ. Thus, the scattering efficiencies Q_{sca} are nearly constants for straight lines in the (λ, d)-plane. The highest values for Q_{sca} (up to 901%) can be found for TM polarized light in a branch defined by the points $d = 64$ nm, $\lambda = 425$ nm and $d = 230$ nm, $\lambda = 1100$ nm. Another branch with high scattering efficiencies Q_{sca} (up to 866%) for even thinner SiNWs is given by the points $d = 16$ nm, $\lambda = 370$ nm and $d = 62$ nm, $\lambda = 720$ nm.

Since these are very common diameters for SiNWs,[2,26] it is possible to use this knowledge to optimize the growth of SiNWs using the particularly large scattering efficiencies Q_{sca} by controlling the SiNW diameters. The assessment of the SiNW diameters can be carried out by determination of the colors of the SiNWs in an optical microscope in dark-field configuration (*cf.* Figure 3). The scattered light analysis can, in principle, be used for *in situ* monitoring of the SiNWs' diameters, when they are individually grown in place in future devices. This *in situ* control during the SiNW growth can be decisive for successfully producing SiNW-based devices since *ex situ* diameter control is normally associated with oxidation of the SiNWs, which can prevent further epitaxy on the SiNWs.[27] An *in situ* control of the diameter could be necessary since not only the optical properties but also the electrical properties of SiNWs are strongly dependent on the diameter.[28] It also provides the option for a fast and low-cost *ex situ* diameter SiNW control to be used when implementing SiNWs in future device concepts. This can even be double checked by measuring the different scattering intensities for the different polarizations. Encouraging for a further use of this method is that the polarization dependence of the scattering efficiencies has already successfully been used with one wavelength ($\lambda = 1548$ nm) to measure the displacement of SiNWs.[26] The minima and maxima of the scattering efficiencies Q_{sca} can be a knowledge that may be important to minimize or maximize the scattering of light for optical SiNW-based sensors.

Absorption Efficiencies for Perpendicular Illumination $\xi = 90°$. The absorption efficiencies Q_{abs} are again a dimensionless number and are about 1 order of magnitude lower

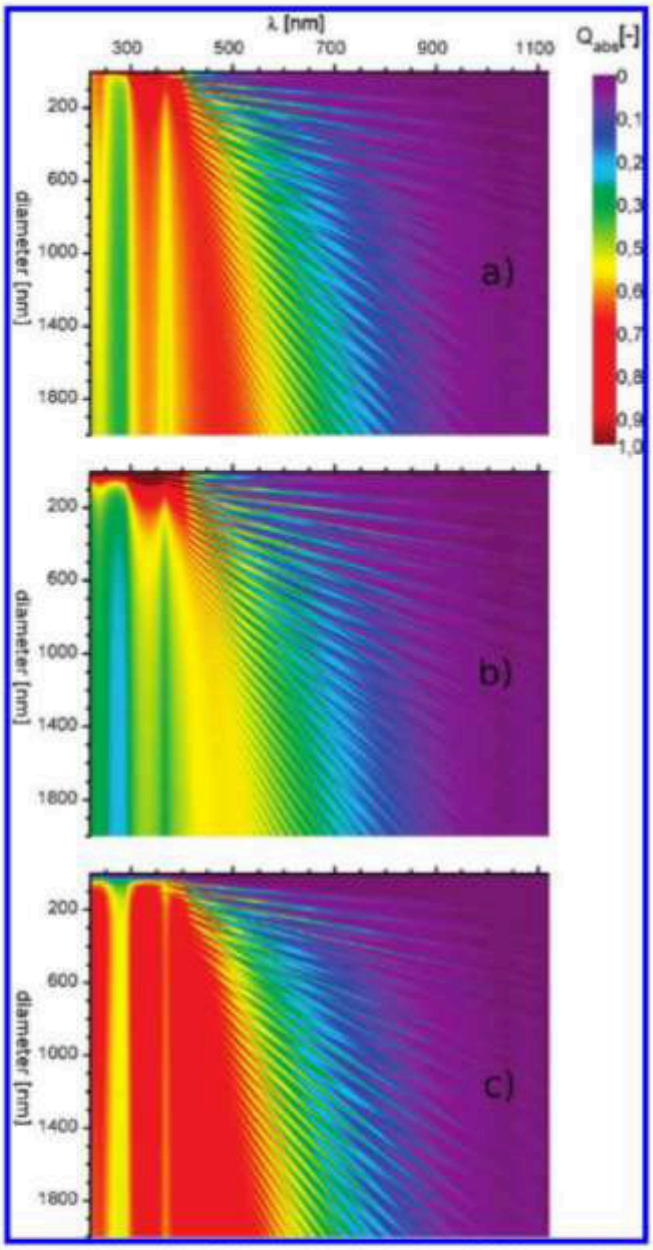

Figure 7. Absorption efficiencies Q_{abs} for d = 2 and 2000 nm and λ = 220 and 1120 nm for (a) nonpolarized light, (b) TM polarized light, and (c) TE polarized light.

than the scattering efficiencies Q_{sca}. This is not surprising because Si is an indirect band gap semiconductor. Note that the color scale implies 0 to 1 for Q_{abs} (Figure 7) and 0 to 10 for Q_{sca} (Figure 4, Figure 5, and Figure 6).

The results for the nonpolarized light (Figure 7a) are in accordance with those published in ref 23. However, in ref 23, it is mentioned that nanowires with diameters bigger than 100 nm do not show pronounced polarization dependence. This is only in qualitative accordance with our calculations; that is, the branches with high Q_{abs} are more or less at the same position in the (λ, d)-plane for the different polarizations, but the values of Q_{abs} show strong polarization dependence for all calculated diameters (*cf.* Figure 7).

The absorption efficiencies Q_{abs} show for λ < 360 nm (corresponding to the smallest direct band gap in Si[25]) only a weak dependence on the diameter d. Here, the direct band gap character of the Si with a high extinction coefficient k is dominating. Even though for larger wavelengths λ, Si is an indirect semiconductor, high absorption efficiencies Q_{abs} are possible because of resonant enhancement effects occurring in the SiNWs. These resonant enhancement effects are restricted to certain wavelengths and diameters, building the basis for a complex branched structure, similar to the structure of the scattering efficiencies Q_{sca} shown before.

A way to use SiNWs as wavelength- and polarization-sensitive photodetectors is as follows. Absorbed photons can produce free carriers in the SiNWs. Consequently, the conductance of undoped SiNWs rises proportional to the absorbed energy of light. Since SiNWs absorb light very specific with respect to the wavelength and polarization of incident light, the photoresistance is as very specific to these properties of the incident light. This method has been used for germanium NWs[21] and very recently as well for SiNWs.[23]

By examining the structure of the branches of high absorption efficiencies Q_{abs}, we find that the slope of the branches decreases for increasing diameters d and decreasing wavelengths λ, and these branches are nearly straight lines. These findings are very similar to what was found for the scattering efficiencies Q_{sca}. This is not surprising when looking at the formula for perpendicular illumination ξ = 90° for Q_{abs}:

$$Q_{abs,TM} = \frac{2}{x}\Re\left[b_0 + 2\sum_{n=1}^{\infty} b_n\right] - Q_{sca,TM} \qquad (7)$$

$$Q_{abs,TE} = \frac{2}{x}\Re\left[a_0 + 2\sum_{n=1}^{\infty} a_n\right] - Q_{sca,TE} \qquad (8)$$

The terms x, b_0, a_0, $Q_{sca,TM}$, and $Q_{sca,TE}$ have the same meaning as in eq 1−6. $\Re$ is only the real part taken, and $Q_{abs,TM}$ and $Q_{abs,TM}$ are the absorption efficiencies for *TM* and TE polarized light, respectively. In the case of perpendicular illumination ξ = 90°, the absorption efficiencies Q_{abs} are only dependent on the terms such as Q_{sca} (*i.e.*, $x = d\pi/\lambda$ and $x\tilde{n}$). This gives analogy to the arguments for Q_{sca} straight lines in the (λ, d)-plane for the absorption efficiencies Q_{abs}. Since Si is an indirect semiconductor, small wavelengths λ close enough to the direct gap are needed to obtain high absorption efficiencies Q_{abs}, despite the resonant enhancement effects. Note that for all 2 nm < d < 2000 nm calculated examples, Q_{abs} > 100% is restricted to wavelengths λ < 474 nm for TE polarized light and λ < 576 nm for TM polarized light. For diameters d smaller than 20 nm and ultraviolet light, the absorption efficiencies Q_{abs} are very different for the different polarizations. For wavelengths between 230 nm < λ < 1120 nm, Q_{abs} is always

smaller than 20% for TE polarized light, while it can reach values larger than 440% for TM polarized light ($Q_{abs,TM}(d = 12\ nm, \lambda = 365\ nm) = 449\%$). This opens up the opportunity to build very efficient nanoscale Si technology based polarization detectors. For larger diameters, the polarization dependence is about the opposite: for diameters d larger than 160 nm, Q_{abs} tends to be higher for TE polarized light than for TM polarized light (*cf.* Figure 7b,c). Furthermore, there is a general trend to higher Q_{abs} for larger diameters d for wavelengths between 380 nm $< \lambda <$ 1120 nm for both polarizations. This is again due to the indirect character of Si for these wavelengths, and it is critical for many optics applications such as solar cells, where the whole solar spectrum up to wavelengths corresponding to the gap of the semiconductor ($\lambda = 1120$ nm for Si[29]) should be absorbed.

For applying SiNWs in solar cell concepts, the following properties are important: For diameters d smaller than 120 nm and wavelengths λ larger than 700 nm, Q_{abs} is always smaller than 7%. For even larger wavelengths ($\lambda > 850$ nm), Q_{abs} does not exeed a comparable value ($Q_{abs} < 7.2\%$) for diameters d up to 200 nm. Although these values seem rather low, they can be sufficient if many SiNWs are used to absorb the light. This thought is supported by the fact that comparably large absorption of thin layers of SiNWs have already been reported.[11]

Note that commonly used multicrystalline Si wafer based solar cells have a thickness of a few hundred micrometers to absorb light from the entire solar spectrum sufficiently. Because of this thickness large charge, carrier diffusion lengths are needed and, consequently, very pure low defective and thus expensive Si is needed. The enhancement of light absorption of SiNWs with respect to Si thin films becomes even more obvious when they are directly compared. For infrared light ($\lambda = 850$ nm), a SiNW with a diameter of 172 nm shows an absorption efficiency $Q_{abs} = 5.37\%$ for nonpolarized light. The absorption $Abs_{bulk\text{-}Si}$ of a Si thin film with the same thickness $z = 172$ nm, even with no reflection at all, can be estimated following the Beer–Lambert law

$$\begin{aligned} Abs_{bulk\text{-}Si} &= 100\% - e^{(-z4\pi k/\lambda)} \\ &= 100\% - e^{(-172\ nm \times 4 \times \pi \times 4.05 \times 10^{-3}/850\ nm)} \\ &= 1.02\% \end{aligned} \quad (9)$$

Here k is the extinction coefficient for $\lambda = 850$ nm, $k(850\ nm) = 4.05 \times 10^{-3}$. The absorption efficiency $Q_{abs} = 5.37\%$ of the SiNW is more than five times higher than the absorption $Abs_{bulk\text{-}Si} = 1.02\%$ of the Si thin film with a perfect anti-reflective coating.

Dependence of the Scattering Efficiencies on the Angle of Incident ξ. Since the angle of incidence ξ is not always 90°, we will discuss how the optical properties are changing when the angle of incidence ξ is changed. Especially, if SiNWs are grown on an amorphous substrate like glass, they will be orientated randomly and all sorts of oblique orientations with respect to the substrate surface normal can occur. Consequently, the angle of incidence ξ will be randomly distributed.

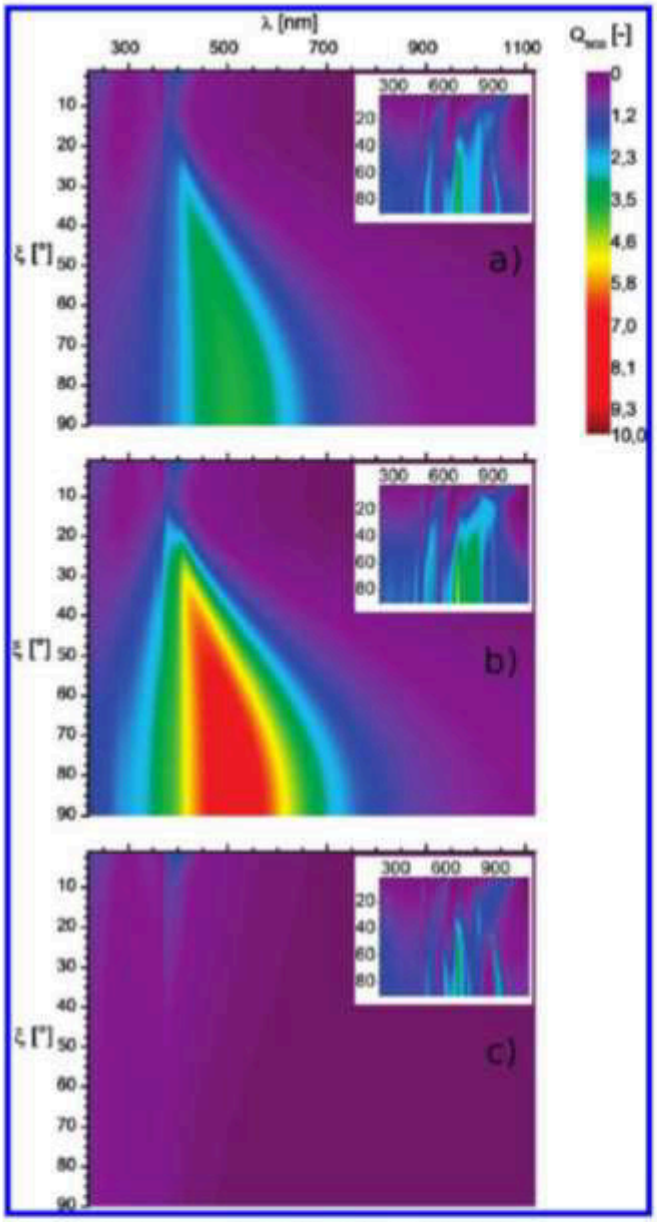

Figure 8. Scattering efficiencies Q_{sca} for a SiNW with a diameter d = 40 nm and λ = 220 and 1120 nm for different angles of illumination ξ for (a) nonpolarized light, (b) TM polarized light, and (c) TE polarized light. Insets: same for a SiNW with a diameter d = 400 nm.

A statistical approach based on the more simplified Rayleigh-type model to calculate the reflectance of thin films of SiNWs has been applied quite successfully by Street and co-workers.[10] The calculations shown in this paper can be used as a basis for more precise calculations of the optical properties of SiNW thin films composed of ensembles of randomly distributed SiNWs. For the discussion of the dependence on the angle of incidence ξ, two typical examples are chosen.

In the first example, a SiNW with a diameter $d = 40$ nm is illuminated. For perpendicular illumination (ξ =

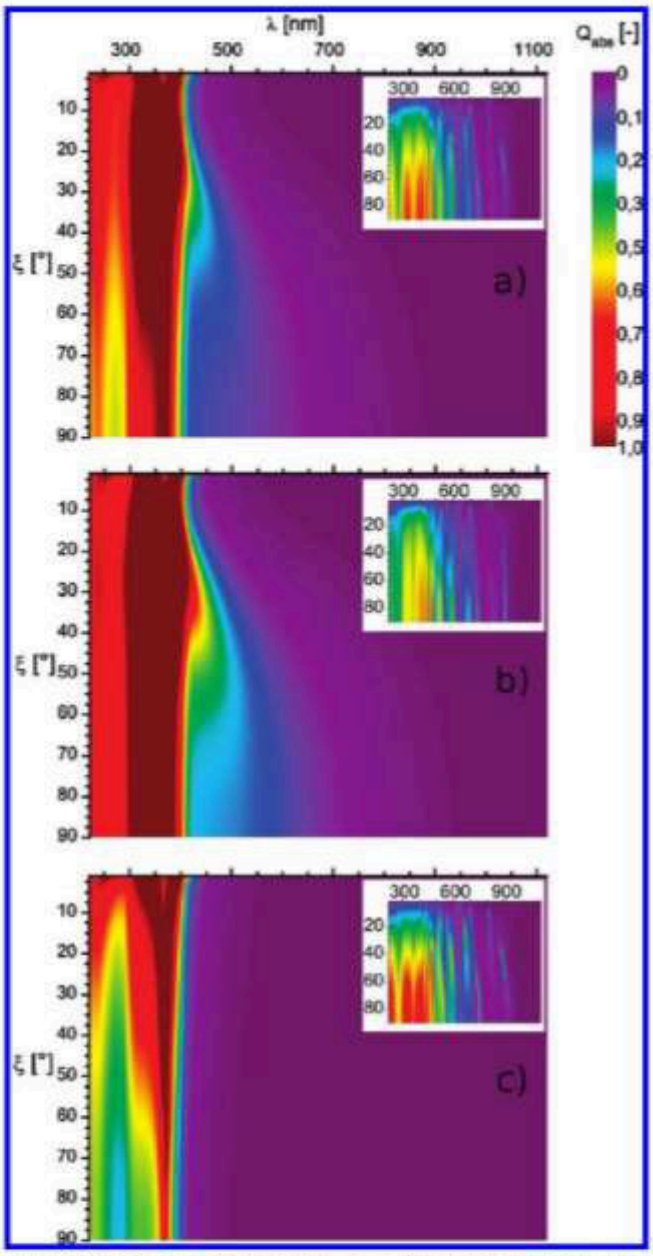

Figure 9. Absorption efficiencies Q_{abs} for a SiNW with a diameter d = 40 nm and λ = 220 and 1120 nm for different angles of illumination ξ for (a) nonpolarized light, (b) TM polarized light, and (c) TE polarized light. Insets: same for a SiNW with a diameter d = 400 nm.

90°), it can be seen that scattering efficiency Q_{sca} does not show a very strucutured dependence on the wavelength λ; that is, there is only one branch in the (λ, d)-plane for TM polarized light (*cf.* Figure 5) and none for TE polarized light (*cf.* Figure 6); however, for the TM polarization, the branch covers a large part of the visible spectrum of light for perpendicular illumination (ξ = 90°). This branch is getting much narrower for smaller ξ (*cf.* Figure 8b). On the other hand, there is no such branch in the (λ, d)-plane for TE polarized light for perpendicular illumination (ξ = 90°). In this case, Q_{sca} is increasing for decreasing ξ for wavelengths λ smaller than 450 nm, up to Q_{sca} = 2.1 for ξ = 1° and λ = 406 nm (*cf.* Figure 8c). Conclusively, it can be stated that the qualitative properties do not change drastically if the angle of incidence ξ is not altered too much. This is encouraging for further engineering of devices using SiNWs because it is not necessary to calibrate the angle of incidence ξ very precisely.

The second example uses the illumination of a *SiNW* with a diameter of d = 400 nm. In this case, there are many branches in the (λ, d)-plane for perpendicular illumination (ξ = 90°) for both polarizations (*cf.* insets in Figure 5 and Figure 6). The branches change with ξ in different ways. For TE polarization, some branches bend to smaller wavelengths λ for smaller ξ (*cf.* inset in Figure 8c), while for the TM polarization, most branches do not show such a behavior (*cf.* inset in Figure 8b). In summary, this gives a rather complicated quantitative dependence of Q_{sca} on λ and ξ. Again, it can be stated that the qualitative optical properties such as light scattering do not change dramatically when the angle of incidence ξ is not altered too much. Since it is still a challenge to build devices based on SiNWs, it is encouraging that the angle of incidence ξ is not very critical, and thus engineering of devices does not require intensive control of this parameter.

For bigger diameters (d > 400 nm), the dependence of optical properties on the angle of incidence ξ of incident light is qualitatively the same but in detail even a bit more complex.

Dependence of the Absorption Efficiencies on the Angle of Incident ξ. To discuss the dependence of the absorption efficiencies Q_{abs} on the angle of incidence ξ, the same two examples have been chosen that are used to discuss the dependence of Q_{sca} on ξ.

The first example is a SiNW with a diameter of d = 40 nm. For perpendicular illumination (ξ = 90°), one branch can be seen in the (λ, d)-plane for both TM polarized light (*cf.* Figure 7b) and TE polarized light (*cf.* Figure 7c). For TM polarized light, there is a broad branch with Q_{abs} > 1 for nearly all angles of incidence ξ for wavelengths λ between 300 and 400 nm (*cf.* Figure 8b). For TE polarized light, Q_{abs} tends to have bigger values for smaller angles of incidence ξ for wavelengths λ smaller than 450 nm. For λ > 450 nm, Q_{abs} is smaller than 6% for all calculated angles of incidence ξ (*cf.* Figure 9c). As mentioned before, the qualitative course of the absorption efficiencies is not very strongly dependent on the angle of incidence ξ. The underlying physics of this behavior is that these small SiNWs act like simple dipoles with respect to incident light.[23]

For potential applications, this finding is advantageous since not much attention has to be paid to focus light on the SiNWs and small angles of incidence are sufficient so that it is possible to focus light on potential devices with cheap, small focal lengths lenses without losing potential predesigned tuning to certain wavelengths.

SiNWs with a diameter $d = 400$ nm show many branches in the (λ, d)-plane for perpendicular illumination ($\xi = 90°$) for both polarizations (*cf.* Figure 7). The branches show the trend that they become increasingly narrow for smaller ξ (*cf.* insets in Figure 9). In addition, there are a few small branches starting at angles different from $\xi = 90°$. This shows that for thicker SiNWs the situation becomes more complicated and the angle of illumination ξ has a stronger influence and thus needs to be more thoroughly considered when building wavelength-sensitive SiNW-based devices.

CONCLUSION

The scattering and absorption efficiencies of SiNWs are calculated using Mie theory depending on polarization as well as the angle of incidence of the illuminating light and the diameters of the SiNWs. Quantitatively, these efficiencies depend strongly on the polarization of the incident light. The scattering efficiencies are generally higher for TM polarized light. The general trend for the absorption efficiencies is more complex. For TM polarized light, the absorption efficiencies are only higher than those for TE polarized light for SiNWs with diameters smaller than ~160 nm. For thicker SiNWs, the opposite holds true. The dependence of these cross sections on the angle of incidence ξ is not very pronounced. Calculated dependencies of scattering and absorption efficiencies very well coincide with experimental findings of scattering of white light in an optical microscope, which results, depending on the diameter of the SiNW, in a differently colored appearance of the SiNWs. The combined experimental and theoretical study of optical properties of individual SiNWs reveals a huge potential of SiNWs to be used as sensitively tunable building blocks in opto-electronic devices such as sensors, solar cells, and photodetectors.

METHODS

Preparation of Samples. The SiNWs are grown on Si wafers following the vapor−liquid−solid mechanism (VLS).[30] The Si is supplied by chemical vapor deposition (CVD) from a silane precursor in argon as the carrier gas at a mixture of 1:1 and a total pressures of 2.0 mbar. The one-dimensional wire growth is catalyzed by commercially available gold colloids (British Biocell Int.[31]). The use of gold colloids as catalysts for the SiNW growth has the potential to gain a certain control over the diameters of the SiNWs.[32] However, under different conditions during the CVD process, SiNWs with mixed diameters can occur due to gold diffusion.[33] Since the sample is placed about 1 mm above the heater, the absolute growth temperature on the wafer surface is unknown but could roughly be estimated to be around 500 °C based on pyrometer and thermocouple measurements.

After the CVD SiNW growth, the SiNWs are removed from the substrate by applying ultrasonic treatment for about 2 min with the sample residing in a small drop of isopropyl alcohol in a capsular. After the treatment, a SiNW isopropyl alcohol suspension is formed that is pipetted on a glass substrate. After drying of the suspension, dispersed, individual SiNWs can be found lying with their long axis flat on the glass substrate (*cf.* Figure 2).

Optical Measurements. The optical measurements are carried out with a Axio Imager (Zeiss Microimaging, Göttingen, Germany) optical microscope using as light source of a tungsten halogen lamp with a continuous spectrum with a color temperature of 3200 K. To experimentally obtain the scattering spectra of individual SiNWs, dark-field configuration is used. In this configuration, the direct light is blocked out and only the scattered light is passed through a pinhole to a spectrometer. The pinhole has a diameter of 100 μm and is coplanar to the real image plane of the tube lens. A multimode fiber is used to connect the pinhole to a Acton Research SpectraPro 2300i microspectrometer (Princeton Instruments, Trenton, NJ) with a grating with 150 lines and a peltier cooled CCD camera. With this setup, the scattered light of individual SiNWs is gathered. To obtain the scattering spectrum of a SiNW, the background from the glass substrate has to be removed and the spectrum has to be normalized with respect to the illuminating light source. This is done using the following equation:

$$I(\lambda)_{\text{normalized}} = \frac{I(\lambda)_{\text{NW,DF}} - I(\lambda)_{\text{BG,DF}}}{I(\lambda)_{\text{BG,BF}}} \quad (10)$$

where $I(\lambda)_{\text{NW,DF}}$ is the intensity of a NW, measured in dark-field (DF) configuration, $I(\lambda)_{\text{BG,DF}}$ is the intensity of the background (BG) of the sample without a NW, measured in dark-field configuration, and $I(\lambda)_{\text{BG,BF}}$ is the intensity of the light source, measured in bright-field (BF) configuration. Throughout this paper, we only show the normalized $I(\lambda)_{\text{normalized}}$ spectra.

Analytical Mie Calculations. For the calculation of efficiencies, Q_{sca} and Q_{abs} using Mie theory, the following assumptions are made: The SiNWs are approximated by infinitely long cylinders with diameter d. These cylinders are assumed to be surrounded by air, which means that the surrounding medium is modeled as being nonabsorbing assuming a refractive index of $n = 1$. The SiNWs themselves are assumed to be composed of pure, undoped silicon with the complex refractive index $\hat{n} = n + ik$ known for bulk silicon as plotted in Figure 1. Here n is the real part of the refractive index, k the extinction coefficient, and i the imaginary number. Values guiding the curve in Figure 1 for the complex refractive index are taken from ref 24.

The parameters that are varied for the Mie calculations are the diameter d of the SiNWs, the wavelength λ, the polarization, and the angle of incidence ξ (*cf.* inset in Figure 1) of the illuminating light. In this paper, efficiencies Q for diameters d ranging from 2 to 2000 nm are calculated. For the smallest diameters ($d < 5$ nm), quantum confinement effects are likely to occur.[34] This of course changes the complex refractive index $\hat{n}$ of the SiNWs and thus the scattering and absorption efficiencies Q_{sca} and Q_{abs}. Our calculations do not account for quantum confinement effects. Therefore, calculations for SiNWs with diameters down to 5 nm can be done. However, the calculated efficiencies Q for $d < 5$ nm SiNWs based on the bulk refractive index data can be used to assess the influence of quantum confinement on the optical properties of these very thin SiNWs by comparing the measured values with the calculated ones. Furthermore, the calculated efficiencies Q can be used as a first approximation even for these very thin SiNWs.

The angle of incidence ξ is the angle between the long axis of the SiNW and the illuminating light, as schematically shown in the inset of Figure 1. The extreme cases are (i) perpendicular illumination, $\xi = 90°$, which means that the SiNWs are lying flat on an anticipated support/substrate while light is shining on the surface of this substrate perpendicularly, and (ii) parallel illumination, $\xi = 0°$, which means that the SiNWs are again lying on that support while the light is incident parallel to the SiNWs long axes. The latter extreme case ($\xi = 0°$) cannot be calculated in the framework of Mie theory because this case would imply that the top or buttom area of the SiNWs has to be considered. Since infinitely long SiNWs are assumed for the Mie calculations, the top and bottom areas are not considered and it is not possible to calculate the efficiencies for $\xi = 0°$ exactly but only for small angles of incidence ξ. In this paper, we restrict ourselves to a minimum angle of $\xi = 1°$.

The efficiencies of both absorption and scattering are first calculated for TE and TM polarized light. The corresponding efficiencies for nonpolarized light Q_{nonpol} can be calculated by averaging over the respective efficiencies for TM and TE polarized lights Q_{TM} and Q_{TE}:

$$Q_{nonpol} = \frac{1}{2}(Q_{TM} + Q_{TE}) \quad (11)$$

Acknowledgment. We thank F. Jahn for the scanning force microscopy measurements. Funding by the European Commission through the state of Thuringia within the project EFRE-SiFafl and ROD-SOL (FP7-NMP-227497) is gratefully acknowledged.

REFERENCES AND NOTES

1. Cui, Y.; Wei, Q.; Park, H.; Lieber, C. M. Nanowire Nanosensors for Highly Sensitive and Selective Detection of Biological and Chemical Species. *Science* **2001**, *293*, 1289–1292.
2. Cui, Y.; Zhong, Z.; Wang, D.; Wang, W. U.; Lieber, C. M. High Performance Silicon Nanowire Field Effect Transistors. *Nano Lett.* **2003**, *3*, 149–152.
3. Sivakov, V.; Andrä, G.; Gawlik, A.; Berger, A.; Plentz, J.; Falk, F.; Christiansen, S. H. Silicon Nanowire-Based Solar Cells on Glass: Synthesis, Optical Properties, and Cell Parameters. *Nano Lett.* **2009**, *9*, 1549–1554.
4. Kayes, B. M.; Atwater, H. A.; Lewis, N. S. Comparison of the Device Physics Principles of Planar and Radial p−n Junction Nanorod Solar Cells. *J. Appl. Phys.* **2005**, *97*, 114302–114312.
5. Tian, B.; Zheng, X.; Kempa, T. J.; Fang, Y.; Yu, N.; Yu, G.; Huang, J.; Lieber, C. M. Coaxial Silicon Nanowires as Solar Cells and Nanoelectronic Power Sources. *Nature* **2007**, *449*, 885–889.
6. Tsakalakos, L.; Balch, J.; Fronheiser, J.; Korevaar, B. A.; Sulima, O.; Rand, J. Silicon Nanowire Solar Cells. *Appl. Phys. Lett.* **2007**, *91*, 233117–233119.
7. Fang, H.; Li, X.; Song, S.; Xu, Y.; Zhu, J. Fabrication of Slantingly-Aligned Silicon Nanowire Arrays for Solar Cell Applications. *Nanotechnology* **2008**, *19*, 255703–255708.
8. Zhang, A.; You, S.; Soci, C.; Liu, Y.; Wang, D.; Lo, Y.-H. Silicon Nanowire Detectors Showing Phototransistive Gain. *Appl. Phys. Lett.* **2008**, *93*, 121110–121112.
9. Servati, P.; Colli, A.; Hofmann, S.; Fu, Y. Q.; Beecher, P.; Durrani, Z. A. K.; Ferrari, A. C.; Flewitt, A. J.; Robertson, J.; Milne, W. I. Scalable Silicon Nanowire Photodetectors. *Physica E* **2007**, *38*, 64–66.
10. Street, R. A.; Wong, W. S.; Paulson, C. Analytic Model for Diffuse Reflectivity of Silicon Nanowire Mats. *Nano Lett.* **2009**, *9*, 3494–3497.
11. Tsakalakos, L.; Balch, J.; Fronheiser, J.; Shih, M.-Y.; LeBoeuf, S. F.; Pietrzykowski, M.; Codella, P. J.; Korevaar, B. A.; Sulima, O. V.; Rand, J.; *et al.* Strong Broadband Optical Absorption in Silicon Nanowire Films. *J. Nanophotonics* **2007**, *1*, 013552–013561.
12. Muskens, O. L.; Borgstrom, M. T.; Bakkers, E. P. A. M.; Rivas, J. G. Giant Optical Birefringence in Ensembles of Semiconductor Nanowires. *Appl. Phys. Lett.* **2006**, *89*, 233117–233119.
13. Muskens, O. L.; Diedenhofen, S. L.; Kaas, B. C.; Algra, R. E.; Bakkers, E. P. A. M.; Gomez Rivas, J.; Lagendijk, A. Large Photonic Strength of Highly Tunable Resonant Nanowire Materials. *Nano Lett.* **2009**, *9*, 930–934.
14. Muskens, O. L.; Diedenhofen, S. L.; van Weert, M. H. M.; Borgström, M. T.; Bakkers, E. P. A. M.; Rivas, J. G. Epitaxial Growth of Aligned Semiconductor Nanowire Metamaterials for Photonic Applications. *Adv. Funct. Mater.* **2008**, *18*, 1039–1046.
15. Muskens, O. L.; Rivas, J. G.; Algra, R. E.; Bakkers, E. P. A. M.; Lagendijk, A. Design of Light Scattering in Nanowire Materials for Photovoltaic Applications. *Nano Lett.* **2008**, *8*, 2638–2642.
16. Bohren, C. F.; Huffman, D. R. *Absorption and Scattering of Light by Small Particles*; Wiley-VCH: Berlin, 1998.
17. Protasenko, V.; Hull, K.; Kuno, M. Disorder-Induced Optical Heterogeneity in Single CdSe Nanowires. *Adv. Mater.* **2005**, *17*, 2942–2949.
18. Protasenko, V.; Bacinello, D.; Kuno, M. Experimental Determination of the Absorption Cross-Section and Molar Extinction Coefficient of CdSe and CdTe Nanowires. *J. Phys. Chem. B* **2006**, *110*, 25322–25331.
19. Giblin, J.; Protasenko, V.; Kuno, M. Wavelength Sensitivity of Single Nanowire Excitation Polarization Anisotropies Explained through a Generalized Treatment of Their Linear Absorption. *ACS Nano* **2009**, *3*, 1979–1987.
20. Giblin, J.; Syed, M.; Banning, M. T.; Kuno, M.; Hartland, G. Experimental Determination of Single CdSe Nanowire Absorption Cross Sections through Photothermal Imaging. *ACS Nano* **2010**, *4*, 358–364.
21. Cao, L.; White, J. S.; Park, J.-S.; Schuller, J. A.; Clemens, B. M.; Brongersma, M. L. Engineering Light Absorption in Semiconductor Nanowire Devices. *Nat. Mater.* **2009**, *8*, 643–647.
22. Aspnes, D. E.; Studna, A. A. Dielectric Functions and Optical Parameters of Si, Ge, GaP, GaAs, GaSb, InP, InAs, and InSb from 1.5 to 6.0 eV. *Phys. Rev. B* **1983**, *27*, 985–1009.
23. Cao, L.; Fan, P.; Vasudev, A. P.; White, J. S.; Yu, Z.; Cai, W.; Schuller, J. A.; Fan, S.; Brongersma, M. L. Semiconductor Nanowire Optical Antenna Solar Absorbers. *Nano Lett.* **2010**, *10*, 439–445.
24. *Handbook of Optical Constants of Solids III*; Palik, E. D., Ed.; Academic Press: New York, 1998.
25. Phillips, J. C. Band Structure of Silicon, Germanium, and Related Semiconductors. *Phys. Rev.* **1962**, *125*, 1931–1936.
26. Nichol, J. M.; Hemesath, E. R.; Lauhon, L. J.; Budakian, R. Displacement Detection of Silicon Nanowires by Polarization-Enhanced Fiber-Optic Interferometry. *Appl. Phys. Lett.* **2008**, *93*, 193110–193112.
27. Lauhon, L. J.; Gudiksen, M. S.; Wang, D.; Lieber, C. M. Epitaxial Core−Shell and Core−Multishell Nanowire Heterostructures. *Nature* **2002**, *420*, 57–61.
28. Kimukin, I.; Islam, M. S.; Williams, R. S. Surface Depletion Thickness of p-Doped Silicon Nanowires Grown Using Metal-Catalysed Chemical Vapour Deposition. *Nanotechnology* **2006**, *17*, S240–S245.
29. Macfarlane, G. G.; McLean, T. P.; Quarrington, J. E.; Roberts, V. Fine Structure in the Absorption-Edge Spectrum of Si. *Phys. Rev.* **1958**, *111*, 1245–1254.
30. Wagner, R. S.; Ellis, W. C. Vapor−Liquid−Solid Mechansim of Single Crystal Growth. *Appl. Phys. Lett.* **1964**, *4*, 89–90.
31. http://www.britishbiocell.co.uk/.
32. Cui, Y.; Lauhon, L. J.; Gudiksen, M. S.; Wang, J.; Lieber, C. M. Diameter-Controlled Synthesis of Single-Crystal Silicon Nanowires. *Appl. Phys. Lett.* **2001**, *78*, 2214–2216.
33. Oehler, F.; Gentile, P.; Baron, T.; Ferret, P. The Effects of HCl on Silicon Nanowire Growth: Surface Chlorination and Existence of a 'Diffusion-Limited Minimum Diameter'. *Nanotechnology* **2009**, *20*, 475307–475312.
34. Ma, D. D. D.; Lee, C. S.; Au, F. C. K.; Tong, S. Y.; Lee, S. T. Small-Diameter Silicon Nanowire Surfaces. *Science* **2003**, *299*, 1874–1877.

6.1.2 A precise optical determination of nanoscale diameters of semiconductor nanowires [CL2]

Gerald, Brönstrup:	Konzeptentwicklung Berechnungen und Evaluierung der Daten Diskussion des Konzepts und der Ergebnisse Diskussion und Korrektur des Manuskripts
Christian, Leiterer:	Messungen und Evaluierung der Daten Diskussion des Konzepts und der Ergebnisse Diskussion und Korrektur des Manuskripts
Norbert, Jahr:	Diskussion und Korrektur des Manuskripts
Christoph, Gutsche:	Herstellung der Nanodrähte Diskussion und Korrektur des Manuskripts
Andrey, Lysov:	Diskussion und Korrektur des Manuskripts
Ingo, Regolin:	Diskussion und Korrektur des Manuskripts
Werner Prost:	Diskussion und Korrektur des Manuskripts
Franz-Josef Tegude:	Diskussion und Korrektur des Manuskripts
Wolfgang, Fritzsche:	Diskussion und Korrektur des Manuskripts
Silke, Christiansen:	Diskussion und Korrektur des Manuskripts

Nanotechnology, **2011**, 22, 38, 385201

IOP Publishing Nanotechnology
Nanotechnology **22** (2011) 385201 (9pp) doi:10.1088/0957-4484/22/38/385201

A precise optical determination of nanoscale diameters of semiconductor nanowires

G Brönstrup[1,4], C Leiterer[2], N Jahr[2], C Gutsche[3], A Lysov[3], I Regolin[3], W Prost[3], F J Tegude[3], W Fritzsche[2] and S Christiansen[1,4]

[1] Max Planck Institute for the Science of Light, 91058 Erlangen, Germany
[2] Nanobiophotonics, Institute of Photonic Technology Jena, 07745 Jena, Germany
[3] Department of Solid State Electronics and CeNIDE, University of Duisburg-Essen, 47057 Duisburg, Germany
[4] Semiconductor Nanostructures, Institute of Photonic Technology Jena, 07745 Jena, Germany

E-mail: gerald.broenstrup@gmail.com

Received 6 April 2011, in final form 12 July 2011
Published 26 August 2011
Online at stacks.iop.org/Nano/22/385201

Abstract
Electrical and optical properties of semiconducting nanowires (NWs) strongly depend on their diameters. Therefore, a precise knowledge of their diameters is essential for any kind of device integration. Here, we present an optical method based on dark field optical microscopy to easily determine the diameters of individual NWs with an accuracy of a few nanometers and thus a relative error of less than 10%. The underlying physical principle of this method is that strong Mie resonances dominate the optical scattering spectra of most semiconducting NWs and can thus be exploited. The feasibility of this method is demonstrated using GaAs NWs but it should be applicable to most types of semiconducting NWs as well. Dark field optical microscopy shows that even slight tapering of the NWs, i.e. diameter variations of a few nanometers, can be detected by a visible color change. Abrupt diameter changes of a few nanometers, as they occur for example when growth conditions vary, can be determined as well. In addition a profound analysis of the elastic scattering properties of individual GaAs NWs is presented theoretically using Mie calculations as well as experimentally by dark field microscopy. This method has the advantage that no vacuum technique is needed, a fast and reliable analysis is possible based on cheap standard hardware.

(Some figures in this article are in colour only in the electronic version)

Introduction

The diameter of a semiconductor nanowire (NW) plays an important role since it influences its optical [1–8] and electrical [9–11] properties substantially. Moreover, electrical and optical properties of NWs are influenced by tapering due to the shape change. Tapering in addition points toward a change in dopant concentrations between top and bottom of the NWs [12]. Two competing doping mechanisms exist: (i) dopant incorporation through the liquid catalyst via the vapor–liquid–solid (VLS) [13] growth mechanism and doping via the NW side walls via a vapor–solid (VS) mechanism [14, 12, 15]. Following these arguments, a tapered NW geometry is related to the VS doping mechanism that results in an essentially underdoped NW core and a highly doped NW shell [12]. To assess the electrical and optical properties of NWs for future device integration a cheap, easy and reliable method is needed to determine the diameters and tapering of individual NWs even *in situ* during growth.

Here, we present such a method based on the optical analysis of the elastic scattering of light of individual NWs. The light scattering of semiconducting NWs is defined by strong Mie resonances, which are very sensitive to the polarization and the wavelength of the illuminating light as well as to the NW diameters. The dependence of scattering on the latter permits an accurate optical determination of NW

diameters with a resolution which is even hard to achieve with a scanning electron microscope (SEM), i.e. in the <10 nm range. In contrast to SEM and atomic force microscope (AFM) based NW diameter determination, the advantage of this approach is its fast (compared to an AFM) and reliable performance and the fact that no vacuum is required (as for the SEM). Concerning the passive optical properties of NWs, such as elastic scattering or absorption of light, papers have been published for individual indirect semiconductor silicon [2, 8] and germanium NWs [3]. Ensembles of direct semiconductor NWs show that direct semiconductor NWs show strong Mie resonances as well [4, 5]. We rely on this fact when proving the applicability of our optical method to determine nanoscale NW diameters of direct and indirect semiconductors. We take GaAs NWs as an example. GaAs itself is a technologically important direct semiconductor for optoelectronic applications and GaAs NW based light-emitting diodes have already been realized [16] or even GaAs NW based solar cells [17, 18]. Therefore, a knowledge of the elastic scattering of individual GaAs NWs of different diameters and potential tapering might be useful for their integration in novel nanoscale optoelectronic devices. To clarify the underlying physics of the presented optical method to determine nanoscale NW diameter we describe the analytical calculation of diameter dependent NW scattering spectra. Moreover, both measured scattering spectra of individual GaAs NWs as well as the results of the theoretical Mie calculations will be shown. By comparing the optically determined diameters of flatly lying GaAs NWs to AFM measurements of their height, the nanoscale resolution of this optical method and the feasibility to detect even very small diameter changes (~10 nm) along the NW axis (as they occur during tapering or can intentionally and abruptly be included by an abrupt change in growth parameters) is proven.

For both cases of diameter changes, abrupt or tapered, a visualization by a change in color in an optical microscope is possible which is based on shifts in the Mie resonances along the long axis of the NWs. Though we restrict ourselves in this paper to GaAs NWs, the described technique to determine NW diameters can easily be applied to different semiconductor NWs as well.

1. Experiments

1.1. Basic principles of optical determination of NW diameters

The underlying physical principle of the proposed optical method to determine the diameters of semiconductor NWs relies on a sensitive change in resonant scattering at nanoscale varying diameters. Experimentally obtained scattering spectra for individual NWs are compared to Mie calculated scattering efficiencies of NWs and fitting is used such that the diameters of the NWs are adjustable fit parameters. Thus, it is possible to determine the NW diameters with nanoscale accuracy.

1.2. Mie calculations

To describe the passive elastic light scattering of individual NWs with diameters smaller than the wavelength of the illuminating light the Maxwell equations have to be solved. This can be done analytically using the well known Mie theory [19]. Based on this theory the scattering efficiencies Q_{sca} of these nanostructures can be calculated. These scattering efficiencies Q_{sca} are dependent on the polarization, the wavelength λ, and on the angle of incidence ξ (compare with figure 2) of the illuminating light. Since it has been shown that the influence of the angle of incidence ξ is rather weak [1] we can limit the calculations to illumination perpendicular to the wires long axis $\xi = 90°$, i.e. the NWs are lying flat on the substrate and are illuminated directly from above. Three different polarizations of the incident light have been analyzed regarding the suitability to determine the NW diameters. In the first case, the light was linearly polarized with the electric field vector lying parallel and the magnetic field vector lying perpendicular to the NWs' long axis (cf figure 2), i.e. the so-called transversal magnetic (TM) polarization [19]. In the second case, the light was also linearly polarized but the polarization was rotated by 90°, i.e. the magnetic field vector was parallel to the NWs' long axis while the electric field vector was perpendicular to the NWs' long axis, i.e. the so-called transversal electric (TE) polarization [19] was applied. In the third case, the light was non-polarized. For the calculations of the scattering efficiencies we assumed that the NWs were well separated, that they were infinitely long compared to the wavelength λ and that they were surrounded by a non-absorbing medium with a refractive index equal to one (like air). The latter is only an approximation to the spectra discussed in this paper since the NWs are lying on a supporting glass substrate. It has been proven experimentally for silicon and germanium NWs that the approximation of infinite length is justified for NWs that have lengths of a few microns [2, 3, 8], while the substrate has some effect on the scattering of light by semiconducting NWs [2], however, this has not been considered in the calculations. Thus, it has been speculated that small deviations of experimentally measured scattering spectra of silicon NWs from calculated scattering cross sections occurred due to the influence of the substrate that was not considered [8]. For the complex refractive index, the bulk values of the particular semiconductor, in this work GaAs [20], can be used. The same calculations can easily be carried out for all kinds of NW materials simply by changing to the particular complex refractive index. For the sake of completeness we state the well known equations to calculate the scattering efficiencies Q_{sca} of NWs for the special case of perpendicular illumination [19]:

$$a_i = \frac{\tilde{n} J_i(\tilde{n}x) J_i'(x) - J_i'(\tilde{n}x) J_i(x)}{\tilde{n} J_i(\tilde{n}x) H^{(1)'}_i(x) - J_i'(\tilde{n}x) H^{(1)}{}_i(x)} \quad (1)$$

$$b_i = \frac{J_i(\tilde{n}x) J_i'(x) - \tilde{n} J_i'(\tilde{n}x) J_i(x)}{J_i(\tilde{n}x) H^{(1)'}_i(x) - \tilde{n} J_i'(\tilde{n}x) H^{(1)}{}_i(x)} \quad (2)$$

$$x = \frac{2\pi}{\lambda} \frac{d}{2} \quad (3)$$

$$\tilde{n} = n + ik \quad (4)$$

$$Q_{sca,TM} = \frac{2}{x} \left[|b_0|^2 + 2 \sum_{i=1}^{\infty} |b_i|^2 \right] \quad (5)$$

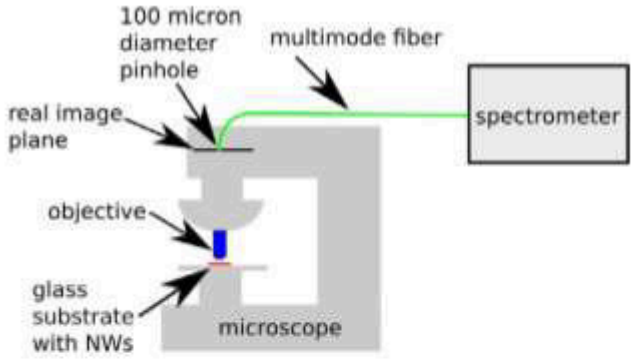

Figure 1. Schematic drawing of the experimental setup used to measure the scattering spectra of individual GaAs NWs. The image of the NWs on the glass substrate is magnified by the objective in the real image plane. In this plane a pinhole with a diameter of 100 μm is used to couple a spectrometer to the microscope with a multi mode fiber. We used an objective with a 50× magnification and thus the spatial resolution is about 100 μm/50 = 2 μm. The microscope is used in dark field configuration, so only scattered light is detected and the intensity of the background signal $I(\lambda)_{\mathrm{BG,DF}}$ from the bare glass substrate is very low.

$$Q_{\mathrm{sca,TE}} = \frac{2}{x}\left[|a_0|^2 + 2\sum_{i=1}^{\infty}|a_i|^2\right] \tag{6}$$

$$Q_{\mathrm{sca,non-pol}} = \tfrac{1}{2}(Q_{\mathrm{sca,TM}} + Q_{\mathrm{sca,TE}}). \tag{7}$$

Here $\tilde{n} = n + ik$ is the complex refractive index of the respective NW material, λ is the wavelength of the illuminating light, J_i are the Bessel functions of first kind of order i and $H^{(1)}$ are the Hankel functions of first kind of order i. $Q_{\mathrm{sca,TM}}$, $Q_{\mathrm{sca,TE}}$ and $Q_{\mathrm{sca,non-pol}}$ are the wavelength and diameter dependent scattering efficiencies for TM, TE and non-polarized light, respectively.

1.3. Sample preparation

For experimental measurements of the optical scattering behavior of individual NWs they were dispersed on a glass substrate. To remove the NWs from the growth substrate a small piece of the growth substrate was placed in a small capsule filled with purified water and the NWs broke off that substrate during sonication. The water/NW suspension of this capsule was pipetted on a specially pre-patterned glass support. The patterning of the glass support was used to identify individual NWs in different experiments. After drying of the suspension the NWs assumed a flat position on the glass support.

1.4. Scattering spectra of individual NWs measured with dark field optical microscopy and determination of their diameters

The scattering spectra of individual NWs have been taken using TM, TE and non-polarized light in an optical Axio Imager microscope (C.-Zeiss Microimaging, Göttingen, Germany) in dark field configuration with a fiber coupled spectrometer. The light source was a tungsten halogen lamp with a continuous spectrum with a color temperature of 3200 K. A linear polarizer has been installed in a way that the NWs were illuminated with polarized light. Only the scattered light was

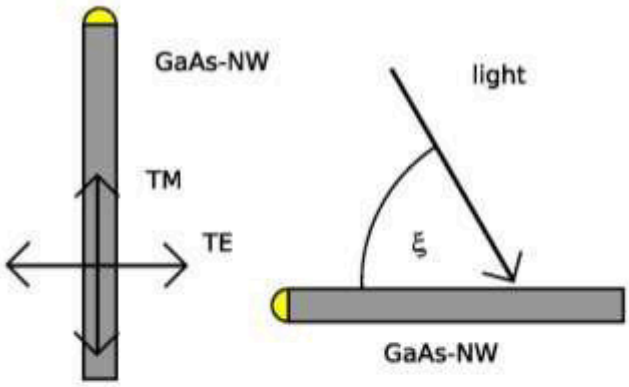

Figure 2. Schematic drawing of the GaAs NW and the incident light. Left: schematic top view, the arrows indicate the planes in which the vectors of the electric field are lying for TM and TE polarized light. Right: schematic side view, the angle of incidence ξ is shown.

detected due to the dark field configuration which blocks the directly transmitted light. This scattered light was passed through a pinhole and a multi mode fiber to an Acton Research SpectraPro 2300i micro-spectrometer (Princeton Instruments, Trenton, NJ, USA) with a grating with 150 lines and a Peltier cooled CCD camera. The pinhole was coplanar to the tube lens of the optical microscope, i.e. the pinhole was in the magnified, real image plane, and had a diameter of 100 μm (compare with figure 1). With this setup the scattered light of individual NWs was collected. These measured spectra were proportional to the product of the intensity of the illuminating lamp and the scattering efficiencies of the NWs, in addition the supporting substrate weakly scattered the light as well. To obtain scattering spectra proportional to the scattering cross sections of the NWs the spectra had to be normalized with respect to the illuminating light and the background from the glass support had to be removed:

$$I(\lambda)_{\mathrm{normalized}} = \frac{I(\lambda)_{\mathrm{NW,DF}} - I(\lambda)_{\mathrm{BG,DF}}}{I(\lambda)_{\mathrm{BG,BF}}} \tag{8}$$

$I(\lambda)_{\mathrm{NW,DF}}$ is the intensity of a GaAs NW, measured in dark field (DF) configuration, $I(\lambda)_{\mathrm{BG,DF}}$ is the intensity of the background (BG) of the glass support without a NW, measured in dark field configuration and $I(\lambda)_{\mathrm{BG,BF}}$ is the intensity of the light source, measured in bright field (BF) configuration. Throughout this paper only the normalized spectra $I(\lambda)_{\mathrm{normalized}}$ are shown. All these quantities were taken for all three polarizations which are discussed in this paper: TM, TE and non-polarized light. The experimentally obtained and normalized scattering spectra $I(\lambda)_{\mathrm{normalized}}$ are proportional to the scattering efficiencies of individual NWs. Therefore a fit to the calculated scattering efficiencies Q_{sca} was carried out:

$$I(\lambda)_{\mathrm{normalized}} = A\,Q_{\mathrm{sca}} \tag{9}$$

'A' is a scaling constant which is necessary because not the total scattering cross section has experimentally been measured but only the relative dependence on the wavelength λ of the illuminating light. In this work the fit was carried out with a Levenberg–Marquardt solver [21]. To get a reasonable

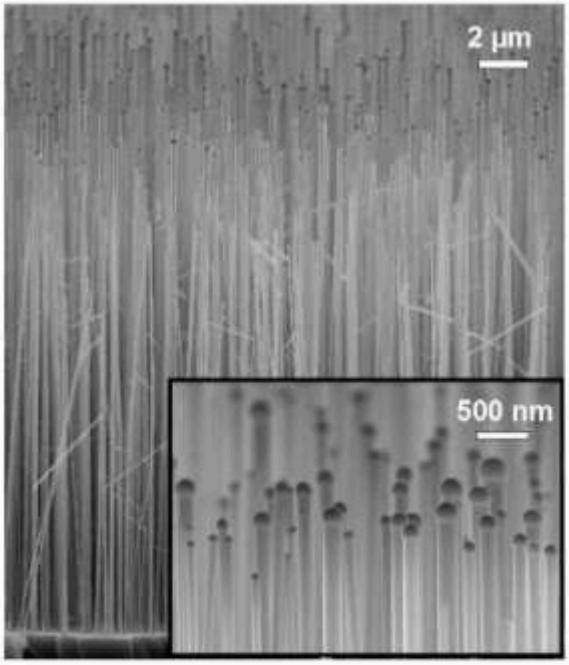

Figure 3. SEM image of the straight as-grown GaAs NWs on (111)B GaAs substrates (first sample, grown at 400 °C). The inset shows a zoom in on the NW tips, here the gold catalyst on top of each VLS grown NW is clearly visible.

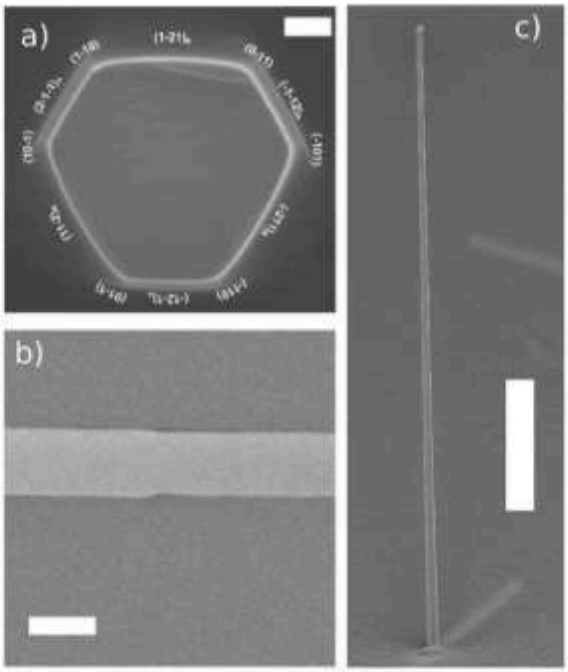

Figure 4. SEM images of the examined GaAs NWs. The scale bars represent 100 nm for (a) and (b) and 3 μm for (c). (a) Top view of a GaAs NW cross section (first sample, grown at 400 °C, see also figure 3), revealing a hexagonal shape. (b) GaAs NW showing a step-like change in the diameter, due to a change of the Ga flow during growth (second sample, grown at 400 °C). (c) GaAs NW showing tapering (third sample, grown at 450 °C): the diameter at the bottom is larger than at the tip.

result the fit was carried out with different starting values, i.e. with different values for the diameters of the NWs and the scaling constant A. The fit with the least square error was automatically picked and the diameter of the NW was consequently extracted as a parameter of that fit.

1.5. AFM height measurements on flatly lying NWs that provide the NW diameters

To prove the accuracy of the NW diameter detection of our described optical method, NW diameters were also determined with an AFM. The measurements were performed on the flatly lying NWs on the glass support after sonication off the growth substrate. It was assumed that the heights of the lying NWs are equal to their diameters. The error of these measurements can roughly be estimated to be around ± 3 nm mainly due to the roughness of the glass substrate and the resolution of the used AFM setup. By use of markers on the pre-patterned glass substrate AFM measurements and optical measurements of identical NWs could be carried out.

1.6. GaAs NW growth

For this study we used GaAs NWs grown by the vapor–liquid–solid (VLS) [13] mechanism on (111)B GaAs wafers. On these wafers the GaAs NWs grow straight and perpendicular to the substrate surface. Non-intentionally doped NWs were realized by metal–organic vapor-phase (MOVPE) epitaxy in an AIX200 radiofrequency (RF) system with a fully non-gaseous source configuration. The NW growth is catalyzed by gold (Au) dots that form upon annealing of a thin, evaporated Au layer of nominally 2.5 nm thickness. The annealing step was carried out at 500 °C for 3 min under As overpressure and resulted in a high density of gold dots with distributed diameters ranging from 30 nm to some 100 nm. GaAs NWs were grown at a total pressure of 50 mbar, using trimethylgallium (TMGa) and tertiarybutylarsine (TBAs) as liquid precursors with a constant V/III ratio of 2.5. The total gas flow of 3.4 l min^{-1} was provided by N_2 as carrier gas, while H_2 was used for the bubblers. Growth was initiated at 450 °C for 3 min followed by a final growth temperature of 400 °C, to obtain untapered wires (compare with figure 3). After 20 min of growth the GaAs NWs were about 13 μm long at diameters between 30 and a few 100 nm (compare with inset in figure 3). A cross sectional cut through a NW as shown in figure 4(a), reveals their faceted and hexagonal shape.

A second sample was grown with GaAs NWs that showed a small and abrupt diameter change along the NW growth axis due to a change in growth conditions (changing the gas composition, i.e. the V/III ratio, during the MOVPE process). The initial GaAs NW segment was grown for 20 min with similar parameters as those for the first sample. The second part was grown for 25 min with a decreased Ga flow leading to a doubled V/III ratio of 5.0 and hence a smaller diameter of the seed particle and upper NW segment, respectively (compare with figure 4(b)). The overall length of these GaAs NWs was about 23 μm.

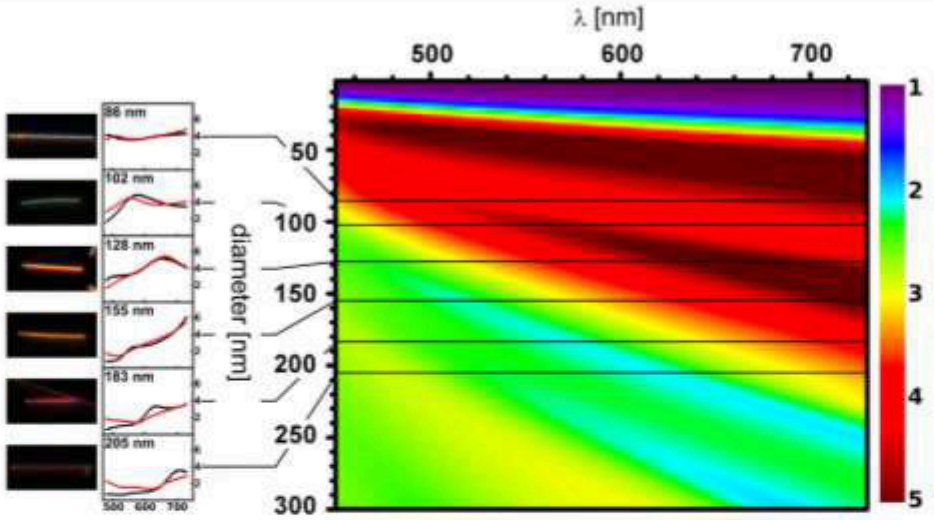

Figure 5. Optical scattering properties of GaAs NWs for TM polarized light. In the left column pictures of individual GaAs NWs, taken with an optical microscope in dark field configuration, are shown. The calculated scattering efficiencies Q_{sca} (red lines) and scaled measured spectra (black lines) are plotted in the middle column. The diameters used to calculate the scattering efficiencies Q_{sca} are stated. They were obtained from the fits of the optical spectra. For diameters smaller than 90 nm the spectra taken with TM polarized light have been used to optically determine the diameters and for diameters larger than 90 nm the spectra taken with TE polarized light have been used for this purpose. On the x-axis the wavelength λ of the illuminating light is given in nanometers. The large plot on the right shows color coded calculated scattering efficiencies Q_{sca} for non-polarized light at normal incidence ($\xi = 90°$) for d = [2 nm, 300 nm] and λ = [450 nm, 730 nm]. The solid black lines indicate the positions of the measured spectra. The color scale on the right side shows the scattering efficiencies Q_{sca}.

The third sample was synthesized using gold particles with diameters of 50 and 100 nm from a colloidal solution, which leads into a drastically decreased NW density. Moreover, the growth temperature was increased to 450 °C. In this case the NW diameters are larger at their re-entrant corner to the substrate compared to their tips (tapering) (compare with figure 4(c)) [22], an effect ascribed to a kinetically enhanced growth rate of the material along the NW sidewalls [23].

2. Results and discussion

2.1. Calculated scattering efficiencies using Mie theory

The calculated scattering efficiencies exhibit a strong dependence on the diameter of the NWs and on the wavelength λ and the polarization of the illuminating light (compare with figures 5–7) as already reported for different indirect semiconducting NWs [2, 3, 8]. On the one hand this strong dependence of the light scattering on the diameter is the physical basis for the optical determination of NW diameters. On the other hand it also shows the potential to tune the light scattering of GaAs NWs to certain wavelengths. The scattering efficiencies for TE polarized light are in general lower than those for TM polarized light (compare with right columns of figures 5 and 6). This is not a special case for GaAs NWs but a common behavior of many semiconducting NWs [2, 4, 5, 8]. There are certain branches of high scattering efficiencies visible in the (λ, d)-plane. These branches are the so-called Mie resonances which are also a common feature of the scattering properties of many semiconducting NWs. Their positions in the (λ, d)-plane have been quantitatively reported for silicon NWs [8]. For GaAs NWs the first of these branches begins at diameters as small as 20 nm (compare with figure 5), i.e. for GaAs NWs that are slightly thicker than those showing quantum confinement effects (QCEs) [24]. Furthermore, the wavelength sensitive light scattering of GaAs NWs occurs not only for wavelengths corresponding to photon energies smaller than the energy of the direct band gap of GaAs, i.e. at wavelengths larger than ~870 nm (not shown) but also for wavelengths down to ~450 nm (compare with figures 5–7). This is different compared to e.g. silicon NWs [2], which only show wavelength sensitive light scattering for wavelengths larger than ~360 nm [8], corresponding to the smallest direct gap of silicon (see e.g. [25]).

2.2. Experimental scattering spectra and optical determination of NW diameters

The scattering spectra of untapered NWs (cf figure 3) were analyzed as described above by fitting the measured optical spectra to the scaled scattering efficiencies of individual GaAs NWs using equation (9). To control the results of the optically obtained diameters they have also been determined with an AFM by measuring the heights of the flatly lying NWs on glass supports (see section 1.5). For diameters larger than ~90 nm the fits for the TE polarization have been much better than those for the TM polarization. The deviations from the theory are probably due to the supporting glass substrate, which was not considered in the calculations. It has already been shown for silicon NWs, that different substrates can lead to different scattering behavior and thus to different colors [2]. An explanation for the lower disturbance by the glass substrate

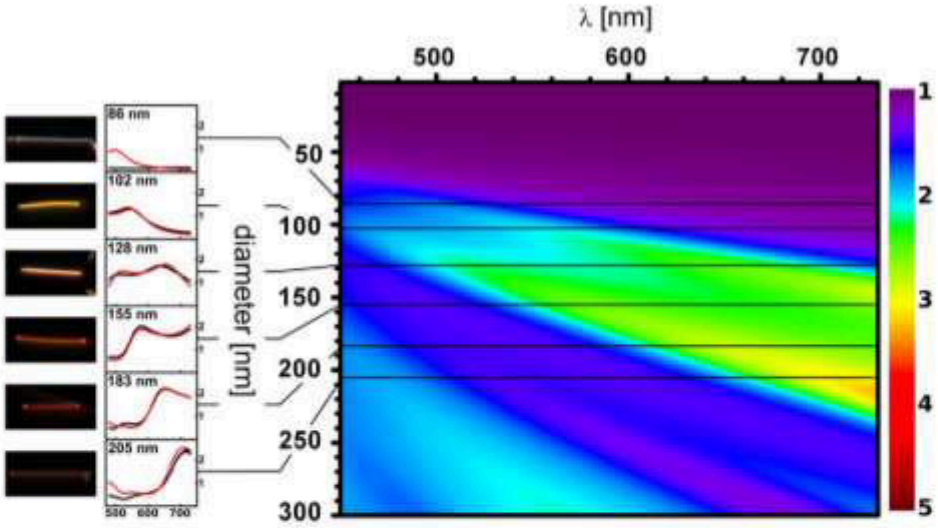

Figure 6. Analogue values are plotted as in figure 5 for TE polarized light.

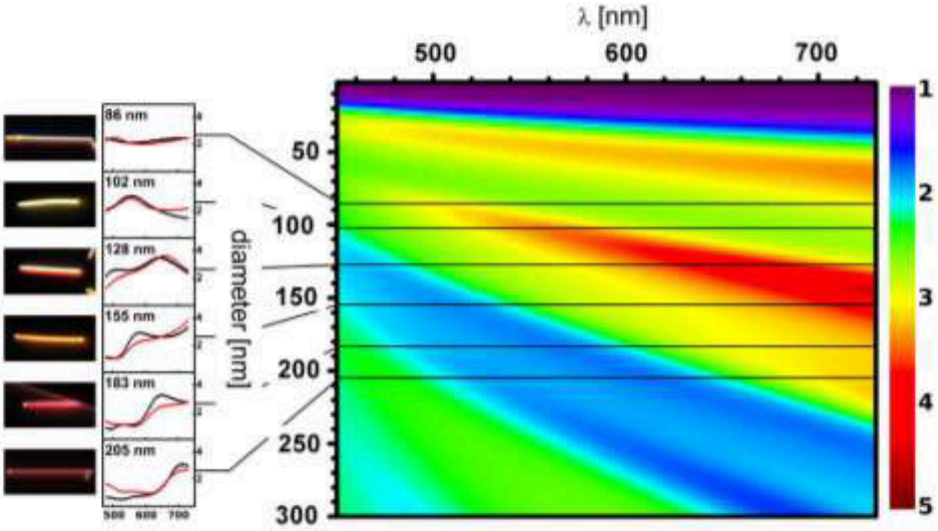

Figure 7. Analogue values are plotted as in figure 5 for non-polarized light.

of the scattering efficiencies for TE polarized light could be a disproportionately high increase of the effects of the substrate with the scattering efficiencies of the NWs.

For the analyzed GaAs NW with a diameter less than ~90 nm it was not possible to use the scattering spectra taken with TE polarized light because the scattering efficiencies are close to zero and do not show any pronounced structure (compare with right column of figure 6). However, for this GaAs NW, the diameter could be optically determined from spectra taken with TM polarized light. The diameters obtained from the fits of the optical spectra are listed in table 1. Only the diameters obtained with the appropriate polarization are shown, i.e. TM polarization for $d \leqslant 90$ nm and TE polarization for $d > 90$ nm. For the other polarizations these diameters were taken to calculate the corresponding scattering efficiencies and are only shown for comparison

Table 1. Diameters of the GaAs NWs. The optically determined diameters are printed in the first row, the diameters of the same NWs obtained by AFM height measurements are printed in the second row. In the third row are the absolute differences of both measurements.

Opt. (nm)	86	102	128	155	183	205
AFM (nm)	83	106	136	167	194	220
$\lvert\Delta\rvert$ (nm)	3	4	8	12	11	15

(middle columns of figures 5–7). The diameters obtained by fitting to the optical spectra were typically a few nanometers smaller than those measured with an AFM (compare with table 1). This is comprehensible, since the GaAs NWs are wrapped in a thin oxide layer [26] that adds to the measured NW heights/diameters. In addition, the surface of the substrate that was used as a support for the flatly lying NWs had a roughness of a few nanometers and the geometry of the GaAs

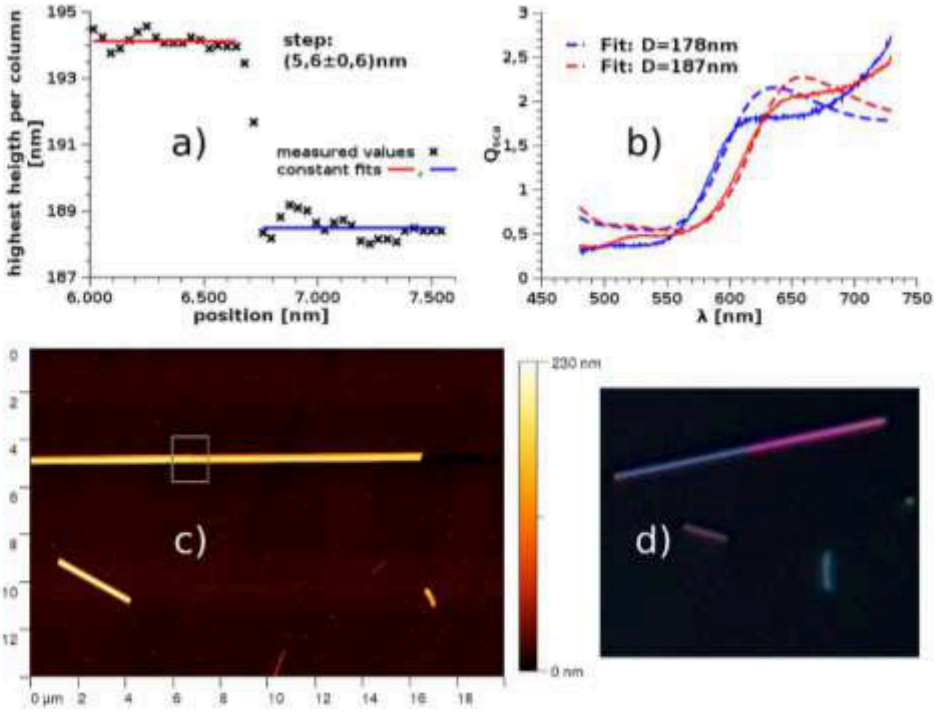

Figure 8. GaAs NWs with step (a) the highest point per column as measured with an AFM (the evaluated area is shown in (c)). (b) Normalized optical scattering spectra taken with TE polarized light and fits of both sides of the step. (c) Picture of AFM measurement, the square indicates the area used to evaluate the height of the step; highest values of each column are shown in (a). (d) Optical dark field micrograph of the same NW taken with non-polarized light, the picture is shown with artificially enhanced contrast.

NWs is not precisely a round cylinder but a slightly faceted cylinder with a hexagonal base (compare with figure 4(a)). Nonetheless it is actually possible to optically determine the diameters of GaAs NWs with a relative error of less than 10% using the presented optical method.

For further analyses of the sensitivity of our optical method, a small, abrupt diameter change was induced during growth by changing the growth conditions. The resulting diameter change in the middle of the GaAs NWs was optically determined by a change in color in the dark field optical micrograph and measured with an AFM (compare with figures 4(b) and 8). In the latter case special attention has been paid to the measurement of the actual diameter change. To reduce the error of the AFM measurements the diameter change was determined by two types of measurements: (i) measuring the NW diameters at both ends of the NWs that had seen different growth conditions and (ii) scanning the AFM tip along the NW long axis thereby directly measuring over the abrupt diameter change. The latter measurement resulted in a step of $(5,6 \pm 0,6)$ nm (as error one standard deviation is given). Assuming cylindrical symmetry, as indicated by SEM studies of the same sample (compare with figure 4(b)), this height difference is equal to the change in NW radius. Thus, the resulting diameter change is $2(5,6 \pm 0,6)$ nm $= (11,2 \pm 1,2)$ nm. Optically, we determined a value of 9 nm which would indicate a relative error of about ~20%. However, since the error of our AFM measurement is in the same order of magnitude, this is only a rough estimation and the error could be even much smaller.

The combination of measured spectra and analytical Mie calculations can not only be used to determine the diameters of the NWs but also to easily explain the different colors as visible in dark field optical microscopy. The different colors of NWs with different diameters are explained with their wavelength and polarization dependent scattering behavior (as shown in the left columns of figures 5–7). This polarization dependence of the colors is especially pronounced for the GaAs NW with a diameter of ~100 nm. This NW changes its color from blue (when illuminated with TM polarized light, compare with figure 5) to orange (when illuminated with TE polarized light, compare with figure 6).

2.3. *Tapered NWs*

All calculations regarding the optical properties of the NWs in this paper are based on the assumption that the NWs have a perfect cylindrical geometry. However, semiconductor NW VLS growth is, depending on the growth parameters, more or less superimposed by VS growth on the NW side facets which results in a tapered geometry. Therefore, we also tried to apply the described method to tapered GaAs NWs. Since already diameter changes of a few nm affect the scattering spectra significantly (compare with figures 5–7, 8(d)) it is reasonable to assume that even a small tapering of the NWs can be identified by a continuous color change. For an experimental proof, tapered GaAs NWs have been grown (figure 4(c)) and put on a glass support for optical microscopy, like the untapered NWs. In figure 9 such a tapered

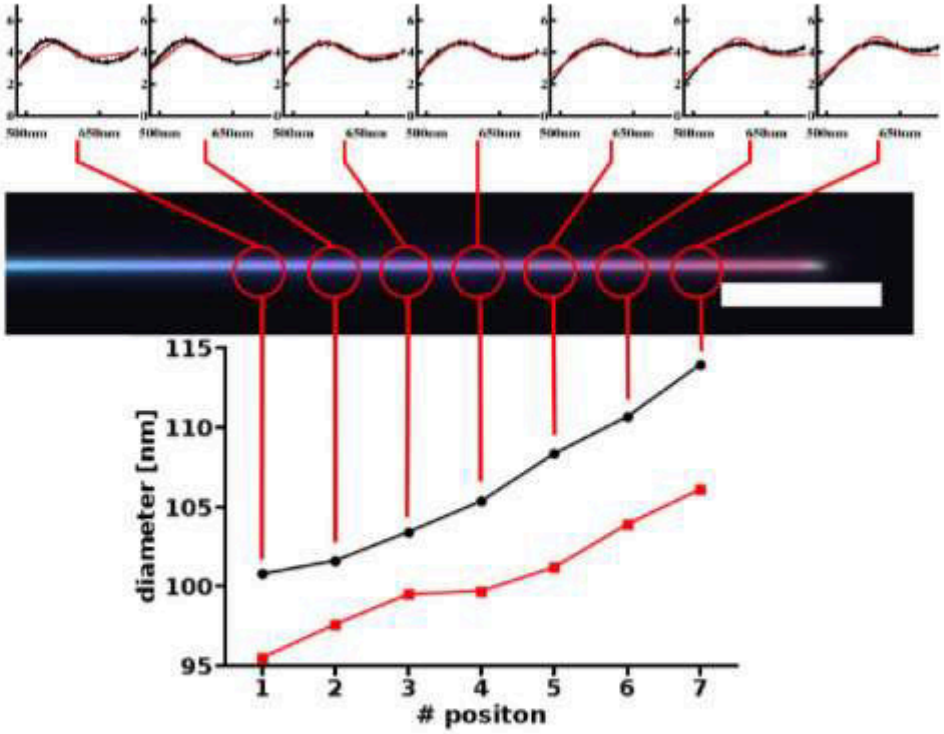

Figure 9. Tapered GaAs NW. First row: experimentally obtained normalized and scaled scattering spectra taken with TM polarized light (black) and the respective fitted values of the scattering efficiencies Q_{sca} (red) and their dependence on the wavelength λ. Second row: optical micrograph of the tapered GaAs NW taken in dark field configuration with non-polarized light. The locations where the spectra are taken are marked by red circles. The scale bar represents 4 μm. Third row: the diameters at the marked locations are displayed as obtained with an AFM (red) and by the fit of the scattering spectra (black) taken with TM polarized light. For the fits of the optical spectra, ideal cylindrical geometry of the NW has been assumed, as a first approximation.

NW is displayed along with the scattering spectra and height measurements performed with an AFM. The GaAs NW is shown as viewed in dark field configuration with an optical microscope, revealing different colors along its growth axis, which can be attributed to a change in the spectral dependence of the scattering efficiency from one end to the other. Hence, an optical microscope can provide evidence of slightly tapered NWs. Moreover, we tried to measure the diameter change along the tapered NWs using the proposed optical method. The red circles in figure 9 indicate locations where scattering spectra were experimentally taken. In this case it was only possible to obtain reasonable results using TM polarized light. The corresponding diameter values, obtained by fitting of these spectra are in good agreement with the AFM values, though they are in general ~5 nm higher. This means again a relative error of less than 10%. It has to be stressed that we have assumed a perfect cylindrical and untapered NW geometry for our calculations. Thus, it can only be considered as a rough approximation of the real geometry, which might cause the observed deviations. Nevertheless, in this case the proposed method was suitable to approximate the diameter and tapering of the GaAs NW (using TM polarized light).

3. Conclusion

A scalable method to optically determine NW diameters based on their scattering spectra has been presented and its applicability has been shown for GaAs NWs. Since the underlying physics of this method are the Mie resonances, which are a common feature of most semiconducting NWs for the wavelengths of visible light, it is not only limited to GaAs NWs but is on the contrary a technique that can be used flexibly for a great variety of NW materials. In particular, spectra taken with linear TE polarized light have been proven to account for NW diameters with less than 10% relative error. Moreover, the described optical method is even sensitive to abrupt diameter changes of only ~10 nm along the NW growth axis. Furthermore, it has been shown that slightly tapered NWs can easily be distinguished from untapered, cylindrical NWs with standard optical microscopy by their continuous color changes. Beyond this method the wavelength and polarization dependence of the scattering spectra of GaAs NWs have been discussed and the colors of individual GaAs NWs as visible in dark field microscopy have been explained.

Acknowledgments

We thank Christian Borschel from the University of Jena for establishing the contact of the different groups. Funding by the European Commission through the state of Thuringia within the project EFRE-SiFaFI and within the FP7 project ROD-SOL (FP7-NMP-227497) are gratefully acknowledged.

References

[1] Cao L, Fan P, Vasudev A P, White J S, Yu Z, Cai W, Schuller J A, Fan S and Brongersma M L 2010 Semiconductor nanowire optical antenna solar absorbers *Nano Lett.* **10** 439–45

[2] Cao L, Fan P, Barnard E S, Brown A M and Brongersma M L 2010 Tuning the color of silicon nanostructures *Nano Lett.* **10** 2649–54

[3] Cao L, White J S, Park J-S, Schuller J A, Clemens B M and Brongersma M L 2009 Engineering light absorption in semiconductor nanowire devices *Nature Mater.* **8** 643–7

[4] Muskens O L, Diedenhofen S L, Kaas B C, Algra R E, Bakkers E P A M, Gomez Rivas J and Lagendijk Ad 2009 Large photonic strength of highly tunable resonant nanowire materials *Nano Lett.* **9** 930–4

[5] Muskens O L, Gomez Rivas J, Algra R E, Bakkers E P A M and Lagendijk Ad 2008 Design of light scattering in nanowire materials for photovoltaic applications *Nano Lett.* **8** 2638–42

[6] Protasenko V, Bacinello D and Kuno M 2006 Experimental determination of the absorption cross-section and molar extinction coefficient of cdse and cdte nanowires *J. Phys. Chem.* B **110** 25322–31

[7] Giblin J, Protasenko V and Kuno M 2009 Wavelength sensitivity of single nanowire excitation polarization anisotropies explained through a generalized treatment of their linear absorption *ACS Nano* **3** 1979–87

[8] Brönstrup G, Jahr N, Leiterer C, Csáki A, Fritzsche W and Christiansen S 2010 Optical properties of individual silicon nanowires for photonic devices *ACS Nano* **4** 7113–22

[9] Xie P, Hu Y, Fang Y, Huang J and Lieber C M 2009 Diameter-dependent dopant location in silicon and germanium nanowires *Proc. Natl Acad. Sci.* **106** 15254

[10] Ford A C, Ho J C, Chueh Y L, Tseng Y C, Fan Z, Guo J, Bokor J and Javey A 2008 Diameter-dependent electron mobility of InAs nanowires *Nano Lett.* **9** 360–5

[11] Agarwal P, Vijayaraghavan M N, Neuilly F, Hijzen E and Hurkx G A M 2007 Breakdown enhancement in silicon nanowire pn junctions *Nano Lett.* **7** 896–9

[12] Perea D E, Hemesath E R, Schwalbach E J, Lensch-Falk J L, Voorhees P W and Lauhon L J 2009 Direct measurement of dopant distribution in an individual vapour–liquid–solid nanowire *Nature Nano* **4** 315–9

[13] Wagner R S and Ellis W C 1964 Vapor–liquid–solid mechansim of single crystal growth *Appl. Phys. Lett.* **4** 89–90

[14] Kolasinski K W 2006 Catalytic growth of nanowires: vapor–liquid–solid, vapor–solid–solid, solution–liquid–solid and solid–liquid–solid growth *Curr. Opin. Solid State Mater. Sci.* **10** 182–91

[15] Dufouleur J, Colombo C, Garma T, Ketterer B, Uccelli E, Nicotra M and Fontcuberta i Morral A 2010 P-doping mechanisms in catalyst-free gallium arsenide nanowires *Nano Lett.* **10** 1734–40

[16] Svensson C P T, Mårtensson T, Trägårdh J, Larsson C, Rask M, Hessman D, Samuelson L and Ohlsson J 2008 Monolithic GaAs/ingap nanowire light emitting diodes on silicon *Nanotechnology* **19** 305201

[17] Czaban J A, Thompson D A and LaPierre R R 2009 GaAs core–shell nanowires for photovoltaic applications *Nano Lett.* **9** 148–54

[18] Colombo C, Heiß M, Grätzel M and Fontcuberta i Morral A 2009 Gallium arsenide p–i–n radial structures for photovoltaic applications *Appl. Phys. Lett.* **94** 173108

[19] Bohren C F and Huffman D R 1998 *Absorption and Scattering of Light by Small Particles* (Berlin: Wiley–VCH)

[20] Aspnes D E and Studna A A 1983 Dielectric functions and optical parameters of Si, Ge, GaP, GaAs, GaSb, InP, InAs, and InSb from 1.5 to 6.0 eV *Phys. Rev.* B **27** 985

[21] Gough B 2009 *GNU Scientific Library Reference Manual* 3rd edn (Godalming: Network Theory Ltd)

[22] Paiano P, Prete P, Speiser E, Lovergine N, Richter W, Tapfer L and Mancini A M 2007 GaAs nanowires grown by Au-catalyst-assisted movpe using tertiarybutylarsine as group-V precursor *ICMOVPE XIII: 13th Int. Conf. on Metal Organic Vapor Phase Epitaxy; J. Cryst. Growth* **298** 620–4

[23] Borgström M, Deppert K, Samuelson L and Seifert W 2004 Size- and shape-controlled GaAs nano-whiskers grown by movpe: a growth study *J. Cryst. Growth* **260** 18–22

[24] Zhang G, Tateno K, Sanada H, Tawara T, Gotoh H and Nakano H 2009 Synthesis of GaAs nanowires with very small diameters and their optical properties with the radial quantum-confinement effect *Appl. Phys. Lett.* **95** 123104

[25] Phillips J C 1962 Band structure of silicon, germanium, and related semiconductors *Phys. Rev.* **125** 1931–6

[26] Tanner B K, Allwood D A and Mason N J 2001 Kinetics of native oxide film growth on epiready GaAs *Mater. Sci. Eng.* B **80** 99–103

6.1.3 Dielectrophoretic manipulation of DNA in microelectrode gaps for single-molecule constructs [CL3]

Andreas, Wolff:	Konzeptentwicklung
	Messungen und Evaluierung der Daten
	Diskussion des Konzepts und der Ergebnisse
	Diskussion und Korrektur des Manuskripts
Christian, Leiterer:	Messungen und Evaluierung der Daten
	Diskussion des Konzepts und der Ergebnisse
	Diskussion und Korrektur des Manuskripts
Andrea, Csaki:	Diskussion und Korrektur des Manuskripts
Wolfgang, Fritzsche:	Diskussion und Korrektur des Manuskripts

Froniers in Bioscience, **2008**, 13, 6834–40

Dielectrophoretic manipulation of DNA in microelectrode gaps for single-molecule constructs

Andreas Wolff, Christian Leiterer, Andrea Csaki and Wolfgang Fritzsche

Nano Biophotonics Department, Institute of Photonic Technology, Jena, Germany

TABLE OF CONTENTS

1. ABSTRACT

The construction with biomolecules and their manipulation represent a key step for developing new miniaturized structures. Such micro or nanometer systems promise a variety of novel features. Dielectrophoresis (DEP) is a powerful tool for trapping and orienting individual molecules in microelectrode arrangements, and was demonstrated to be applicable to DNA. This relatively rigid biomolecule could (after defined immobilization) act as template for further modifications and functionalizations, e.g. metallization. Parameters of the DEP process were adapted to the given electrode layout and for trapping a few or even a single DNA strand. Characterization with atomic force microscopy (AFM) extends the standard method of fluorescence imaging by resolving the resulting structures with single molecule resolution.

2. INTRODUCTION

The fabrication of novel miniaturized, functional structures for applications in micro electronic, computing or detection and biosensing are a key goal of modern nanotechnology. The realization of nanostructures using biological or biomimetic strategies is one possible approach with a huge potential regarding miniaturization and self-assembly. Promising new hybrid structures (containing e.g. nanoscale metal or magnetic structures) combine the desired functionality with molecular-scale units and offer novel electric or magnetic features with the prospect of smaller and faster circuits. Advantages are also smaller sample volumes and reduced costs.
Biomolecules like DNA, enzymes or antibodies are in the nm range and exhibit interesting properties regarding manipulation and construction. The capability to self assemble into highly ordered structures is one of their decisive features (1,2). So, it is possible to use them as building blocks for bottom up architectures together with nanoparticles or nanowires/-tubes (3-5). Such hybrid systems of nanoparticles and biomaterials provide new dimensions in the rapidly growing research field of bioelectronics and nano photonics.

A controlled handling of single molecules is essential for the fabrication and the investigation of highly defined devices based on molecules. Especially linearly stretched DNA is quite suitable for the demonstration of different applications that contain structures with nanometer addressability such as molecular electronics, real-time PCR, or single molecule sequencing. There is a variety of approaches aimed at stretching and aligning of individual DNA molecules. Most of them utilize the hydrodynamic flow, e.g. molecular combing (6-8). Optical tweezers (9) and magnetic fields (10) are also suitable for such approaches, as well as scanning force microscopy methods.
These methods are usually developed for well-defined tasks and work well in the given environment. But problems of reproducibility, accommodation to different technical surroundings and, in particular, of addressing only a few or even single molecules simultaneously are still remaining.

In order to align DNA and beside the use of an external flow, dielectrophoresis represents another interesting approach with a high potential for the defined molecular manipulation (11). It allows the separation of cells, nanoparticles and DNA as well as their manipulation in an electrical environment. It uses the fact that a polarizable particle exhibit dielectrophoretic activity in the presence of an alternating electric field.
The induced dipole can cause electrokinetic effects like rotation, deformation and orientation. In a spatially inhomogeneous field, DEP leads to the lateral movement towards the highest field strength. The force does not require the particles to be charged and depends on the medium, the polarizability, shape and size of the objects as well as on the frequency and the electric field gradient (11,12).

Washizu and coworkers were the first to demonstrate a DEP method to stretch DNA along field lines and positioned it onto electrode edges (13). They described two effects, the dielectrophoretic attraction towards the electrode gaps and the electrostatic orientation of the DNA. So in ongoing studies it was possible to determine both DNA size distribution and activities of nuclease by measuring the apparent length of stretched DNA in the micrometer range. Therefore, they used a field of $1x10^6$ V/m and a frequency of about 1 MHz between aluminium microelectrodes (14).
Application of static as well as oscillating fields make it possible to move the trapped DNA strands from one edge of a gold film to the other (15). This is quite useful for the manipulation of small quantities or molecules in microdevices.
The design of the electrodes (especially the shape) is of key importance for a defined DEP. The influence of the electrode shape on the precision of positioning DNA molecules was demonstrated (16). The prevalent electrode material is gold, microstructured on glass or silicon substrates. Quadrupole electrode geometries were investigated with gaps ranging from 3 to 100 micrometer, in order to trap DNA and proteins could be trapped and their electrical resistance could be measured (17).

This paper describes the trapping of lambda DNA by DEP with two different electrode layouts. Thereby parameters (DNA concentration, time, temperature, voltage and frequency) could be optimized semi empirical using *in situ* and real time fluorescence imaging during the trapping process by vary one of these parameters.
Beside standard fluorescence imaging, it was important to characterize the gaps with high resolution techniques like atomic force microscopy for a detailed view of the structure and the amount of the collected DNA. AFM allows for molecular resolution without the need for sample metallization, and is therefore a valuable tool for detailed characterization beyond optical resolution.
The intention is to align single DNA strands over a given electrode gap in order to provide a scaffold for subsequent steps such as nanoparticle binding and/or metallization for potential applications in nanoelectronics and biosensing.

3. MATERIALS AND METHODS

Dielectrophoresis experiments were performed on microstructured chips with a size of 12.8 x 12.8 mm. The gold electrodes of 100 nm thickness were prepared on silicon oxide substrates by sputtering and standard photolithographic lift-off processes.
The designs of the 10-micrometer-gap-chip (a 42 electrode gap array) and on the 2-micrometer-gap-chip (a 4 electrode gap array) are shown in figure 1. The microstructured chips were cleaned with acetone, water and ethanol for 10 min each and dried in a N_2 stream; a plasma cleaning step with 50 W for 10 min followed. No additionally adhesions layer for DNA immobilization was used.
The most commonly used DNA species for single molecule manipulations is linearized lambda phage DNA (lambda DNA) which is double-stranded. This macromolecule has a size of 48500 base pairs with a contour length of 16.5 micrometer when fully stretched. It combines a sufficient length with easy access due to its commercial availability and the comprehensive literature about its biophysical properties. Another investigated DNA species is single-stranded M13 DNA (18).
The lambda DNA stock solution (300 ng/ micro liter; Fermentas, St. Leon-Rot, Germany) was diluted to working solutions of 0.02 ng/ micro liter or 0.004 ng/micro liter respectively.
In order to monitor DNA movement as well as conformation, DNA can be stained with intercalating dyes like YOYO™, TOTO™, DAPI or acridine orange. For imaging the DNA during and/or after the dielectrophoresis it was stained using the fluorescence dye YOYO-1 (MoBiTec, Göttingen, Germany). The chips were covered with nearly 200 micro liter of the working solution without wetting the contact pads. The voltage was applied with a frequency generator Agilent 3320A (Agilent, Böblingen, Germany) in the range of 0.5 V up to 10 V. The used frequencies were between 1 kHz and 1 MHz for 1 to 20 min.
Fluorescence imaging was conducted using an Axiotech microscope (Carl Zeiss, Jena, Germany), equipped with a Sensicam CCD camera (PCO Computer Optics, Kehlheim, Germany) or an AxioImager A1m microscope with Axio Cam MRc5 (Carl Zeiss, Jena, Germany). All experiments were performed with an immersion objective under liquid phase conditions and room temperature. Single images or a series of images were taken during the experiments or at the end of the experiment. High-resolution topographic images were obtained in tapping mode with the scanning force microscope NanoScopeIII using a Dimension 3100 measurement head (Digital Instruments, Santa Barbara, CA) and scanning electron microscope (SEM) Joel JSM 6700 (Joel Europe, Zaventem, Belgium).

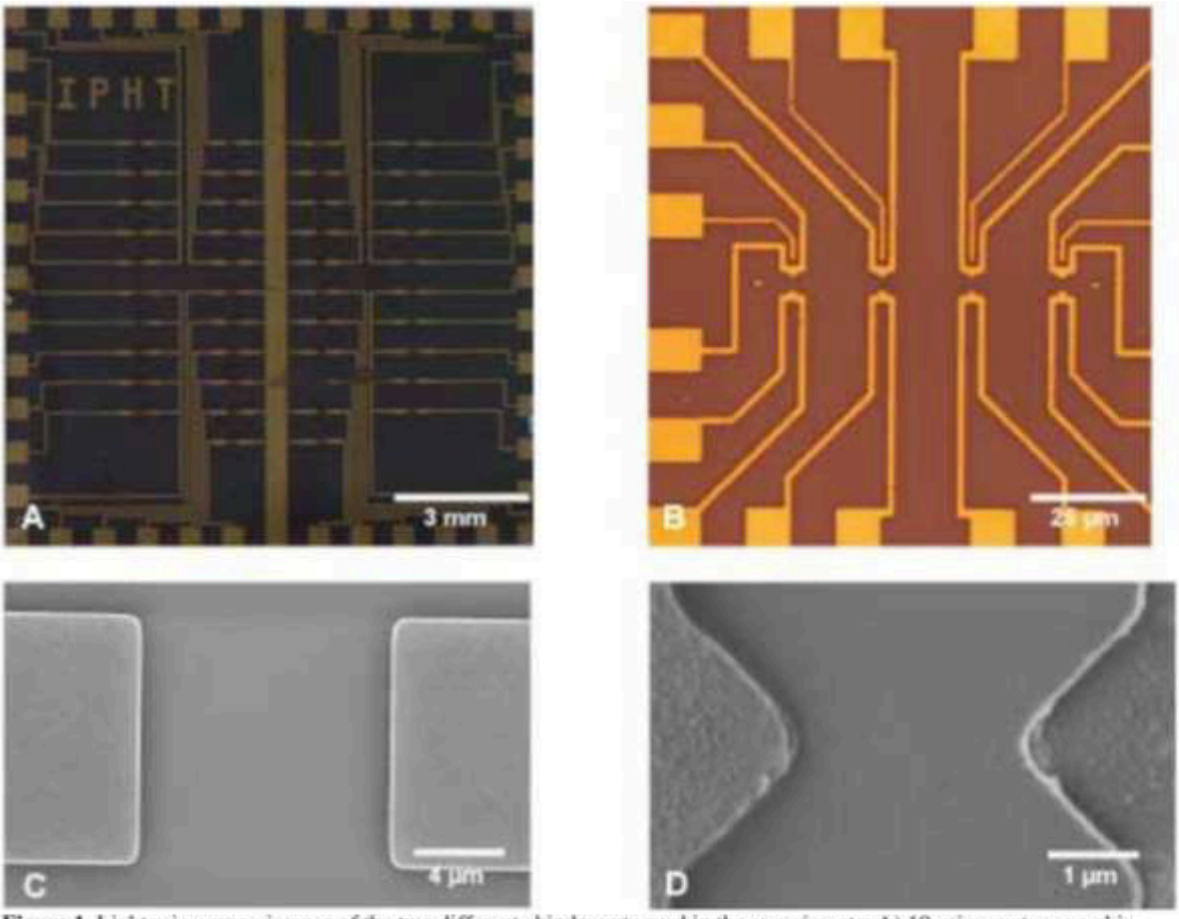

Figure 1. Light microscope images of the two different chip layouts used in the experiments: A) 10-micrometer-gap-chip with 42 electrode gaps and B) 2-micrometer-gap-chip, with arrangements of 4 smaller tapered electrode gaps. The SEM images show detailed views of one 10 micrometer electrode gap (C) and 2 micrometer electrode gap (D).

4. RESULTS AND DISCUSSION

First experiments were conducted to determine optimal conditions for dielectrophoretic trapping of lambda DNA in microelectrode gaps. As shown in figure 2, initial results exhibit the problem of the "all-or-none effect"; the yield of the DNA in the gaps differs considerably. A voltage of 6 V is collecting only a few, not stretched strands at the electrode edge (figure 2A). On the other hand, voltages of 8 V or higher cause an assembly of thick bundles and also lead to trapping of impurities (figure 2B and C). The shape of the DNA material in figure 2B is probably due to drying effects, of the pinned DNA on the electrodes, after the DEP process and before imaging with the fluorescence microscope. The control of the trapping process was also given by the *in situ* real time fluorescence imaging during the process, where such a shape could not be observed. Further investigation regarding this problem are still ongoing and seem to confirm this.

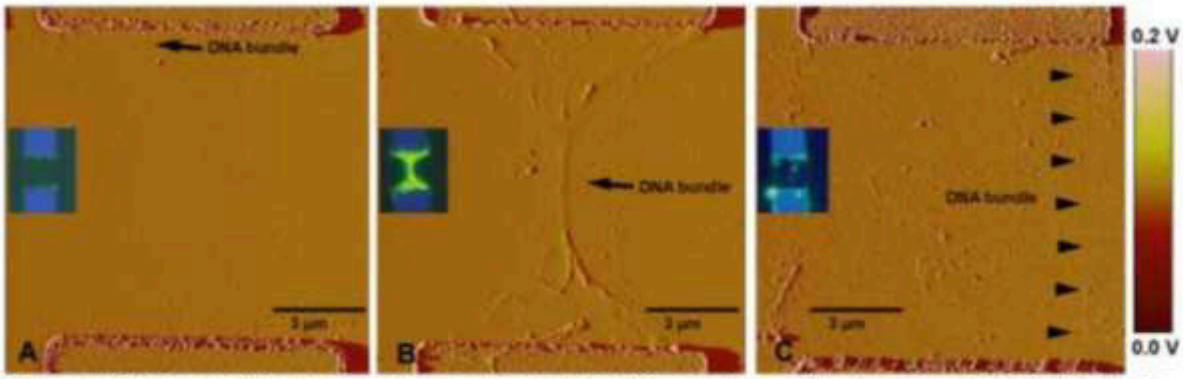

Figure 2. AFM images of the 10 micrometer gaps after applying different voltages with a frequency of 100 kHz. The insets show the corresponding fluorescence images. A) 6V: no fully stretched DNA is bridging the gap. B) 8V: a bulk of DNA fibers is bridging the gap. C) 10V: beside a couple of DNA structures, impurities are trapped in the electrode gap.

After this unsatisfied results a set of different frequencies as well as voltage series (data not shown) were utilized. The effect of the applied frequency is given in figure 3. At a low frequency of 10 kHz an alignment of DNA strands on the electrode edges in the gap is visible (figure 3A), but no molecule is actually bridging the gap. At a frequency of 100 kHz the DNA was both collected at the edges and stretched over the gap (figure 3B). A tremendeous amount of DNA between the electrodes results from high frequencies like 1 MHz as shown in figure 3C. A bright spot of stained molecules is covering the entire electrode gap.
Studies using the 2-micrometer-gap layout confirm and extend these results. At a frequency of 10 kHz an alignment of DNA strands along the electrode wires is clearly visible and the gap remains empty (figure 3D). However, at100 kHz DNA bundles are focused in the electrode gap and only a few molecules are attached to the electrode outside the gap (figure 3E).
These results are in agreement with investigations of Namasivayam (19) and Asbury (15). It is supposed that different regions of the inhomogeneous counterion cloud (that surrounds the negatively charged backbone of the DNA) contribute in polarization of a DNA strand. For trapping DNA in electrode gaps, 100 kHz proved to be the optimum frequency. It is also visible that the shape of the smaller 2-micrometer-gap arrangement is more suitable for DNA trapping applications. The increased field gradient at the tip of such a tapered electrode seems to enhance the accuracy of the positioning of single strands, so all further experiments were done with this layout.

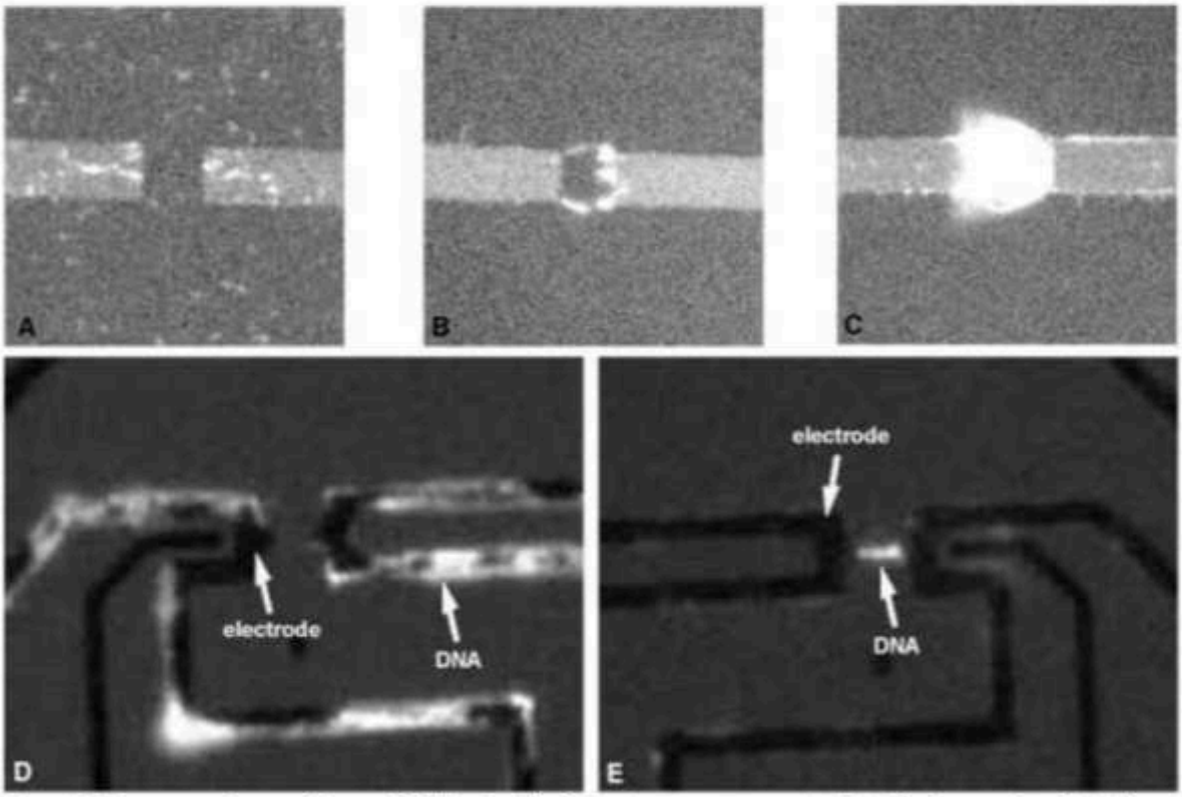

Figure 3. Fluorescence images of trapped DNA in the 10 micrometer gap arrangement obtained by frequencies of: A) 10 kHz, B) 100 kHz, C) 1 MHz. D) 2 micrometer gap chip with DNA along the electrode structures by a frequency of 10 kHz. E) DNA trapped in the gap by a frequency of 100 kHz.

For applications in the field of nano structuring and nano wires, single DNA molecules or thin bundles are preferred in the electrode gaps. Further experiments were aiming at this target. Therefore the gaps were more precisely characterized with an atomic force microscope. In order to detect even single DNA molecules between the electrodes. DEP parameters from the first experiments were taken and adjusted to tune to single DNA molecule trapping. Figure 4 shows a chip where voltages from 1 to 4 V were applied to four different gaps. A frequency of 100 kHz was taken as an optimum from previous experiments because higher frequencies yield an undesired excess of DNA molecules in the gap.
A detailed look at the gaps with the AFM exposes the single strands or bundles bridging the gap from the tip of the electrodes. It points out that with higher voltages more DNA is trapped and an assembly to bundles become apparent. In the gap at which 1V was applied single DNA strands or very thin bundles of a few DNA molecules could be found. At higher voltages the bundles become thicker especially from the tip of the electrode towards the gap. It is assumed that the DNA has contact with one end to the electrode and is pinned down there. Outgoing from this point the DNA is spanning the gap. A terminal binding of DNA strands with a high affinity to gold electrodes is known (20,21). Such binding can be enforced with an additional thiol group at the DNA strand end (19).

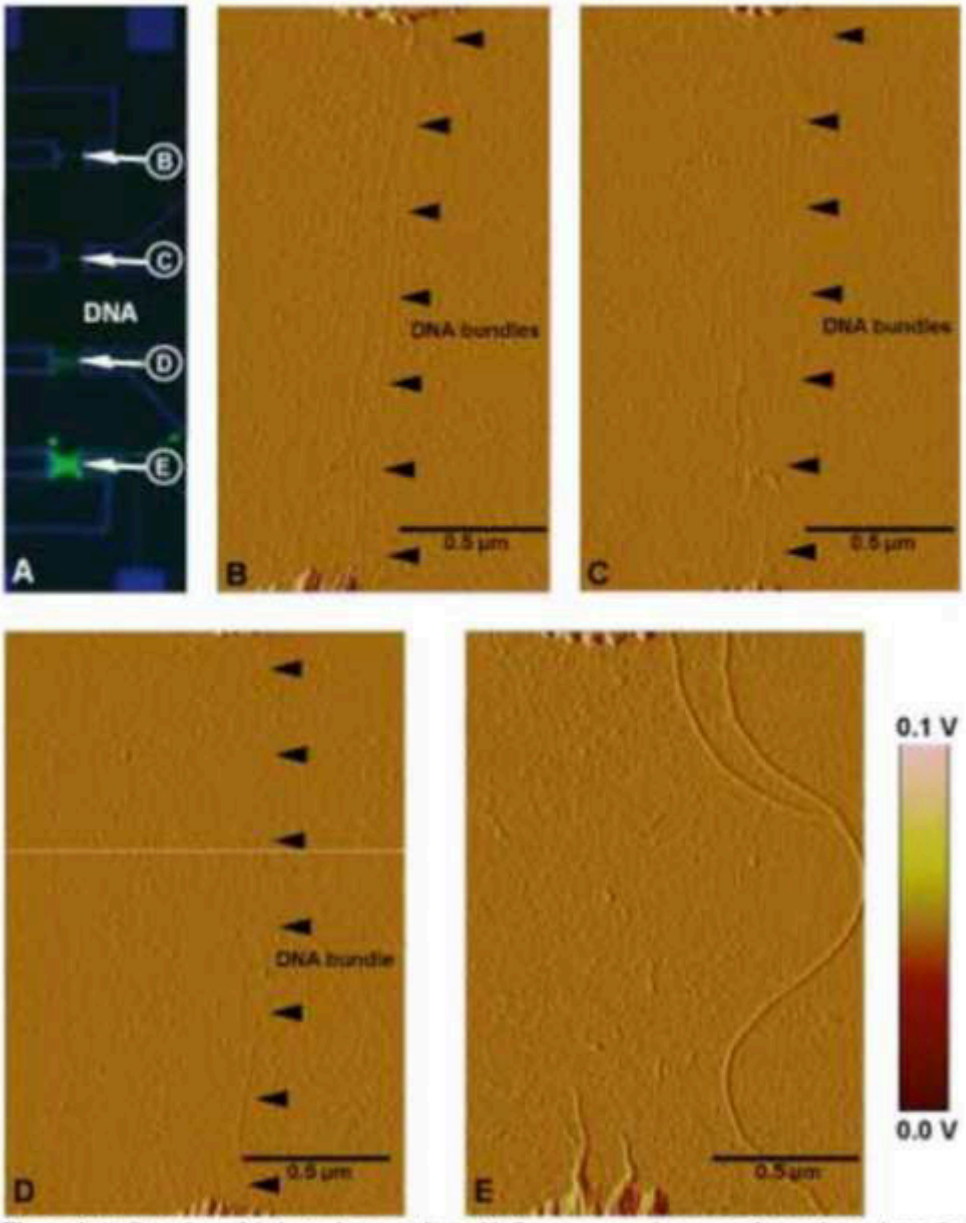

Figure 4. A) Overview of 4 electrode gaps taken with fluorescence microscope. Increasing voltages in 1V steps were applied top down. B-E) detail images of the gaps taken with AFM.

A further decrease of the applied voltage was carried out to reduce the amount of DNA molecules in the gap. It turns out that the concentration of DNA in the applied solution (0.02 ng/ micro liter) appears to be too low in order to align molecules between the electrodes in the given time of 10 min. A satisfying result could be achieved by applying the electric field for 20 min (figure 5). So, two thin bundles as well as single molecules could be found.

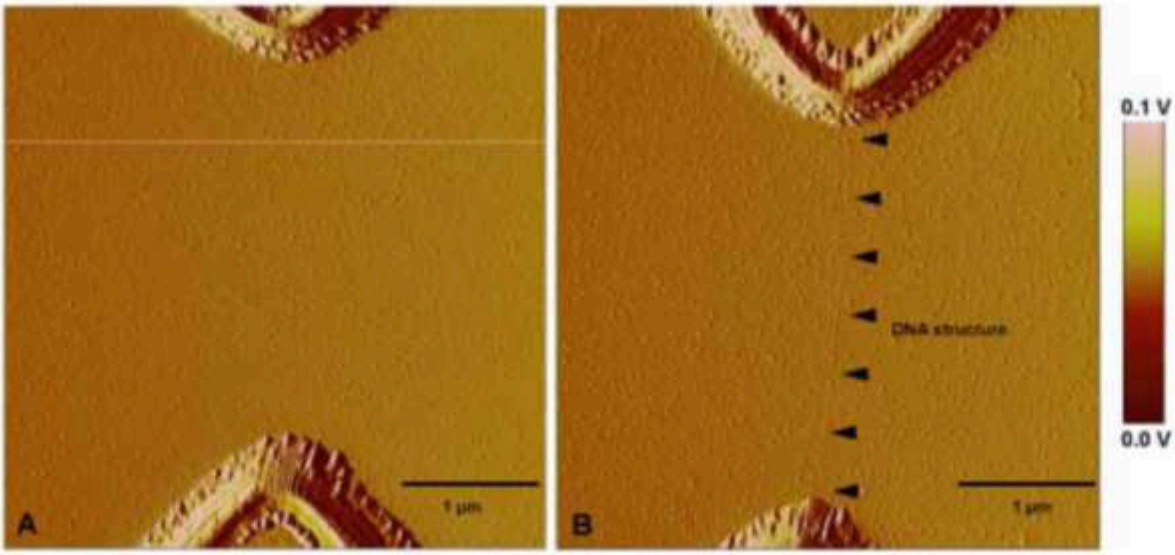

Figure 5 AFM images of A) an empty gap at a voltage of 0.5 V for 10 min. B) Two individual DNA structures spanned over the gap after applying a voltage for 20 min.

We conclude that DEP is a useful tool for spatial manipulation of DNA in micrometer sized electrode gaps.
The combination of different imaging techniques like online *in situ* fluorescence imaging and atomic force microscopy allows the characterization and optimization of the DNA trapping process. Especially the investigation of electrode gaps with AFM after dielectrophoretic positioning and stretching steps may improve the optimization processes regarding single molecule manipulation. So single DNA strands can be resolved on microstructured substrates. Thus, DEP parameters derived from first experiments could be further defined. It is important to understand that such optimized DEP conditions are valid for a given parameter group. The interaction of focusing the electrical field, attained by increasing the frequency, enhanced field intensity, by rising the applied voltage and field radius, given by the DNA concentration results in a defined DNA structure, bridging the electrode gap.
Hier relativieren, dass es nur gültig bei einen bestimmten Parameterkomplex, Zusammenspiel. Fokussierungseffekt (Frequenz), Erhöhung der Feldintensität (U), Radius (Konzentration), definierter Brücke? (Zeit und niedrigere Spannung!), Temperatur und Abstand immer gleich. So optimum erreicht – eine Molekül schön klar als Brücke, ohne Elektrolyse Effekt und pipapo.
The tradeoff between efficiency and accuracy could be overcome with a frequency of 100 kHz and a voltage of 0.5 V for the given parameter group. So, it is possible to attach and stretch DNA strands nearly from the one electrode to the other. Higher voltages induce extended field intensities and radii. An increased action radius influenced neighbor electrode gaps. This leads to additional amounts of DNA in the gap. Higher frequencies lead to better focusing effects (radii) during the trapping and also to defined DNA structures, like single molecule bridging the gap. This effect has also been observed by Tuukkanen (22). The advantage of lower frequencies is the possible application of higher voltages and therewith briefer trapping times (19), but for our conditions it lead to unspecific accumulation of residues and thick DNA bundles. So that for single molecule applications low concentrated DNA solutions, relatively low voltage and longer trapping times (20 min) are preferred.
The difference in gap width also plays an enormous role on DEP experiments. The advantage of electrodes with a defined geometry could be shown and has been described in the literature as well (sinusoidal (23), trapezoidal (24) or triangular (16)). The change to the 2-micrometer-gap-chip with smaller electrode gaps led to better results concerning the localization of the DNA strands. An important point was the use of AFM that could resolve individual DNA structures and thereby clarify the local molecular arrangement. The presented work demonstrates the successful utilization of DEP for single-molecular manipulation, thereby opening the way towards single molecule DNA constructs for future application in nanoelectronics or biosensorics.

5. ACKNOWLEDGMENTS

We like to thank Franka Jahn for SEM imaging and Grit Festag for proof reading of the manuscript. This work has been supported by the Volkswagen Stiftung (VW Project: I/80 070, SOBSI) and the European Project NUCAN (NMP-STREP 013775).

6. REFERENCES

1. N. C. Seeman: De novo design of sequences for nucleic acid structural engineering. *J Biomol Struct Dyn*, 8, 573-81(1990)

2. N. C. Seeman: The use of branched DNA for nanoscale fabrication. *Nanotechnology*, 2, 149-159(1991)

3. N. C. Seeman: DNA nanotechnology: novel DNA constructions. *Annu Rev Biophys Biomol Struct*, 27, 225-48(1998)

4. N. C. Seeman: DNA nanotechnology. *materials today*, 24-30(2003)

5. H. Yan: Materials science. Nucleic acid nanotechnology. *Science*, 306, 2048-9(2004)

6. A. Bensimon, A. Simon, A. Chiffaudel, V. Croquette, F. Heslot and D. Bensimon: Alignment and Sensitive Detection of DNA by a Moving Interface. *Science*, 265, 2096-2098(1994)

7. D. Bensimon, A. J. Simon, V. Croquette and A. Bensimon: Stretching DNA with a Receding Meniscus: Experiments and Models. *Physical Review Letters*, 74, 4754-4757(1995)

8. X. Michalet, R. Ekong, F. Fougerousse, S. Rousseaux, C. Schurra, N. Hornigold, M. van Slegtenhorst, J. Wolfe, S. Povey, J. S. Beckmann and A. Bensimon: Dynamic molecular combing: stretching the whole human genome for high-resolution studies. *Science*, 277, 1518-23(1997)

9. T. T. Perkins, S. R. Quake, D. E. Smith and S. Chu: Relaxation of a Single DNA Molecule Observed by Optical Microscopy. *Science*, 264, 822 -826(1994)

10. S. B. Smith, L. Finzi and C. Bustamante: Direct mechanical measurements of the elasticity of single DNA molecules by using magnetic beads. *Science*, 258, 1122-6(1992)

11. H.A. Pohl, Dielectrophoresis: The behavior of matter in nonuniform electric fields. London:*Cambridge University Press*, London (1978)

12. R. Hölzel and F. F. Bier: Dielectrophoretic manipulation of DNA. *IEE Proceedings Nanobiotechnology*, 150, 47-53(2003)

13. M. Washizu and O. Kurosawa: Electrostatic Manipulation of DNA in Microfabricated Structures. *IEEE Transactions of Industrial Applications*, 26, 1165-1172(1990)

14. M. Washizu, O. Kurosawa, I. Arai, S. Suzuki and N. Shimamoto: Applications of electrostatic stretch-and-positioning of DNA. *IEEE Transactions on Industry Applications*, 31, (1995)

15. C. L. Asbury and G. v. d. Engh: Trapping of DNA in Nonuniform Oscillating Electric Fields. *Biophysical Journal*, 74, 1024-1030(1998)

16. F. Dewarrat, M. Calame and C. Schönenberger: Orientation and Positioning of DNA Molecules with an Electric Field Technique. *Single Molecules*, 3, 189-193(2002)

17. L. Zheng, J. P. Brody and P. J. Burke: Electronic manipulation of DNA, proteins, and nanoparticles for potential circuit assembly. *Biosens Bioelectron*, 20, 606-19(2004)

18. R. Holzel, N. Gajovic-Eichelmann and F. F. Bier: Oriented and vectorial immobilization of linear M13 dsDNA between interdigitated electrodes--towards single molecule DNA nanostructures. *Biosens Bioelectron*, 18, 555-64(2003)

19. V. Namasivayam, R. G. Larson, D. T. Burke and M. A. Burns: Electrostretching DNA molecules using polymer-enhanced media within microfabricated devices. *Anal Chem*, 74, 3378-85(2002)

20. J. Allemand, D. Bensimon, L. Jullien, A. Bensimon and V. Croquette: pH-dependent specific binding and combing of DNA. *Biophys. J.*, 73, 2064-2070(1997)

21. G. Maubach and W. Fritzsche: Precise Positioning of Individual DNA Structures in Electrode Gaps by Self-Organization onto Guiding Microstructures. *Nano Letters*, 4, 607-611(2004)

22. S. Tuukkanen, A. Kuzyk, J. J. Toppari, H. Häkkinen, V. P. Hytönen, E. Niskanen, M. Rinkiö and P. Törmä: Trapping of 27 bp–8 kbp DNA and immobilization of thiol-modified DNA using dielectrophoresis. *Nanotechnology*, 18, 295204-295214(2007)

23. S. Suzuki, T. Yamanashi, S. Tazawa, O. Kurosawa and M. Washizu: Quantitative analysis of DNA orientation in stationary AC electricfields using fluorescence anisotropy. *IEEE Transactions on Industry Applications*, 34, 75-83(1998)

24. T. Kawabata and M. Washizu: Dielectrophoretic detection of molecular bindings. *IEEE Transactions on Industry Applications*, 37, 1625-1633(2001)

Abbreviations: DEP: dielectrophoresis; AFM: atomic force microscopy

Key Words Atomic force microscopy, Dielectrophoresis, DNA, Microstructures, Nanotechnology.

Send correspondence to: Dr. Wolfgang Fritzsche, Institute of Photonic Technology Albert-Einstein-Str. 9, 07745 Jena, Germany, Tel:+49(0)-3641-206-304, Fax:+49(0)-3641-206-344, wolfgang.fritzsche@ipht-jena.de

6.1.4 Assembling gold nanoparticle chains using an AC electrical field: Electrical detection of organic thiols [CL4]

Christian, Leiterer:	Konzeptentwicklung Sensorherstellung Echtzeitmessungen und Evaluierung der Daten Diskussion des Konzepts und der Ergebnisse Diskussion und Korrektur des Manuskripts
Steffen, Berg:	Sensorherstellung Endpunktmessungen und Evaluierung der Daten
Antti-Pekka, Eskelinen:	Herstellung der Chipsubstrate Diskussion und Korrektur des Manuskripts
Andrea, Csaki:	Diskussion und Korrektur des Manuskripts
Matthias, Urban:	Unterstützung bei den Messungen
Päivi, Törmä:	Diskussion und Korrektur des Manuskripts
Wolfgang, Fritzsche:	Diskussion des Konzepts und der Ergebnisse Diskussion und Korrektur des Manuskripts

Sensors and Actuators B, **2013**, 176, 368–373

Sensors and Actuators B 176 (2013) 368–373

Contents lists available at SciVerse ScienceDirect

Sensors and Actuators B: Chemical

journal homepage: www.elsevier.com/locate/snb

Short communication

Assembling gold nanoparticle chains using an AC electrical field: Electrical detection of organic thiols

Christian Leiterer[a,*], Steffen Berg[a], Antti-Pekka Eskelinen[b], Andrea Csaki[a], Matthias Urban[a], Päivi Törmä[b], Wolfgang Fritzsche[a]

[a] Institute of Photonic Technology, Albert-Einstein-Straße 9, 07745 Jena, Germany
[b] Aalto University, Applied Physics, FI-00076 Aalto, Finland

ARTICLE INFO

Article history:
Received 9 August 2012
Received in revised form
25 September 2012
Accepted 26 September 2012
Available online 2 October 2012

Keywords:
Gold nanoparticle
Dielectrophoresis
Sensor
Bioanalytics
Micro integration
Nano transducer

ABSTRACT

Here we present the utilization of gold nanoparticle (AuNP) chains assembled between two electrodes using an AC electrical field as a potential nanosensor for molecular detection. We describe an easy way to assemble, monitor and characterize the resulting nanoparticle chains electrically. Furthermore, parallelizability and sensing ability of the assembled structures will be addressed. The assembled pearl-chain like structures have the potential to recognize binding events of small molecules with DC current. Bound molecules influencing the charge transfer along the particle chain and therefore generate a signal that can be read electrically. We demonstrate that the produced AuNP-chains can be used for molecular sensing, by measuring the resistances changes due to the interaction with thiols, which are known to bind strongly to gold. The resulting signal was monitored in end-point as well as real-time measurements.

1. Introduction

Noble metal nanoparticles have been addressed as potential key elements in biosensors over many years [1]. Films of densely packed noble metal nanoparticles stabilized by thin layers of organic molecules respond with a significant increase of their electrical resistance when exposed to certain organic vapors. This effect depends on the species of organic compound as well as the alkyl chain length of the usually utilized stabilization layer molecule [2]. Such colloidal metal–insulator–metal ensemble (MIME) sensors were introduced more than a decade ago [3], and include usually an at least micrometer-sized area covered by nanoparticles. A further shrinkage of these arrangements from 2D to 1D case would allow for a better separation of the various possible conduction mechanisms and therefore a better understanding of the involved processes. Moreover, it would also open these sensors for further miniaturization and the resulting potential for higher multiplexing and/or minimized sample volume.

1D arrangements of metal nanoparticles have been assembled with a thickness in the micrometer and a length in the millimeter range [4–12]. These nanoparticle assemblies are clearly distinguishable from bulk material, because their conductivity is significantly (and therefore measurable) influenced due to the binding of molecules to its surface. This effect can be detected when a high surface to volume ratio of these nanostructures can be achieved. The electrical properties of assembled nanoparticle chains or single nanoparticles have been characterized in the past through DC measurements and impedance spectroscopy in order to get a deeper understanding of the conduction mechanism from particle to particle [13–15]. Surprisingly, the prospects for molecular sensing have been addressed very rarely [16,17], despite the fact that a sensing device based on nanoparticle conductivity could provide a label free detection of molecular binding in real-time. Furthermore, such a device can be read-out electrically, which requires far less expensive equipment than established optical methods.

For the development and characterization of such a sensing device based on nanoparticle conductivity, many steps have to be taken. The key element, the nanoparticles, should be assembled between two electrodes in an inexpensive manner, which must be in the nanoscale and provide the high surface to volume ratio necessary for molecular sensing with electrical read-out.

This article addresses and solves problems concerning these requirements. It is demonstrated that nanoparticle chains consisting of various sized AuNPs can be assembled between nano- and micro-scale electrodes in an inexpensive manner using an

* Corresponding author. Tel.: +49 3641 206 349; fax: +49 3641 206 399.
E-mail addresses: christian.leiterer@ipht-jena.de, Christian.leiterer@gmail.com (C. Leiterer).

0925-4005/$ – see front matter © 2012 Elsevier B.V. All rights reserved.
http://dx.doi.org/10.1016/j.snb.2012.09.088

AC electrical field. This technique can be utilized in parallel with high efficiency, even in nanoscale electrode gaps. Furthermore, the assembled nanoparticle chains can be used for electrical detection of an organic thiol. Endpoint and real-time measurements are possible, which points out the opportunity to measure even binding kinetics with this system.

2. Experimental

2.1. Micro- and nano electrode substrates

For AC field assembly of the gold nanoparticles, microelectrodes were prepared on thermally oxidized silicon substrates by standard photolithography lift-off. Two electrode layouts with different shape and gap size were fabricated: 1 μm gap-size rounded electrodes (Fig. 1, top left) and 10 μm gap-size rectangular electrodes (Fig. 1, top right). Both electrode layouts are made from 100 nm sputtered gold layer. Nanoelectrodes were prepared by standard e-beam lithography of 50 nm gold layer using also lift-off technique. 50 electrode gaps with average gap-sizes between 40 and 100 nm were fabricated, here all electrode gaps can be contacted in parallel (Fig. 1, bottom).

2.2. Colloidal AuNP

For the assembly of the AuNP-chains, commercially available AuNP were obtained from BBI (British BioCell, UK) with diameters of 5 nm, 15 nm, 30 nm and 60 nm. These particles were used for the DEP in the provided concentrations (5 nm: 1.0×10^{13} P/ml, 15 nm: 1.4×10^{12} P/ml, 30 nm: 2.0×10^{11} P/ml, and 60 nm: 2.6×10^{10} P/ml).

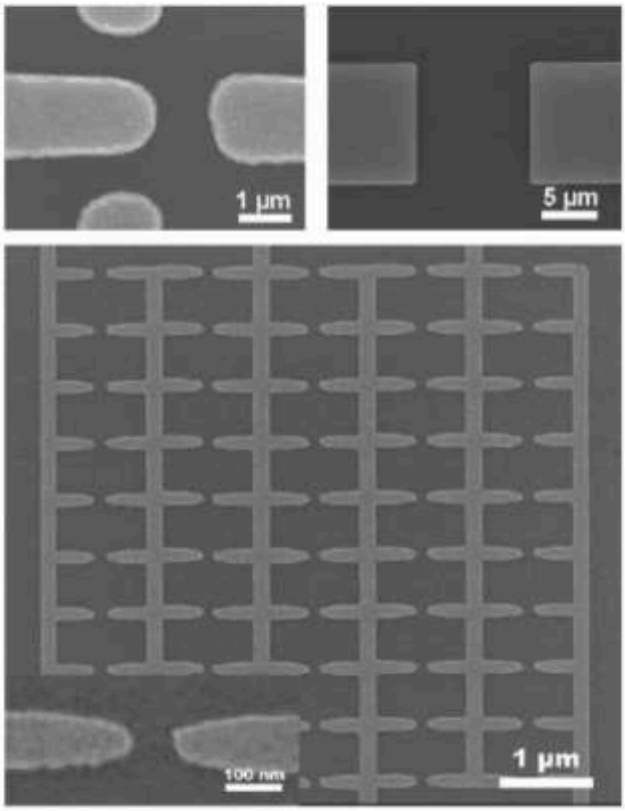

Fig. 1. SEM images of the utilized micro- and nanostructured electrodes with 1 μm (top left), 10 μm (top right) and ~40–100 nm (bottom) electrode gaps. The e-beam fabricated nanoscale gaps allow for parallel connections.

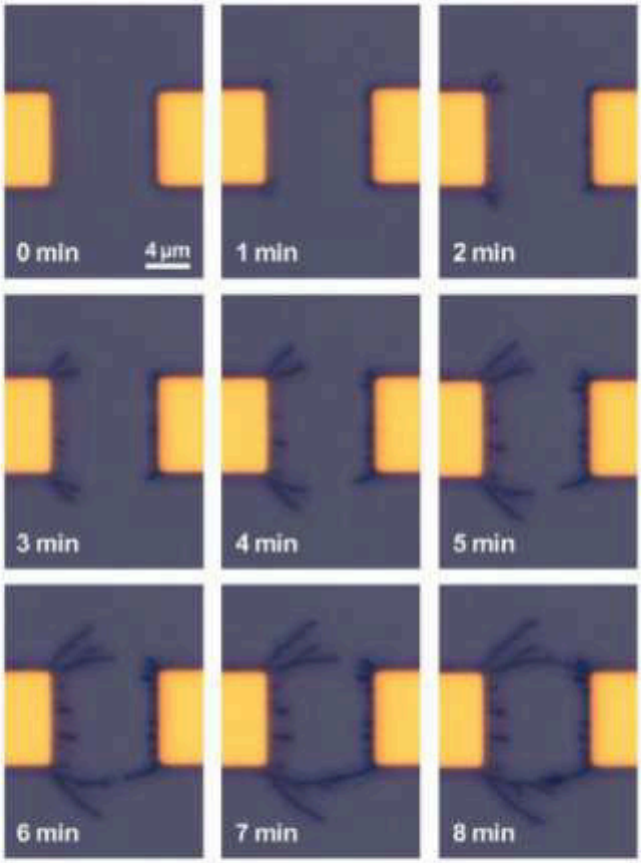

Fig. 2. Assembly of AuNP-chains (30 nm AuNP) in an AC electrical field (1 kHz). For efficient assembly control, the voltage was successively decreased from 2.5 to 1.0 V over the course of several minutes. After 8 min the two-sided assembly of the AuNP-chain is finished, resulting in gap closure.

2.3. Assembly of AuNP in an AC electrical field

In order to assemble nanoparticle chains from the colloidal solutions, a function generator (Agilent 33220A, Agilent Technologies, Böblingen, Germany) was used as a power supply, providing up to 20 MHz, 20 Vpp at open circuit. For our purpose frequencies from 1 kHz to 1 MHz and voltage from 0.7 V to 2.5 V were applied. Average duration of the AC controlled assembly was from 5 to 40 min.

The experimental procedure for the AC assembly is quiet simple: a droplet of the colloidal solution is applied to the chip with a pipette. As soon as voltage is applied to the electrodes, the assembly of the particle into pearl-chain like structures starts taking place (Fig. 2).

To be able to monitor the assembly of the particle chains electrically in real-time, the voltage across a resistor arranged in series to the gap was measured using a digital oscilloscope (DSO 3202A, Agilent-Technologies, USA).

2.4. Detection of an organic thiol

As analyte, 1-mercapto-6-hexanol (Sigma–Aldrich, Taufkirchen, Germany) diluted in ethanol was used. The thiol group of the organic molecule binds to gold nanoparticles with high affinity forming a dense monolayer.

This binding induces a change in resistance, which was monitored using an ampere meter with an integrated DC power supply (Sourcemeter 2400, Keithley Instruments, Cleveland, OH, USA). Endpoint and real-time measurements were performed.

2.5. Characterization of the AuNP-chains

The AuNP-chains were characterized optically (Micro-scope Z1.m/A1.m with CCD camera AxioCam MRc5, Carl Zeiss, Jena, Germany) and by scanning electron microscopy (DSM 960, Carl Zeiss, Jena, Germany) to control quality and sub-structure of the AuNP-chains during and after assembly.

3. Results and Discussion

3.1. Assembly of AuNP chains in 10 μm electrode gaps

To assemble AuNP (colloidal, 60 nm) into chain-like structures, an AC electrical field at a frequency of 1 kHz, 2.5 V was found to work in a fast and reproducible manner for this electrode gap size. The assembly starts at the corners of the rectangular electrodes because the highest field intensities are present here. The particle chain spreads like a growing crystal until final connection. The process was visualized in real-time with an optical microscope (Fig. 2, video 1). The overall process takes about ~8 min.

Also, this process can be monitored simply by electrical means. We demonstrate this by measuring the voltage across a resistor connected in series with the electrode gap using an oscilloscope. In order to have the same force applied to the particle as without the resistor the voltage must be raised accordingly. The following figure (Fig. 3) shows the monitored voltage which also represents the growing of the particle chain. The increasing voltage across the resistor is driven by the decreasing resistance in the electrode gap due to the particle assembly (and therefore decreasing gap). Two phases in the assembly of the particle chains became apparent. In the first phase, particle chains are growing as already shown in Fig. 2. In this phase, the voltage across the resistor in series increases linear (Fig. 3, diagram logarithmic scaled, line b: 0–800 s and c: 0–1300 s). In the second phase, the assembling particle chains from each electrode finally connect with each other, resulting in a voltage peak (Fig. 3, line b: after 800 s and c: after 1400 s).

Line b and c in Fig. 3 correspond to particle assembly under exact same conditions, consequently the time particle chains are assembled until connection cannot be predicted, which corresponds to other experiments made.

Also a negative control is shown using the same particle solution at 1 Mhz, 1.5 V (Fig. 3, line a: below assembly threshold). No significant change in voltage over time could be measured, therefore no particle chain assembled.

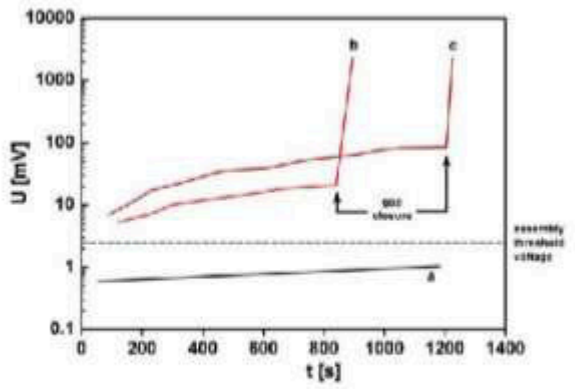

Fig. 3. On-line electrical characterization of the assembly process. When the applied voltage is below the assembly threshold, no significant change in voltage over time is observed (dotted line for 1.5 Vpp). However, for voltages above this threshold such as 2.5 Vpp, the assembly process results in a steady increase in the voltage (measured at a serial resistor) until a certain point where a voltage jump is observed. This point relates to the closure of the gap.

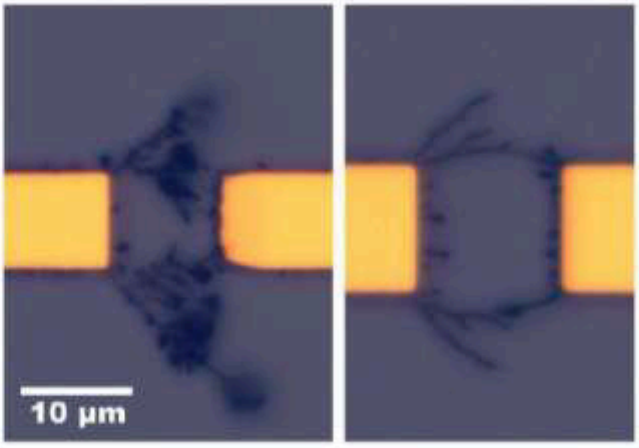

Fig. 4. Comparison of AuNP-chains assembled with constant voltage (left, 2.5 V, 1 kHz) and successively decreased voltage (right, 2.5–1.0 V, 1 kHz).

The ability to monitor the assembly electrically is of high importance because it allows recognizing the moment of contact very exactly, which is not possible using microscopy. The reason why the point of contact is so crucial is that the system is on short-cut at comparatively high voltage at this moment, which can destroy the particle chain immediately after being assembled.

Furthermore, it gives the opportunity to the shutdown of the voltage in order to prevent damaging the particle chain upon short-cut. This automation could be realized quiet easily using a transistor, which switches off the power supply as soon as the voltage across the resistor in series with the gap increases over a certain value. Also, it is important to be able to monitor the process electrically if particle chains have to be produced with high throughput on an industrial scale.

In order to improve the AC driven assembly of the nanoparticle chains, a successive decrease of the applied voltage during the assembly process (8 min) results in more defined particle chains. This was done by control software, which scaled down the applied voltage over time stepwise from 2.5 V to 1.0 V. If the voltage is kept constant over time the electrical field would increase due to growing of the particle chain. Therefore a successively reduction of the voltage leads to a more constant field strength. In the following figure we compare the typical shape of a particle chain assembled with constant voltage and with successive decreasing voltage (Fig. 4).

Having a closer look at the particle chain using SEM imaging reveals the substructure of the particle chain. The AuNPs assembled with an AC field at 1 kHz are fused to a rather continuous nanowire; no individual AuNPs can be resolved anymore (Fig. 5).

Another way to characterize a particle chain is DC resistance measurements. These measurements can as well give information about the internal structure of the particle chains, without the need for sophisticated (and thereby costly) ultramicroscopic technique like SEM. This allows for a very useful fast and reliable quality assurance right after the assembly. Lower resistance corresponds to fused continuous particle chains (Fig. 5, 0.6–1.8 kΩ), higher resistance corresponds to non-fused pearl-chain like structures (Fig. 6, 0.8–60 MΩ). Moreover, SEM was found to be destructive, resulting either in open circuits (destruction of particle chain) or in a significant drop in resistance, especially experienced with the pearl-chain structures. We assume that the decrease in resistance is caused by carbonaceous deposition during SEM measurements in the particle junctions.

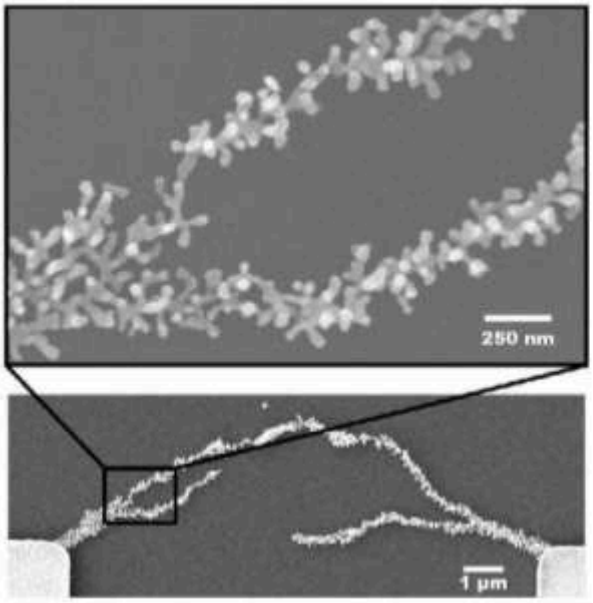

Fig. 5. Scanning electron micrograph of the assembled AuNP-chain (1 kHz, ~2.5 V). The AuNP form a continuous nanowire with a resistance of about 5 kΩ.

3.2. Assembly of AuNP chains in 1 µm electrode gaps

The assembly of AuNP chains in 1 µm electrode gaps was performed with an AC field at 1 MHz using a constant voltage. Different sizes of AuNPs (60 nm, 15 nm, and 5 nm) were investigated. In contrary to the particle chains assembled at 1 kHz, these chains showed pearl-chain-formation after assembly, which means that the assembled nanoparticles are not fused to a continuous nanowire (Fig. 6). AuNP-pearl-chains are showing in average two orders of magnitude higher resistance (0.8–60 MΩ) than the fused nanowires assembled in 10 µm electrode gaps. Due to their higher resistance, this assembly process is not critical upon shortcut. Therefore particle chains of different thicknesses can be assembled (Fig. 6). The thickness can be thereby controlled by assembly duration and voltage. Lower voltage and longer duration means hereby-thick particle chains and higher voltage, shorter duration results in thinner particle chains. The frequency was always held constant at 1 Mhz.

Depending on the applied voltage and particle size these pearl-chains can also be fused into a continuous nanowire in an additional step (data not shown).

3.3. Assembly of AuNP chains in nano-electrode gaps

Beside nanowire formation in micrometer gaps, we demonstrate the formation of AuNP-pearl-chains in much smaller nano-electrode gaps of less than 100 nm gap size. Fifty gaps are assembled here in parallel with high (>90%) efficiency. The starting parameters for the assembly are the same as used with the 1 µm gap, but with the shrinking gap size lower voltage must be applied (0.7–1.3 V) to avoid the destruction of the AuNP-chains and the electrode material. Overall resistance of these arrays of parallel connected AuNP-chains was in the range of 1–50 MΩ (Fig. 7).

Using nanoelectrode gaps nanoparticle chains consisting of few particles can be assembled. With these results we demonstrate that this technique to assemble particle chains works highly parallel and efficiently at the nanoscale.

3.4. Detection of an organic thiol

Thiols are known to have high affinity to gold. This attachment causes the resistance of the gold nanoparticle chain to increase, which can be used as a detection signal. Different mechanisms were discussed how this influence can explained, while the most common explanation is that tunneling barriers between particles (metal–insulator–metal) are influenced due to molecule binding [18]. In our case, 1-mercapto-6-hexanol (MCH) is used to verify the electrical sensing abilities in solution of the assembled AuNP-chains. The obtained results should be the basis for future developments of the sensing capabilities of nanoparticle chains as sensing device. Here the change in resistance of the AuNP-chains upon incubation with MCH was measured.

Endpoint measurements were performed on fused AuNP chains (10 µm gap) and AuNP-pearl-chains (1 µm gap) resulting the resistance to increase about ~10% on fused AuNP-chains and up to ~2000 times on AuNP-pearl-chains (Fig. 8). Pure solvent without MCH showed no change in resistance.

Measurements with only the solvent but no MCH yielded no measurable change in resistance. For both gap sizes, MCH

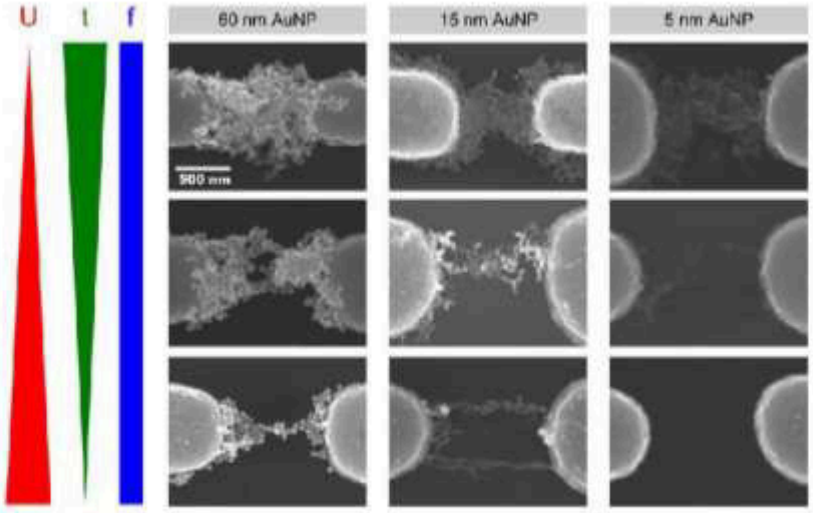

Fig. 6. AuNP-chains with different particle diameter (60 nm, 15 nm, and 5 nm) have been assembled in a 1 µm electrode gap under similar conditions (1 MHz, 5–40 min, 1–2.5 V). The voltage increases and the time decreases from top to bottom row. Their resistance reaches from 300 kΩ (upper left) to ~3 GΩ (bottom center).

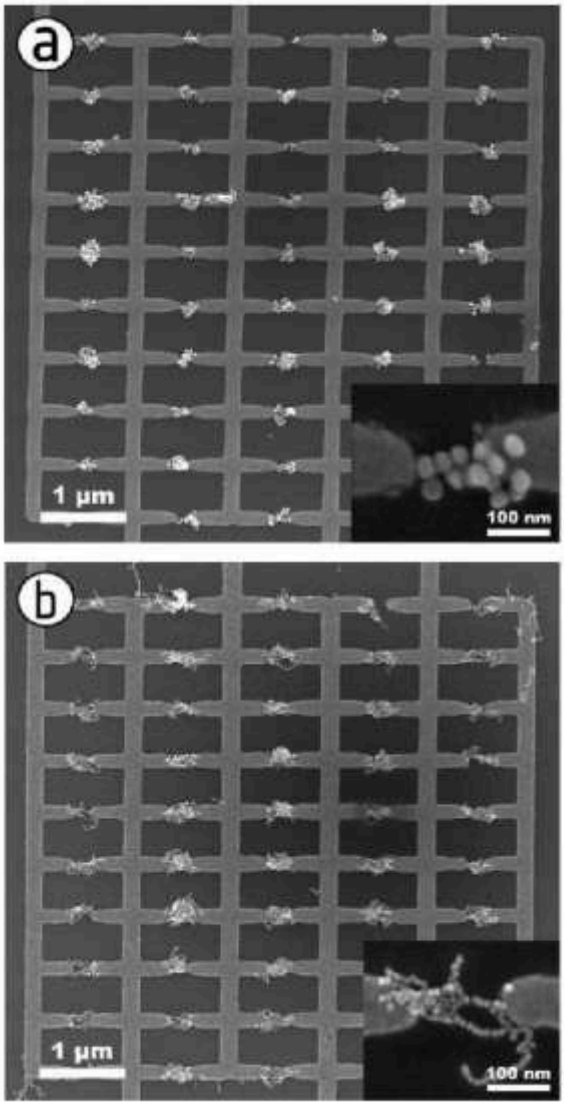

Fig. 7. AuNP were assembled in parallel in a nano gap array using 30 nm (a) and 15 nm (b) particles. The average resistance of these chains (all 50 in parallel) is about 3 MΩ (30 nm) and 30 MΩ (15 nm).

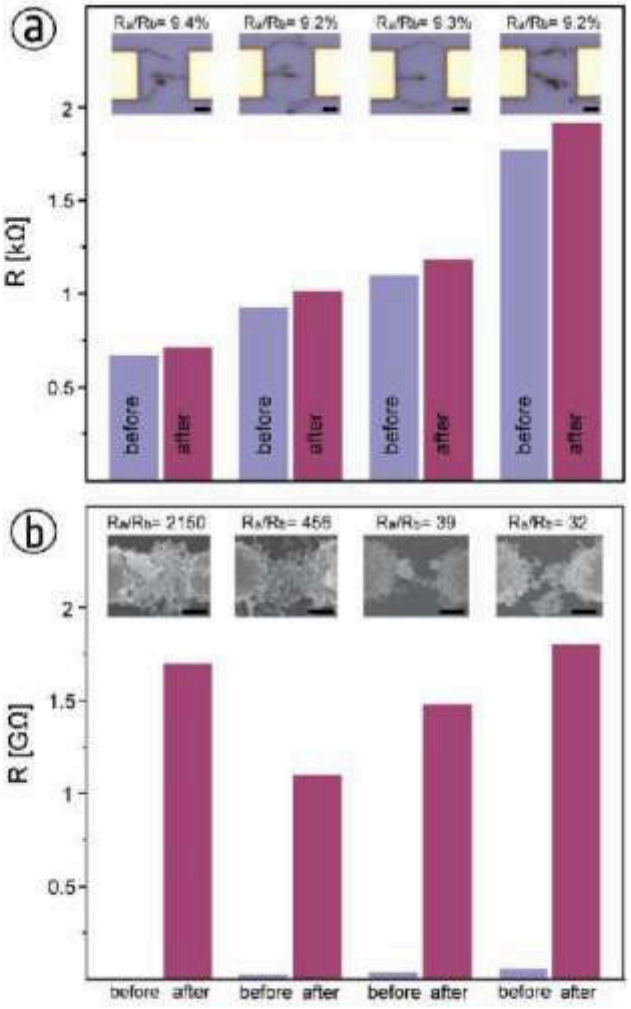

Fig. 8. Endpoint measurements of the AuNP-chain resistance in air. Fused AuNP-chains (a, 10 µm gap, cf. Fig. 5) showing a low change in resistance (~9%), while AuNP-pearl-chains (b, 1 µm gap, cf. Fig. 6) showing a huge change (up to ~2000 times) in resistance when the analyte (10 mM MCH) is applied.

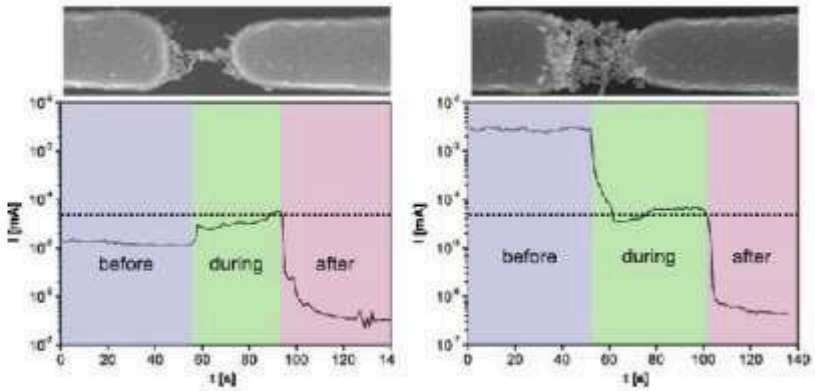

Fig. 9. Real-time resistance measurements when the analyte (10 mM MCH) is applied. The raise in the current in high resistance AuNP chains (left) during on-line measurement occurs due to the fact that the current flows through the solvent which has higher conductance (blue line: $R_{(solvent)}$). Only AuNP chains (right) with lower resistance are suitable for on-line detection. Here the thiol binding can be monitored in real-time. (For interpretation of the references to color in this figure legend, the reader is referred to the web version of this article.)

incubation resulted in a significant resistance increase (Fig. 8): the typical resistance of fused wires (10 μm gap) in the lower kΩ range increased by about 10% upon MCH addition, while the pearl-chain arrangement (1 μm gap) with starting resistances in the GΩ range showed an increase by more than two orders of magnitude.

In on-line measurements the change in resistance due to MCH was measured in real-time. In order to be able to conduct on-line measurements, the AuNP-chain has to have a lower resistance than the solvent of the molecule (Fig. 9, right); otherwise the solvent leak current hinders sensoric applications (Fig. 9, left). Fig. 9 shows on-line measurements of an AuNP-chain with resistance both higher and lower than the solvent. In advantage to endpoint measurements, on-line measurements have the potential to monitor binding kinetics of molecules in biology or pharmacology, which is an important task in this field.

4. Conclusion

In conclusion we were able to demonstrate the assembling of nanoparticle chains at the micro- (1 and 10 μm) and nano-scale (40–100 nm). Hereby two kinds of nanoparticle assemblies could be discriminated: fused highly conductive assemblies made at 1 kHz with limited abilities for sensing, and pearl chain like structures made at 1 MHz with quiet promising sensing potential. The assembly process and characterization of the nanoparticle assemblies was realized with low-cost equipment by using a high frequency AC power-supply for assembling particle chains and DC multimeter/oscilloscope to monitor current or voltage. It was also shown that nanoparticles could be assembled in 50 nanosized electrode gaps in parallel, which confirmed the parallelizability of assembly for high-throughput fabrication.

Furthermore we demonstrated the electrical detection of thiol molecules in solution by endpoint and real-time measurements using the assembled nanoparticle chains.

These results propose a promising way to detect biomolecules using assembled nanosensors. The system itself was kept simple and cost-efficient, allowing for a future commercial use.

In future similar systems might work for the label free, sequence specific detection of DNA in an array format similar to a microarray. Also the detection of sulfurous gases in bioreactors, as well as the identification of proteins similar to an ELISA assay is conceivable.

Acknowledgements

We thank Robert Kretschmer, Norbert Jahr and Janina Wirth for valuable comments and discussion and Franka Jahn for SEM imaging. Furthermore, we also thank BMBF project NAWION (FKZ: 16SV5386K, V4MNI014), TKWFK project Microplex (FKZ: PE113-1), DAAD project PPP Finland (FKZ: 50020468) and Academy of Finland (project numbers 134630, 135000, 141039) for financial support.

References

[1] E. Katz, I. Willner, Integrated nanoparticle-biomolecule hybrid systems: synthesis, properties, and applications, Angewandte Chemie International Edition 43 (2004) 6042–6108.
[2] Y. Joseph, I. Besnard, M. Rosenberger, B. Guse, H.-G. Nothofer, J.M. Wessels, et al., Self-assembled gold nanoparticle/alkanedithiol films: preparation, electron microscopy, XPS-analysis, charge transport, and vapor-sensing properties, The Journal of Physical Chemistry B 107 (2003) 7406–7413.
[3] H. Wohltjen, A.W. Snow, Colloidal metal–insulator–metal ensemble chemiresistor sensor, Analytical Chemistry 70 (1998) 2856–2859.
[4] K.D. Hermanson, Dielectrophoretic assembly of electrically functional microwires from nanoparticle suspensions, Science 294 (2001) 1082–1086.
[5] K.H. Bhatt, O.D. Velev, Control and modeling of the dielectrophoretic assembly of on-chip nanoparticle wires, Langmuir 20 (2004) 467–476.
[6] R. Kretschmer, W. Fritzsche, Pearl chain formation of nanoparticles in microelectrode gaps by dielectrophoresis, Langmuir 20 (2004) 11797–11801.
[7] R.J. Barsotti, M.D. Vahey, R. Wartena, Y.-M. Chiang, J. Voldman, F. Stellacci, Assembly of metal nanoparticles into nanogaps, Small 3 (2007) 488–499.
[8] B.C. Gierhart, D.G. Howitt, S.J. Chen, R.L. Smith, S.D. Collins, Frequency dependence of gold nanoparticle superassembly by dielectrophoresis, Langmuir 23 (2007) 12450–12456.
[9] X. Xiong, A. Busnaina, S. Selvarasah, S. Somu, M. Wei, J. Mead, et al., Directed assembly of gold nanoparticle nanowires and networks for nanodevices, Applied Physics Letters 91 (2007) 063101.
[10] A. Zoy, A.A. Nassiopoulos, A.G. Nassiopoulou, Self-assembly of single thin Au nanoparticle chains on Si along V-groove-etched lines between micrometre-distant electrodes by dielectrophoresis, Nanotechnology 18 (2007) 345608.
[11] X. Xiong, A. Busnaina, Direct assembly of nanoparticles for large-scale fabrication of nanodevices and structures, Journal of Nanoparticle Research 10 (2008) 947–954.
[12] S. Kumar, S.-H. Yoon, G.-H. Kim, Bridging the nanogap electrodes with gold nanoparticles using dielectrophoresis technique, Current Applied Physics 9 (2009) 101–103.
[13] S.I. Khondaker, K. Luo, Z. Yao, The fabrication of single-electron transistors using dielectrophoretic trapping of individual gold nanoparticles, Nanotechnology 21 (2010) 095204.
[14] L. Bernard, M. Calame, S.J. van der Molen, J. Liao, C. Schönenberger, Controlled formation of metallic nanowires via Au nanoparticle ac trapping, Nanotechnology 18 (2007) 235202.
[15] C.T. Harrower, D.R. Oliver, Electronic transport in dielectrophoretically grown nanowires, Journal of Materials Science 41 (2006) 8166–8172.
[16] J.M. Slocik, S.N. Kim, T. Auvil, E.R. Goldman, J. Liu, R.R. Naik, Single domain antibody templated nanoparticle resistors for sensing, Biosensors and Bioelectronics 25 (2010) 1908–1913.
[17] J. Lee, S. Mubeen, C.M. Hangarter, A. Mulchandani, W. Chen, N.V. Myung, Selective and rapid room temperature detection of H2S using gold nanoparticle chain arrays, Electroanalysis 23 (2011) 2623–2628.
[18] A. Zabet-Khosousi, A.-A. Dhirani, Charge transport in nanoparticle assemblies, Chemical Reviews 108 (2008) 4072–4124.

Biographies

Christian Leiterer studied biochemistry at the Friedrich-Schiller-University in Jena. Right now he is completing his PhD at the IPHT (Institute of Photonic Technology).

Steffen Berg studied biomedical-engineering at the University of Applied Science in Jena. He finished his diploma thesis 2011 at the IPHT Jena.

Antti-Pekka Eskelinen received his MSc degree in Physics from University of Jyväskylä, Finland and he is at the moment a PhD student at the Aalto University, School of Science, Espoo, Finland. His research interests are DNA nanotechnology and plasmonics.

Andrea Csáki studied biology at the Friedrich-Schiller-University Jena (Germany). Diploma thesis and following PhD work were completed in the research group of Dr. Wolfgang Fritzsche at the IPHT Jena. Following her PhD work ("DNA based molecular nanoconstructions: one selected model and their applications by using DNA/DNA and DNA/nanoparticle complexes in planar technical surrounding conditions", 2003) she is working as research scientist on the field of molecular plasmonics at the IPHT.

Matthias Urban studied biomedical-engineering at the University of Applied Science in Jena. He is curently working as an engineer at the IPHT in Jena and is especially interessted in applied electronics and device development.

Päivi Törmä is a professor at the Department of Applied Physics, Aalto University, Finland, leading the Quantum Dynamics group since 2007. She received her PhD at the University of Helsinki and was PostDoc at the University of Ulm and the University of Innsbruck. Her research interests are quantum dynamics, plasmonics and DNA-nanotechnology.

Wolfgang Fritzsche heads the Nano Biophotonics Department at the Institute of Photonic Technology (IPHT) in Jena, Germany since 2001. He received his PhD at the Max-Planck-Institute for Biophysical Chemistry in Göttingen and was PostDoc at Iowa State University. His research interests are molecular plasmonics and nanotechnology with a special focus on DNA-nanostructure complexes and their integration into chip environments for bioanalytical and nano photonic applications.

6.1.5 Applying contact to individual silicon nanowires using a dielectrophoresis (DEP) based technique [CL5]

Christian, Leiterer:	Konzeptentwicklung Herstellung des Sensors Messungen und Evaluierung der Daten Diskussion des Konzepts und der Ergebnisse Diskussion und Korrektur des Manuskripts
Gerald, Brönstrup:	Herstellung der Nanodrähte Diskussion und Korrektur des Manuskripts
Norbert Jahr:	Diskussion und Korrektur des Manuskripts
Matthias, Urban:	Unterstützung bei den Messungen
Cornelia Arnold:	Entwicklung des Chiplayouts Diskussion und Korrektur des Manuskripts
Silke Christiansen:	Diskussion und Korrektur des Manuskripts
Wolfgang, Fritzsche:	Diskussion des Konzepts und der Ergebnisse Diskussion und Korrektur des Manuskripts

Journal of Nanoparticle Research 15, **2013**, 5, 1-7

J Nanopart Res (2013) 15:1628
DOI 10.1007/s11051-013-1628-z

BRIEF COMMUNICATION

Applying contact to individual silicon nanowires using a dielectrophoresis (DEP)-based technique

Christian Leiterer · Gerald Broenstrup · Norbert Jahr · Matthias Urban · Cornelia Arnold · Silke Christiansen · Wolfgang Fritzsche

Received: 7 January 2013 / Accepted: 30 March 2013

Abstract One major challenge for the technological use of nanostructures is the control of their electrical and optoelectronic properties. For that purpose, extensive research into the electrical characterization and therefore a fast and reliable way of contacting these structures are needed. Here, we report on a new, dielectrophoresis (DEP)-based technique, which enables to apply sufficient and reliable contact to individual nanostructures, like semiconducting nanowires (NW), easily and without the need for lithography. The DEP contacting technique presented in this article can be done without high-tech equipment and monitored in situ with an optical microscope. In the presented experiments, individual SiNWs are trapped and subsequently welded between two photolithographically pre-patterned electrodes by applying varying AC voltages to the electrodes. To proof the quality of these contacts, I–V curves, photoresponse and photoconductivity of a single SiNW were measured. Furthermore, the measured photoconductivity in dependence on the wavelength of illuminated light and was compared with calculations predicting the absorption spectra of an individual SiNW.

Keywords Nanowire · Dielectrophoresis · Contact · Silicon

C. Leiterer (✉) · N. Jahr · M. Urban · C. Arnold · S. Christiansen · W. Fritzsche
Institute of Photonic Technology, Albert-Einstein-Straße 9, 07745 Jena, Germany
e-mail: christian.leiterer@gmail.com

G. Broenstrup · S. Christiansen
Max-Planck-Institute for the Science of Light, Günther-Scharowsky-Str. 1, Bau 24, 91058 Erlangen, Germany

Introduction

One-dimensional nanostructures such as nanowires (NW) or carbon nanotubes have just recently reached sufficient maturity to be used in nanoelectronic (Thelander et al. 2008; Hsueh et al. 2007; Tans et al. 1998; Cui 2001; McEuen et al. 2002; Evoy et al. 2004; Baughman et al. 2002) and optoelectronic devices (Svensson et al. 2008; Zhou et al. 2007; Kim et al. 2007; Dayeh et al. 2007). Due to their small-size, well-defined shape and crystalline structure that determine their unique physical properties especially semiconducting nanowire are of special interest in the scientific community. In addition, many bottom-up synthesis approaches to obtain NW or carbon nanotubes are particularly inexpensive and promise ultra-sensitive detection abilities (Wang and Gates 2009). The main challenge left to fabricate market-ready devices with nanowires as key elements is to find a way to apply electrical contact to them in a reliable, parallel, and inexpensive manner (Erdem Alaca 2009).

Here, we address this fundamental challenge by presenting a method which is able to establish reliable electrical contacts to semiconducting NW such as

Published online: 07 April 2013

SiNW based on DEP. It is parallelizable and does not require expensive equipment to apply electrical contact to NW on pre-patterned electrode arrays. Therefore, this method can be used for fast and easy electrical characterization of nanoscale structures in a standard laboratory. For years, dielectrophoresis (DEP) has proven to be a promising technique for the integration of individual micro- and nanoscale objects (Pohl and Crane 1971; Smith et al. 2000; Mueller et al. 1996; Chen et al. 2001; Washizu et al. 1994; Raychaudhuri et al. 2009; Wolff et al. 2008; Kretschmer and Fritzsche 2004). However, often the contacted structures show high contact resistance and therefore require additional lithographic or chemical treatment to realize the desired ohmic contact. With the described method, we could overcome this problem. However, the presented technique does not claim to provide better contacts than established methods like contacting by E-beam lithography or using thermal annealing. Nevertheless, this method can be especially favorable for sensitive samples which can be damaged by the harsh conditions coming along with the previous mentioned methods.

The DEP technique consist of three simple steps controlled by an applied AC field: (1) pulling the nanowire to the electrode (Fig. 1a), (2) trapping the nanowire in the desired position (Fig. 1b), and (3) fixation and realization of contact by voltage pulse-induced welding to the nanowire (Fig. 1c). The applicability is shown exemplary for SiNW, but the technique can be applied to other dispersed nanostructures such as nanoparticle or nanowires made from conducing or semiconducting materials.

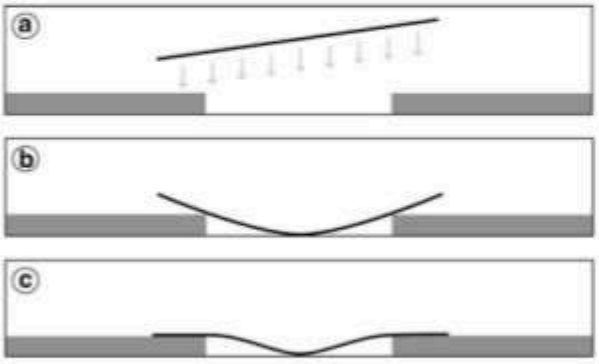

Fig. 1 Scheme for DEP trapping and fixing. **a** The NW is attracted to the microelectrode gap by DEP. **b** The NW is fixed on the electrodes by DEP and welded **c** to the electrodes by short pulses with higher voltage

In the experiments, we show that it is possible to establish contacts which are stable under application of up to 3 μA through a single *n*-doped SiNW. Furthermore, we could characterize contacts by I–V curves, and proof the applicability by measuring photoresponse and wavelength-dependent photoconductivity of a single SiNW using a halogen light source and metal interference filters for tuning the illuminated wavelength. Furthermore, with the obtained data from the wavelength-dependent photoconductivity measurements show an agreement with the calculated absorption maximum of the measured SiNW.

Experimental

SiNW synthesis

The SiNWs are realized by the bottom-up vapor–liquid–solid (VLS) growth technique (Wagner and Ellis 1964). The VLS growth of SiNW is based on the metal (here gold) catalyzed one-dimensional growth using silane as the source of silicon for the NW growth. Silane in Argon (4 sccm silane and 4 or 3.5 sccm argon) is used in a chemical vapor deposition process (CVD) in a home built reactor using pieces of Si (111) wafers as the growth substrate. Two samples are grown at temperatures of ~600 °C, one with undoped SiNW (620 °C) and one with phosphorous-doped *n*-type SiNW (640 °C) at a total chamber pressure of 2.0 mbar. To dope SiNW, 0.5 sccm of 2 % PH_3 in Helium is admitted into the chamber during growth as well. SiNW grown under similar conditions have shown a phosphor doping of roughly 10^{19}–10^{20} at./cm^3 (Schmid et al. 2009). The VLS-grown SiNWs from both samples were removed from their growth substrates by sonication in deionised water.

Dielectrophoresis-assisted welding technique to apply contact to NW

The proposed technique for trapping and contacting of NW is described in detail as follows: the NW, dispersed in deionized water or in another non-conducting solution, is applied to a microchip prepared using standard photolithography to realize the microelectrodes on a glass or silicon substrate. A schematic is shown to illustrate how the DEP

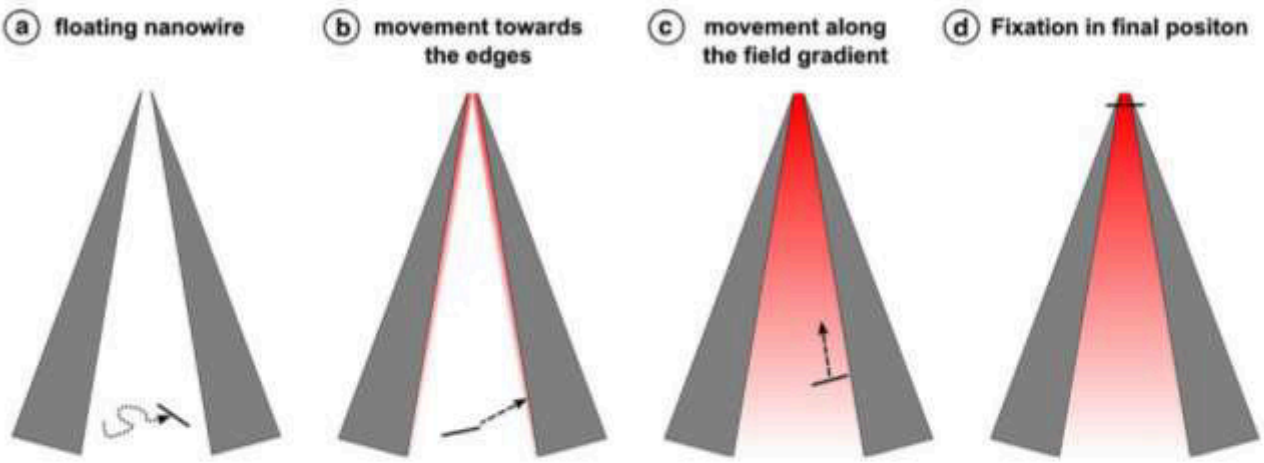

Fig. 2 Schematic illustration of DEP-induced trapping and fixation of single nanowire. A nanowire floating far away from the electrode gap can be moved easily toward it by using such tapered electrode geometry. **a** A nanowire floating near the electrode, no voltage is applied. **b** By applying voltage to the electrodes, the NW is drawn to an electrode quickly, without sticking to it. **c** Due to the increasing field intensity (due to the decrease of the electrode distance), the nanowire is moving toward the electrode gap until it reaches its final position. **d** In the final position, the nanowire can be fixed by applying a short higher voltage pulse so that a sufficient electrical contact can be established

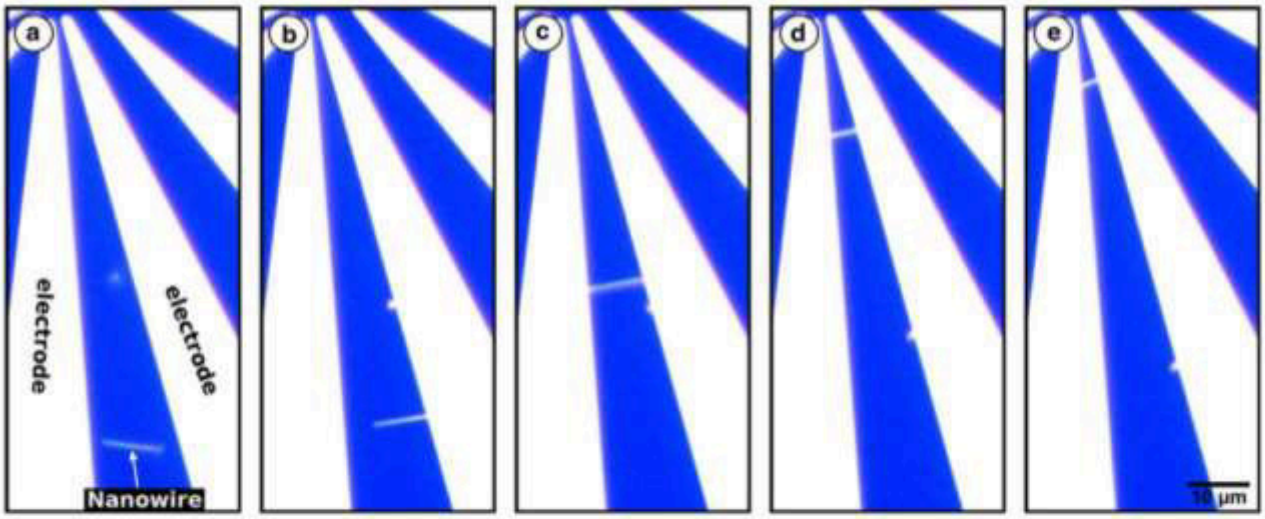

Fig. 3 Real-time imaging of the DEP trapping and welding: a single SiNW during DEP trapping and fusing. **a** Floating of a dispersed SiNW next to the microelectrodes. **b** 0.3 V is applied between the two neighboring electrodes, the SiNW moves to the electrodes. **c**, **d** Continuous application of the voltage leads to SiNW moving along the field gradient to the electrode tips. **e** SiNW is fixed by welding in the final position by application of several short AC pulses at 5 V

technique can be used to apply contact to a nanowire, even for low nanowire concentrations (Fig. 2). Promoted by tapered electrode geometry, nanostructures can be moved along following a field gradient toward their desired position (electrode gap of about 4 µm at the tip, cf. Fig. 4). In this position, the nanostructures can be fixed and contacted, which will be described in detail later on. By using similar electrode geometries and DEP conditions, this technique presents a low cost method to contact and characterize individual nanostructures electrically, even if there are only present in low concentrations. To start the trapping process, an AC voltage (1 MHz, 0.3 V) is applied to the electrodes until a NW is attracted to them. As soon as the NW is touching one of the electrodes, it is slowly drawn to the electrode gap located in the center of the chip following the field gradient (Fig. 3a). The tapered geometry of the electrodes on the chip promotes this

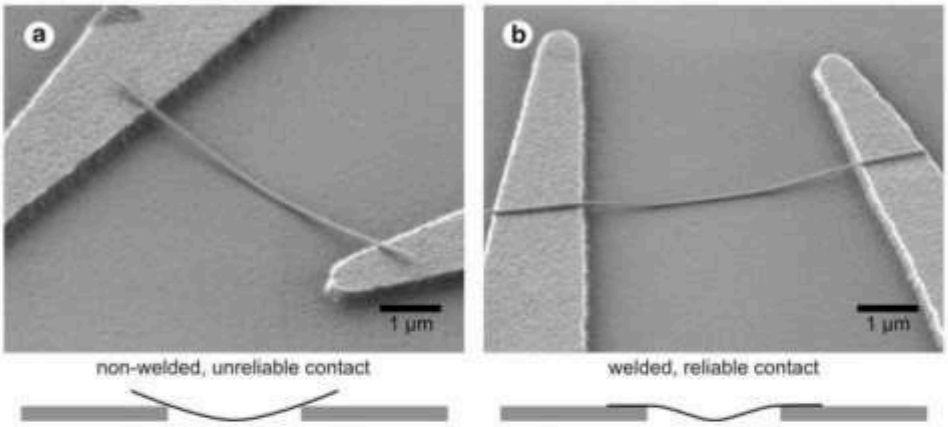

Fig. 4 SEM image of DEP-trapped SiNW. The schematic image on the *bottom* illustrates the behavior of the SiNW on the electrode. **a** Trapped SiNW without welding having insufficient contact to the electrodes. **b** SiNW welded to the electrodes with short pulse of higher voltage is closely clinging on the electrodes, which provides reliable contacts for electrical measurements

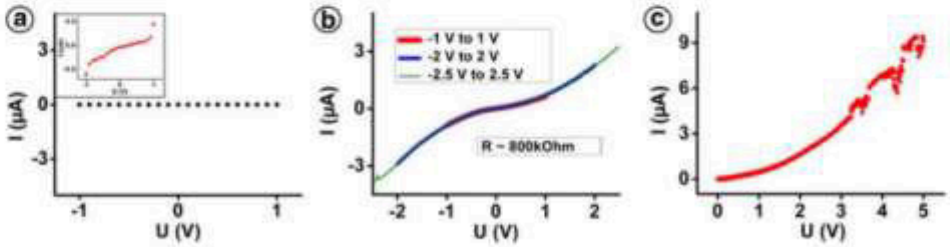

Fig. 5 **a** I–V characteristic of a non-welded *n*-type SiNW showing ~3 orders of magnitude higher resistance. **b** I–V characteristic of an individual *n*-type SiNW using the described welding technique. The *curves* are showing stable a current and no changes during several measurements. **c** Typical I–V characteristic of a *n*-type SiNW using welding technique. The current is showing unstable behavior above 3 V

movement. The NW moves toward the electrode gap and will stay at this point as long as the voltage is applied. In the next step, the NW is welded to the electrodes using a much higher AC voltage than in the first attachment step. This step is the key to establish low contact resist between NW and electrode and will be described in detail later on. The entire attachment and welding processes can be monitored in real-time using an optical microscope (AxioImager Z1m/AxioCam MRc5, Carl Zeiss, Jena, Germany) (Fig. 3).

The DEP method also permits to select a single NW with desired properties such as length, shape, or diameter. Undesired NW can be easily deselected by turning off the voltage. The NW will then be released and moved away from the electrodes due to *Brownian motion*. An appropriate single NW can be firmly attached (welding) to the electrode by using several short AC pulses (0.2–1 s) at 5 V, 1 MHz. After the welding process, the remaining dispersed NWs are removed by washing with deionized water prior to drying using compressed air.

In order to study the quality of the contacts made with our technique, two kinds of SiNW were contacted for subsequent measurements: undoped SiNWs are utilized to demonstrate photoconductivity of single SiNW, and *n*-type SiNW are used to characterize the electrical properties of a single SiNW by measuring I–V curves. All measurements are carried out using DC voltage applied by a sourcemeter (Model 2400, Keithly, Cleveland, OH).

Results and discussion

A SiNW contacted with the proposed technique (welded) is compared to a non-welded SiNW by SEM imaging (Fig. 4). The ends of the SiNW shown in Fig. 4b are closely clinging on the electrodes due to the welding process, while the terminal regions of a non-welded SiNW have only contact to the edges of the electrodes. These small contact areas explain the insufficient contact for electrical measurements.

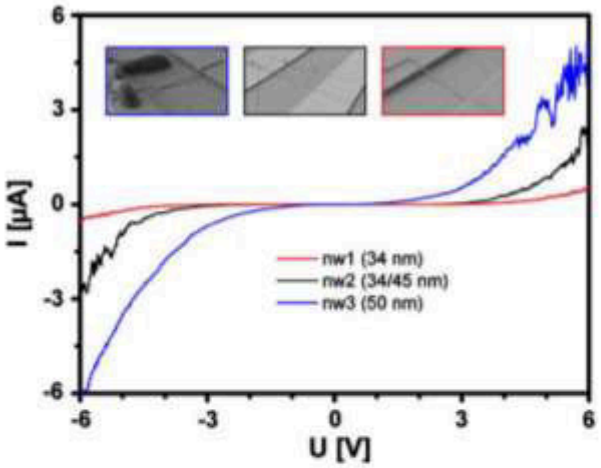

Fig. 6 I–V characteristics of single nanowires. Resistance of the nanowire decreases with increasing diameter. Their resistivity measured at 6 V reaches from ~1–10 MΩ

For the electrical characterization, the welded SiNW, I–V characteristics are recorded for an individual *n*-type SiNW. If the SiNW is welded to electrodes, it shows an average resistance of about 800 kΩ [Fig. 5, $I(-2\ \text{V})$ to $-2.9\ \mu\text{A}$, $I(+2\ \text{V})$–$2.3\ \mu\text{A}$]. If not, its resistance is about 3 orders of magnitude higher, so that there is nearly no measurable contact (Fig. 5a). To proof that the proposed technique provides stable contacts, several I–V measurements are recorded using identical conditions with increasing voltage (Fig. 5b). The resulting I–V curves show nearly identical behavior, no hysteresis is visible. Further, I–V measurements with voltages above 3 V show destabilization of the current; above 5 V the NW is irreversibly damaged (Fig. 5c).

In order to proof the reproducibility of the technique, several NWs with different diameters were contacted and I–V characteristics were recorded. The results show that nanowire with large diameter showing less resistivity as expected. All NWs have a length of between 5 and 7 µm which does not seem to have a strong influence. The contact area between nanowire and electrode is about half its length at all samples and therefore provides stable contact. The according results are shown in Fig. 6.

Furthermore, it is possible to measure photoconductivity of a single undoped SiNW contacted by the proposed technique. Therefore, the contacted SiNW is illuminated using a mercury arc-discharge lamp (X-Cite 120Q, Lumen Dynamics, Mississauga, Canada). In order to take a look at the photoresponse of an individual SiNW, the illuminated light is switched on and off several times while recording the current (Fig. 7a). The current follows the illumination with essentially no delay. However, the measurements are not intended to measure the photoresponse time and thus the time resolution of the experiment is on the order of tenths of a second. During illumination, the current is about 300 times higher ($I \sim 30$ nA) than the current measured for the non-illuminated intentionally undoped SiNW ($I \sim 0.1$ nA).

In a next step, the wavelength dependence of the photoconductivity of a single-welded SiNW is analyzed and compared to its calculated absorption efficiency. In order to be able to compare the calculated wavelength depended absorption with the measured photocurrent, the photocurrent I_{ph} is normalized with respect to the intensity of the

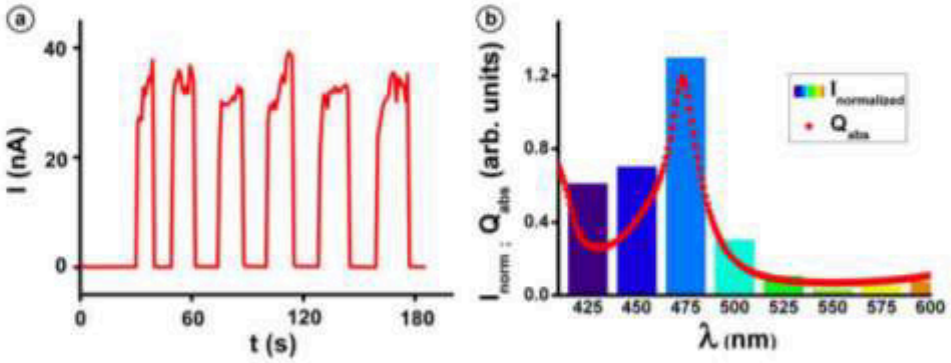

Fig. 7 Photoresponse of a single undoped SiNW contacted by DEP-assisted welding. 10 V (DC) was applied in (**a**, **b**). **a** Photoresponse over the time for an alternately illuminated (on/off) SiNW using the full spectra (*white light*). **b** Wavelength dependency of the normalized photocurrent I_{norm} (using monochromatic light provided by metal interference filters) correlated with calculated absorption efficiencies Qabs of the SiNW

illuminating light I_L. It is assumed that the photocurrent I_{ph} is proportional to I_L. Thus, the normalized photocurrent I_{norm} is given by $I_{norm} = I_{ph} / I_L$. In this experiment, interference filtering permits the illumination with a selected, tunable wavelength of a step width of 25 nm. For the normalization, the intensity of the illuminating light IL for each filter is measured using an optical microscope in bright field geometry with a fiber-coupled spectrometer (SpectraPro 2300i, Princeton Instruments, Trenton, NJ).

For the comparison, the optical absorption efficiencies of SiNW for non-polarized light are calculated using Mie theory (Bohren 1983). For this purpose, the refractive index of bulk silicon (Palik 1998) is assumed for the SiNW. The calculations show that the absorption efficiency of an individual SiNW strongly depends on its diameter. This can be explained by the so called optical antenna effect (Cao et al. 2010; Brönstrup et al. 2010, 2011). The diameter of the illuminated SiNW is measured by SEM imaging, yielding a diameter of $\sim$130 nm.

Finally, the results show that the normalized photocurrent I_{norm}, induced by the illuminated light strongly depends on its wavelength as well, and the experimentally observed values are in good agreement with our calculated absorption efficiency (Fig. 7b).

Conclusion

The dielectrophoretic contacting and welding technique provide not only an efficient tool to trap and align individual nanoscale objects such as NW, but also offers the option to integrate bottom-up nanoscale structures into top-down electronics without using any expensive post processing techniques and nanolithography steps. Hereby tapered electrodes can be used as "electrical tweezers" to wire single nanostructures for subsequent electrical characterization realizing a reliable contact. The *n*-type SiNWs contacted to titanium electrodes have proven to be stable for up to at least 3 μA. Furthermore, it was possible to measure the photoresponse and the photocurrent as a function of the illuminating wavelength of an individual SiNW. In order to verify the measured results of the wavelength-dependent photocurrent, the data was compared to the Mie calculated absorption efficiency for the utilized SiNW. Good agreement between calculated and experimental data could be obtained.

Acknowledgments We thank Andrea Csaki and Janina Wirth for valuable comments and discussions, and Franka Jahn for SEM imaging. The work was supported by BMBF Project NAWION (FKZ: 16SV5386K, V4MNI014) and DAAD Project PPP Finland (FKZ: 50020468).

References

Baughman RH, Zakhidov AA, De Heer WA (2002) Carbon nanotubes—the route toward applications. Science 297:787–792

Bohren C (1983) Absorption and scattering of light by small particles. Wiley, New York

Brönstrup G, Jahr N, Leiterer C, Csáki A, Fritzsche W, Christiansen S (2010) Optical properties of individual silicon nanowires for photonic devices. ACS Nano 4:7113–7122

Brönstrup G, Leiterer C, Jahr N, Gutsche C, Lysov A, Regolin I, Prost W, Tegude FJ, Fritzsche W, Christiansen S (2011) A precise optical determination of nanoscale diameters of semiconductor nanowires. Nanotechnology 22:385201

Cao L, Fan P, Vasudev AP, White JS, Yu Z, Cai W, Schuller JA, Fan S, Brongersma ML (2010) Semiconductor nanowire optical antenna solar absorbers. Nano Lett 10:439–445

Chen XQ, Saito T, Yamada H, Matsushige K (2001) Aligning single-wall carbon nanotubes with an alternating-current electric field. Appl Phys Lett 78:3714

Cui Y (2001) Functional nanoscale electronic devices assembled using silicon nanowire building blocks. Science 291:851–853

Dayeh SA, Soci C, Yu PKL, Yu ET, Wang D (2007) Transport properties of InAs nanowire field effect transistors: the effects of surface states. J Vac Sci Technol B 25:1432

Erdem Alaca B (2009) Integration of one-dimensional nanostructures with microsystems: an overview. Int Mater Rev 54:245–282

Evoy S, DiLello N, Deshpande V, Narayanan A, Liu H, Riegelman M, Martin BR, Hailer B, Bradley J-C, Weiss W, Mayer TS, Gogotsi Y, Bau HH, Mallouk TE, Raman S (2004) Dielectrophoretic assembly and integration of nanowire devices with functional CMOS operating circuitry. Microelectron Eng 75:31–42

Hsueh T-J, Chang S-J, Hsu C-L, Lin Y-R, Chen I-C (2007) Highly sensitive ZnO nanowire ethanol sensor with Pd adsorption. Appl Phys Lett 91:053111

Kim A, Ah CS, Yu HY, Yang J-H, Baek I-B, Ahn C-G, Park CW, Jun MS, Lee S (2007) Ultrasensitive, label-free, and real-time immunodetection using silicon field-effect transistors. Appl Phys Lett 91:103901–103903

Kretschmer R, Fritzsche W (2004) Pearl chain formation of nanoparticles in microelectrode gaps by dielectrophoresis. Langmuir 20:11797–11801

McEuen PL, Fuhrer MS, Park H (2002) Single-walled carbon nanotube electronics. IEEE Trans Nanotechnol 1:78–85

Mueller T, Fiedler S, Schnelle T, Ludwig K, Jung H, Fuhr G (1996) High frequency electric fields for trapping of viruses. Biotechnol Technol 10 Online. http://www.springerlink.com/index/10.1007/BF00184018

Palik E (1998) Handbook of optical constants of solids. III (Academic Press) Online. http://www.worldcat.org/oclc/190842545

Pohl H, Crane J (1971) Dielectrophoresis of cells. Biophys J 11:711–727

Raychaudhuri S, Dayeh SA, Wang D, Yu ET (2009) Precise semiconductor nanowire placement through dielectrophoresis. Nano Lett 9:2260–2266

Schmid H, Björk MT, Knoch J, Karg S, Riel H, Riess W (2009) Doping limits of grown in situ doped silicon nanowires using phosphine. Nano Lett 9:173–177

Smith PA, Nordquist CD, Jackson TN, Mayer TS, Martin BR, Mbindyo J, Mallouk TE (2000) Electric-field assisted assembly and alignment of metallic nanowires. Appl Phys Lett 77:1399

Svensson CPT, Mårtensson T, Trägårdh J, Larsson C, Rask M, Hessman D, Samuelson L, Ohlsson J (2008) Monolithic GaAs/InGaP nanowire light emitting diodes on silicon. Nanotechnology 19:305201

Tans SJ, Verschueren ARM, Dekker C (1998) Room-temperature transistor based on a single carbon nanotube. Nature 393:49–52

Thelander C, Froberg LE, Rehnstedt C, Samuelson L, Wernersson L-E (2008) Vertical enhancement-mode InAs nanowire field-effect transistor with 50-nm wrap gate. IEEE Electron Device Lett 29:206–208

Wagner RS, Ellis WC (1964) Vapor–liquid–solid mechanism of single crystal growth. Appl Phys Lett 4:89

Wang MCP, Gates BD (2009) Directed assembly of nanowires. Mater Today 12:34–43

Washizu M, Suzuki S, Kurosawa O, Nishizaka T, Shinohara T (1994) Molecular dielectrophoresis of biopolymers. IEEE Trans Ind Appl 30:835–843

Wolff A, Leiterer C, Csaki A, Fritzsche W (2008) Dielectrophoretic manipulation of DNA in microelectrode gaps for single-molecule constructs. Front Biosci 13:6834–6840

Zhou H, Wissinger M, Fallert J, Hauschild R, Stelzl F, Klingshirn C, Kalt H (2007) Ordered, uniform-sized ZnO nanolaser arrays. Appl Phys Lett 91:181112

6.1.6 DNA hybridization assay at individual, biofunctionalized zinc oxide nanowires [CL6]

Christian, Leiterer:	Konzeptentwicklung Messungen und Evaluierung der Daten Diskussion des Konzepts und der Ergebnisse Diskussion und Korrektur des Manuskripts
Barbara, Seise:	Konzeptentwicklung Messungen und Evaluierung der Daten Diskussion des Konzepts und der Ergebnisse Diskussion und Korrektur des Manuskripts
Irma, Slowik:	Messungen und Evaluierung der Daten Diskussion und Korrektur des Manuskripts
Gerald, Brönstrup:	Herstellung der Nanodrähte Diskussion und Korrektur des Manuskripts
Raphael, Niepelt:	Diskussion und Korrektur des Manuskripts
Karina, Weber:	Diskussion und Korrektur des Manuskripts
Carsten, Ronning:	Diskussion und Korrektur des Manuskripts
Silke, Christiansen:	Diskussion und Korrektur des Manuskripts
Wolfgang, Fritzsche:	Diskussion des Konzepts und der Ergebnisse Diskussion und Korrektur des Manuskripts

Journal of Biophotonics, **2013**, 6, No. 2, 143–147

J. Biophotonics 6, No. 2, 143–147 (2013) / DOI 10.1002/jbio.201200023

Journal of BIOPHOTONICS

LETTER

DNA hybridization assay at individual, biofunctionalized zinc oxide nanowires

Christian Leiterer[*, **,1], *Barbara Seise*[**,1], *Irma Slowik*[2], *Gerald Brönstrup*[3], *Raphael Niepelt*[2], *Karina Weber*[1], *Carsten Ronning*[2], *Silke Christiansen*[1,3], *and Wolfgang Fritzsche*[1]

[1] Institute of Photonic Technology, Albert-Einstein-Straße 9, 07745 Jena, Germany
[2] Institute for Solid State Physics, Friedrich Schiller University of Jena, Max-Wien-Platz 1, 07743 Jena, Germany
[3] Max-Planck-Institute for the Science of Light, Günther-Scharowsky-Str. 1, Bau 24, 91058 Erlangen, Germany

Received 13 February 2012, revised 15 March 2012, accepted 16 March 2012
Published online 16 April 2012

Key words: DNA, silicon nanowire, zinc oxide, silanization, hybridization

Reliable and efficient identification of DNA is a major goal in on-site diagnostics. One dimensional nanostructures like nanowires (NW) represent potential sensor structures due to their extreme surface-to-bulk ratio, enabling enhanced biomolecule binding which results in optimal signals. While silicon NW are already well studied, NW made from other materials with promising properties like ZnO are not yet established as NW sensor material for bioanalytics. Here we demonstrate the DNA functionalization of ZnO NW even at the single NW level and their successful application in a DNA hybridization assay.

Immobilization of capture DNA on the nanowires (left). Hybridization of immobilized capture DNA with dye labelled target DNA (center). Fluorescence detection of dye labelled double-stranded DNA (right).

1. Introduction

One dimensional nanostructures such as semiconducting nanowires (NW) and carbon nanotubes become more and more suitable transducer elements for chemical [1] and biological sensors [2–10]. Because of their particularly favorable surface-area-to-volume ratio, they are promising ultra-sensitive key elements in future sensing devices [11–13]. Furthermore, these structures can be fabricated in high quantities at low cost using bottom up techniques such as chemical synthesis and vapor-liquid-solid (VLS) growth, and are therefore preferred compared to the more expensive lithographic (top-down) nanostructures.

Silicon nanowires (SiNWs) are promising transducer for bioanalytics with electrical readout, which was demonstrated for both top-down [3, 6, 9, 14, 15] and bottom-up [2, 16–18] structures. While Si technology is widely established in semiconductor industry, the performance of SiNWs can be limited due to the native oxide layer occurring when exposed to and oxygen containing atmosphere [19]. Other materials like ZnO do not have this problem and show a high stability under ambient conditions. Moreover, ZnO provides superior electronic properties regard-

* Corresponding author: e-mail: christian.leiterer@gmail.com, Phone: +49 3641 206 349, Fax: +49 3641 206 399
** These authors contributed equally to this work

Journal of BIOPHOTONICS

ing a large, direct band gap in the visible region, and show exitonic luminescence at room temperature. However, in order to access this potential, the development of techniques for mass production as well as manipulation and biofunctionalization is required. Whereas ZnONW synthesis is established [20], biofunctionalization of ZnONW (such as with DNA) was rarely attempted [21, 22].

Here, we characterize capture DNA functionalization of single ZnONW. We therefore demonstrate the successful hybridization of fluorescently-labeled target DNA to their complementary capture DNA immobilized at the NW surface. The specificity of this reaction is characterized using non-complementary DNA as negative control. The results show that such one dimensional ZnO nanostructures can be biofunctionalized and therefore serve as useful substrates for future microarray devices. One advantage of these one dimensional nanostructures is their potential to serve as a highly sensitive transducer with electrical readout. Such a sensor would detect changes in conductivity of the NW due to a field effect induced by the binding of natively charged biomolecules, which work like a gate-electrode in a field effect transistor. This approach enables marker free DNA or protein detection systems.

2. Experimental

2.1 Preparation of SiNW samples

The SiNW are grown by the bottom-up VLS mechanism [23] based on the gold (Au nanoparticles, 60–80 nm) catalyzed one-dimensional growth using silane as the source of silicon for the NW growth. Further details are described in [24]. Silane in Argon (4 sccm silane and 4 sccm or 3.5 sccm argon) is used in a chemical vapor deposition process (CVD) in a home built reactor using pieces of Si (111) wafers as growth substrate. The samples are grown at temperatures of ~600 °C with a total chamber pressure of 2.0 mbar. The VLS-grown SiNW were removed from their growth substrates by sonication in deionized water or imprinting technique. Typical wire dimensions are 30–150 nm in diameter and 5–15 µm in length.

2.2 Preparation of ZnONW samples

The ZnONW samples were synthesized via vapor-liquid-solid (VLS) process [25]. ZnO powders as source material were positioned at the center of a horizontal tube furnace, which was heated to 1350 °C. Silicon substrates covered with a 5–10 nm thick Au film were placed at a position in the furnace where the temperature ranges around 1050 °C. The vapor was transported by Ar gas flow of 50 sccm to the substrates, at a pressure of 100 mbar and growth time between 30 and 40 min. The ZnONWs evolve in a typical spaghetti-like structure with wire diameters around 100–300 nm and wire lengths of up to some tens of µm.

2.3 Silanization of NW samples

In order to be able to perform a silanization reaction on the NW surface, both the SiNW and ZnONW samples were chemically activated using oxygen plasma which hydroxylates the surface (Plasma System 200 G, Technics Plasma GmbH, München). The etching process is carried out at a pressure of 1.6 mbar at 380 W for at least 30 min.

The silanization of the NW surface was performed as described previously [26]. Briefly, incubation was at 70 °C for 3 h using glycidoxypropyltrimethoxysilane (GOPS) in water-free toluene [27], prior to several washing steps in pure toluene and drying with compressed air.

2.4 Biomodification and hybridization of the NW

Amino-modified oligonucleotides are used for the immobilization of the capture DNA to the GOPS-silanized NW surface. The amino-group is located on the 5'-terminus of the oligonucleotides and forms an imine in a condensation reaction with the epoxy group of the GOPS, which provides a stable attachment of the capture DNA to the surface (Figure 1). The terminal amino-modified oligonucleotides are applied at a concentration of 10 µM in 5 × PBS (pH 7.4) and are incubated on the NW substrate until desiccation. Subsequently the NW are exposed to UV light, washed afterwards in 15 mM tris-HCl (pH 8.0) and dried using compressed air [28].

In order to proof the ability of the NW to act as a substrate for the sequence specific detection of DNA, a DNA hybridization reaction was performed with complementary as well as non-complementary target DNA at room temperature in 5 × PBS (pH 7.4) for at least 2 hrs. The used oligonucleotides are listed in Table 1. Complementary implies the sequence complementarity to the target DNA.

The following three different approaches for the DNA modification of NW are illustrated in Figure 3

LETTER

J. Biophotonics 6, No. 2 (2013) 145

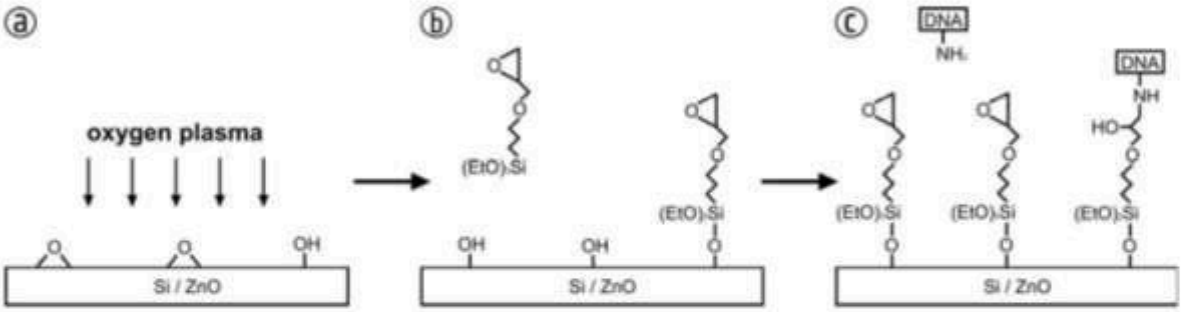

Figure 1 Scheme of the chemical reaction used to immobilize the capture DNA to the surface of ZnONW and SiNW. (**a**) Activation of the NW surface by oxygen plasma resulting in surface hydroxylation. (**b**) Silanization of the surface with glycidoxypropyltrimethoxysilane (GOPS). (**c**) Amino-modified capture DNA reacts with GOPS forming a stable attachment of the capture DNA to the surface.

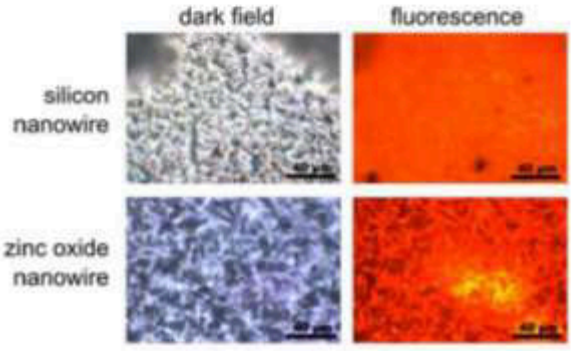

Figure 2 (online color at: www.biophotonics-journal.org) Immobilization of fluorescence labeled capture DNA to SiNW and ZnONW. Dark field and fluorescence measurements are compared confirming DNA binding at the NW.

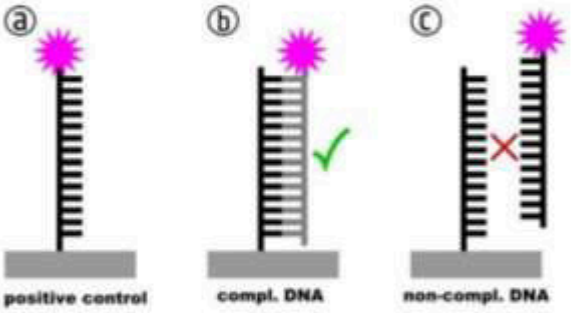

Figure 3 (online color at: www.biophotonics-journal.org) Three different approaches on SiNW and ZnONW samples, respectively, are compared. (**a**) Positive control: Immobilization of Cy3-labeled capture DNA. (**b**) Complementary DNA: Cy3-labeled target DNA hybridized to complementary capture DNA. (**c**) Non-complementary DNA: Cy3-labeld target DNA applied to non-complementary capture DNA.

and compared later on in the results and discussion section:

Approach 1: The **positive control**, which is an amino-modified and Cy3-labelled DNA, is immobilized onto the NW to proof the successful immobilization of capture DNA to the NW (Figure 3a). No further hybridization is done.

Approach 2: Complementary capture **DNA** (see Table 1) is immobilized onto the NW. The Cy3-labelled target DNA (see Table 1) is used in a following hybridization reaction to proof the successful binding (Figure 3b).

Approach 3: Non-Complementary capture **DNA** (see Table 1) is immobilized onto the NW. The Cy3-labelled target DNA (see Table 1) is used in a subsequent hybridization reaction to proof absence of significant non specific binding as an important feature for future application (Figure 3c).

Table 1 List of used DNA and oligonucleotides, respectively.

purpose	sequence	modification
Positive control	5′-AGA ATC AAG GAG CAC ATG CTG AAA AAA-3′	5′-Cy3 3′-NH_2
Complementary capture DNA	5′-TTT TTT CAG CAT GTG CTC CTT GAT TCT ATG-3′	5′-NH_2
Non-Complementary capture DNA	5′-ACT GAC TGA CTG ACT GAC TGA CTG GGC GGC GAC CT-3′	3′-NH_2
Target DNA	5′-CAT AGA ATC AAG GAG CAC ATG CTG AAA AAA-3′	5′-Cy3

Journal of BIOPHOTONICS

3. Results and discussion

3.1 Binding of fluorescence labeled DNA to NW substrates

First the efficient immobilization of Cy3 labeled DNA (positive control, see Table 1) to capture-DNA modified NWs is demonstrated. Optical dark field microscopy represents an established method to visualize sub-wavelength structures and was utilized here to image un-labeled NWs. Dark field and fluorescence images are compared in Figure 2 to show the successful binding of the fluorescence labeled DNA to the NW.

These modified NW can be easily removed from the substrate using ultrasonics or imprinting technique. The resulting fluorescence marked single NW are visible by fluorescence and dark field imaging. Semiconducting NW such as SiNW exhibit different color when observed in dark field. The visible color depends on the diameter of the NW as we have shown previousely [24, 29]. Thinner SiNW show a bluish color while thicker ones appear more reddish or even white. As it is visible in Figure 4, NWs of a variety of thicknesses are homogeneously DNA modified.

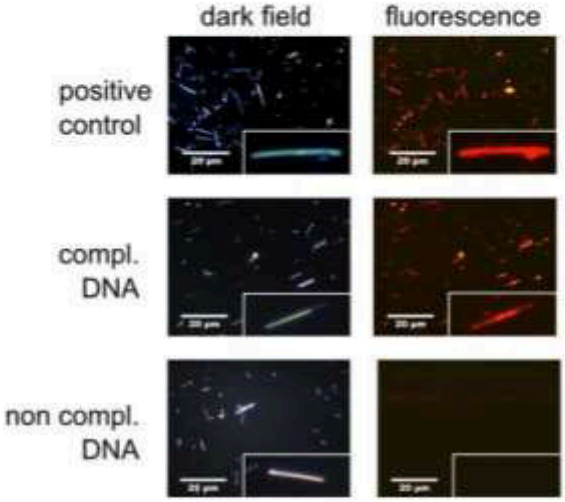

Figure 4 (online color at: www.biophotonics-journal.org) SiNW modified with DNA according to the different approaches (cf. Figure 3). Dark field and fluorescence measurements are compared to show that DNA immobilization and hybridization occurs on the NW. Insets are showing single SiNWs. A strong fluorescence signal of the NWs for the positive control and the complementary target DNA is visible while the NWs with non-complementary target DNA are only visible in the dark field but show no detectable fluorescence signal.

3.2 Detection of sequence specific DNA hybridization on single SiNW and ZnONW

Furthermore, we show the successful detection of complementary target DNA by specific (sequence-complementary) binding on the surface of capture DNA-modified single SiNW and ZnONW. Therefore, the NW are chemically modified with a silane and capture DNA was immobilized as described in the experimental section. Three different approaches from the experimental section are compared in the following results:

In Figures 4 (SiNW) and 5 (ZnONW), NW with the non-complementary capture DNA show no detectable fluorescence, while NW with complementary capture DNA show a bright fluorescence signal. The positive control shows no significant differences in fluorescence intensity compared to the complementary sample in Figures 4 and 5. Therefore, a highly efficient hybridization to the modified NW was achieved.

With these results a sequence-specific DNA recognition is demonstrated on individual ZnONWs. When comparing the fluorescence signal of SiNW and ZnONW, no significant differences in DNA binding efficiencies are visible. Both materials are equally fitting for DNA modification and DNA de-

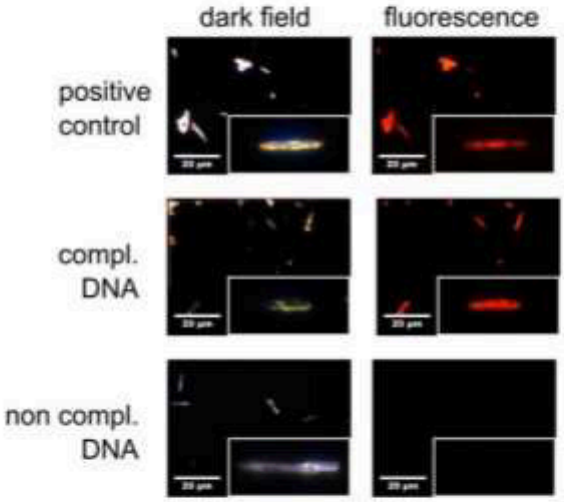

Figure 5 (online color at: www.biophotonics-journal.org) ZnONW modified with DNA accordingly to the different approaches. Dark field and fluorescence measurements are compared in order to show that the immobilization and hybridization of DNA occurs on the NWs. Insets are showing single ZnONWs. A strong fluorescence signal for the positive control and the complementary target DNA is visible. NWs with non-complementary target DNA show no specific fluorescence signal.

LETTER

J. Biophotonics 6, No. 2 (2013) 147

tection using fluorescently-labeled DNA-probes. SO ZnO represents a suitable material for nanoscale DNA sensors.

4. Conclusion

Terminal amino-modified DNA could be immobilized onto ZnONW using standard silane chemistry, which is already established in microarray fabrication for planar silicon or glass substrates. The NW were directly modified on their growth substrate and subsequently being transferred for further investigation or processing. Moreover, it could be demonstrated that the capture DNA immobilized on SiNW and ZnONW serve as basis for following DNA hybridization experiments. The successful detection of complementary DNA was presented. Because non-complementary DNA shows no detectable signal, a high specificity is achieved. With these results we showed the applicability of SiNW and ZnONW, modified with DNA by silane chemistry, for microarray-like NW devices. In future, these results will be used to develop a microarray for the detection of DNA based on the utilized NW. Such microarrays have a great potential to use changes in surface charges due to field effect as signal for the DNA detection as an alternative to fluorescence readout. The results will enable marker-free sequence analysis of DNA with electrical detection.

DNA-functionalized SiNW and ZnONW present highly specific biosensors with a promising high sensitivity for the detection of complementary DNA upon hybridization reaction.

Acknowledgements We thank A. Csaki for valuable comments and discussion. Furthermore, we also thank BMBF project NAWION (FKZ: 16SV5386K, V4MNI014) for financial support.

References

[1] Y. Cui, Science **291**, 851–853 (2001).
[2] J. Hahm and C. M. Lieber, Nano Lett. **4**, 51–54 (2004).
[3] G.-J. Zhang, G. Zhang, J. H. Chua, R.-E. Chee, E. H. Wong, A. Agarwal, K. D. Buddharaju, N. Singh, Z. Gao, and N. Balasubramanian, Nano Lett. **8**, 1066–1070 (2008).
[4] Y. Cui, Science **291**, 851–853 (2001).
[5] E. Stern, J. F. Klemic, D. A. Routenberg, P. N. Wyrembak, D. B. Turner-Evans, A. D. Hamilton, D. A. LaVan, T. M. Fahmy, and M. A. Reed, Nature **445**, 519–522 (2007).
[6] G. J. Zhang, Z. H. H. Luo, M. J. Huang, G. K. I. Tay, and E.-J. A. Lim, Biosens. Bioelectron. **25**, 2447–2453 (2010).
[7] W. C. Maki, N. N. Mishra, E. G. Cameron, B. Filanoski, S. K. Rastogi, and G. K. Maki, Biosens. Bioelectron. **23**, 780–787 (2008).
[8] G.-J. Zhang, M. J. Huang, J. J. Ang, E. T. Liu, and K. V. Desai, Biosens. Bioelectron. **26**, 3233–3239 (2011).
[9] Z. Li, Y. Chen, X. Li, T. I. Kamins, K. Nauka, and R. S. Williams, Nano Lett. **4**, 245–247 (2004).
[10] M. A. Bangar, D. J. Shirale, H. J. Purohit, W. Chen, N. V. Myung, and A. Mulchandani, Electroanalysis **23**, 371–379 (2011).
[11] B. L. Allen, P. D. Kichambare, and A. Star, Adv. Mater. **19**, 1439–1451 (2007).
[12] J. Wang, Analyst **130**, 421 (2005).
[13] F. Patolsky, G. Zheng, and C. M. Lieber, Anal. Chem. **78**, 4260–4269 (2006).
[14] S.-W. Ryu, C.-H. Kim, J.-W. Han, C. J. Kim, C. Jung, H. G. Park, and Y.-K. Choi, Biosens. Bioelectron. **25**, 2182–2185 (2010).
[15] G.-J. Zhang, J. H. Chua, R.-E. Chee, A. Agarwal, S. M. Wong, K. D. Buddharaju, and N. Balasubramanian, Biosens. Bioelectron. **23**, 1701–1707 (2008).
[16] F. Patolsky, Proc. Natl. Acad. Sci. **101**, 14017–14022 (2004).
[17] G. Zheng, F. Patolsky, Y. Cui, W. U. Wang, and C. M. Lieber, Nat. Biotechnol. **23**, 1294–1301 (2005).
[18] Y. Cui, Science **293**, 1289–1292 (2001).
[19] Y. Cui, Z. Zhong, D. Wang, W. U. Wang, and C. M. Lieber, Nano Lett. **3**, 149–152 (2003).
[20] Z. L. Wang, Mat. Sci. Engin.: R: Reports **64**, 33–71 (2009).
[21] C. D. Corso, A. Dickherber, and W. D. Hunt, Biosens. Bioelectron. **24**, 805–811 (2008).
[22] A. Choi, K. Kim, H.-I. Jung, and S. Y. Lee, Sens. Actuators B Chem. **148**, 577–582 (2010).
[23] R. S. Wagner and W. C. Ellis, Appl. Phys. Lett. **4**, 89 (1964).
[24] G. Brönstrup, N. Jahr, C. Leiterer, A. Csáki, W. Fritzsche, and S. Christiansen, ACS Nano **4**, 7113–7122 (2010).
[25] C. Borchers, S. Müller, D. Stichtenoth, D. Schwen, and C. J. Ronning, Phys. Chem. B **110**, 1656–1660 (2006).
[26] R. Niepelt, U. C. Schröder, J. Sommerfeld, I. Slowik, B. Rudolph, R. Möller, B. Seise, A. Csaki, W. Fritzsche, and C. Ronning, Nanoscale Res. Lett. **6**, 511 (2011).
[27] R. Möller, A. Csáki, J. M. Köhler, and W. Fritzsche, Nucleic Acids Res. **28**, E91 (2000).
[28] T. Schüler, A. Nykytenko, A. Csaki, R. Möller, W. Fritzsche, and J. Popp, Anal. Bioanal. Chem. **395**, 1097–1105 (2009).
[29] G. Brönstrup, C. Leiterer, N. Jahr, C. Gutsche, A. Lysov, I. Regolin, W. Prost, F. J. Tegude, W. Fritzsche, and S. Christiansen, Nanotechnology **22**, 385201 (2011).

7 Publikationen

7.1 Peer-reviewed Publikationen

Applying contact to individual silicon nanowires using a dielectrophoresis (DEP) based technique. Christian Leiterer, Gerald Brönstrup, Norbert Jahr, Matthias Urban, Cornelia Arnold, Silke Christiansen, Wolfgang Fritzsche. Journal of Nanoparticle Research, (2013), 15 (2012), 5, 1-7.

Assembling gold nanoparticle chains using an AC electrical field: Electrical detection of organic thiols. Christian Leiterer, Steffen Berg, Antti-Pekka Eskelinen, Andrea Csaki, Matthias Urban, Päivi Törmä, Wolfgang Fritzsche. Sensors and Actuators B 176 (2013) 368– 373.

DNA hybridization assay at individual, biofunctionalized zinc oxide nanowires. Christian Leiterer, Barbara Seise, Irma Slowik, Gerald Brönstrup, Raphael Niepelt, Karina Weber, Carsten Ronning, Silke Christiansen, Wolfgang Fritzsche. Journal of Biophotonics 6 (2013) 143–147.

Far-Field Imaging for Direct Visualization of Light Interferences in GaAs Nanowires. Rachel Grange, Gerald Brönstrup, Michael Kiometzis, Anton Sergeyev, Jessica Richter, Christian Leiterer, Wolfgang Fritzsche, Christoph Gutsche, Andrej Lysov, Werner Prost, Franz-Jospeh Tegude, Thomas Pertsch, Andreas Tünnermann, Silke Christiansen. Nano Letters 12 (2012) 5412–5417.

Micromanipulation of sepsis relevant bacteria with dielectrophoresis. Ulrich-Christian Schröder, Uwe Glaser, Christian Leiterer, Andrea Csaki, Wolfgang Fritzsche, Michael Bauer, Jürgen Popp, Ute Neugebauer. Infection 39 (2011) 104-105.

A precise optical determination of nanoscale diameters of semiconductor nanowires. Gerald Brönstrup, Christian Leiterer, Norbert Jahr, Christoph Gutsche, Andrej Lysov, Ingo Regolin, Werner Prost, Franz-Joseph Tegude, Wolfgang Fritzsche, Silke Christiansen. Nanotechnolgy 22 (2011) 385201.

Optical properties of individual silicon nanowires for photonic devices. Gerald Brönstrup, Norbert Jahr, Christian Leiterer, Andrea Csaki, Wolfgang Fritzsche, Silke Christiansen. ACS Nano 4 (2010) 7113–7122.

Dielectrophoretic manipulation of DNA in microelectrode gaps for single-molecule constructs. Andreas Wolff, Christian Leiterer, Andrea Csaki, Wolfgang Fritzsche. Frontiers in Bioscience 13 (2008) 6834–6840.

7.2 Buchkapitel

DEP-Based integration of G-quadruplex structures. Christian Leiterer, Andreas Kopielski, Irit Lubitz, Alexander Kotlyar, Antti-Pekka Eskelinen, Päivi Törmä, Wolfgang Fritzsche. Guanine quartets – structure and application, **in Press.**

G-Wire Synthesis and Modification with Gold Nanoparticle. Christian Leiterer, Andrea Csaki, Wolfgang Fritzsche. DNA Nanotechnology, Methods in Molecular Biology Volume 749 (2011) 141-150.

Plasmonic nanoparticles - noble material for sensoric application. Andrea Csaki, Steffen Berg, Norbert Jahr, Christian Leiterer, Thomas Schneider, Andrea Steinbruck, David Zopf, Wolfgang Fritzsche. Nanotechnology Science and Technology, Gold nanoparticles: Properties, characterization and fabrication (2010) 245-261.

7.3 Andere Publikationen

DNA-Hybridisierungs-assay basierend auf der Biofunktionalisierung von Nanodrähten. Christian Leiterer, Barbara Seise, Irma Slowik, Gerald Brönstrup, Raphael Niepelt, Karina Weber, Carsten Ronning, Silke Christiansen und Wolfgang Fritzsche. VDE/VDI Proceeding (2012).

Micronano integration of nanoscale objects for parallel biosensorics. Christian Leiterer, Steffen Berg, Norbert Jahr, Gerald Brönstrup, Silke Christiansen, Andrea Csaki, Wolfgang Fritzsche. SPIE Proceedings 8068 (2012).

Ultrasensitive nanosensors based on electronic effects in nanoscale structures. Christian Leiterer, Steffen Berg, Thomas Schneider, Norbert Jahr, Ondrej Stranik, Gerald Broenstrup, Silke Christiansen, Andrea Csaki, Wolfgang Fritzsche. SPIE Proceedings 8068 (2012).

Integration of DNA molecules in microelectronic environment using dielectrophoresis. Christian Leiterer, Andrea Csaki, Norbert Jahr, Robert Kretschmer, Wolfgang Fritzsche. SPIE Proceedings 7397 (2009).

Integration of molecular structures in electrode gaps by dielectrophoresis. Andrea Csaki, Steffen Berg, Christian Leiterer, Robert Kretschmer, Andreas Wolff, Wolfgang Fritzsche. SPIE Proceedings 7035 (2008).

DNA based nanoscale constructions and their microintegration via guided self-assembly for nanoelectronic applications. Andrea Csaki, Christian Leiterer, Andrea Steinbruck, Andreas Wolff, Wolfgang Fritzsche. AIP Proceedings 1062 (2008).

7.4 Konferenzbeiträge

7.4.1 Vorträge

DNA-Hybridisierungs-assay basierend auf der Biofunktionalisierung von Nanodrähten. Christian Leiterer, Barbara Seise, Irma Slowik, Gerald Brönstrup, Raphael Niepelt, Karina Weber, Carsten Ronning, Silke Christiansen und Wolfgang Fritzsche. 4. GMM Workshop Mikro-Nano-Integration, Berlin (Germany), 12.11.2012 - 13.11.2012.

Integration of nanostructures using AC electrical fields as an approach to low-cost electrical sensing of optical or chemical signals. Christian Leiterer, Gerald Brönstrup, Barbara Seise, Norbert Jahr, Matthias Urban, Cornelia Arnold, Karina Weber, Silke Christiansen, Wolfgang Fritzsche. International symposium in DNA-Nano Sensors, Jena (Germany), 10.05.2012 - 12.05.2012.

Mikrointegration von Nanostrukturen mittels Dielektrophorese (DEP). Christian Leiterer, Gerald Brönstrup, Norbert Jahr, Matthias Urban, Cornelia Arnold, Silke Christiansen, Wolfgang Fritzsche. 3. GMM-Workshop Mikro-Nano-Integration. Stuttgart (Germany), 03.03.2011 - 04.03.2011.

Microintegration of DNA-framework molecules using dielectrophoresis for nanoelectronic applications. Christian Leiterer, Andreas Wolff, Andrea Csaki, Wolfgang Fritzsche. Nanoelectronics-Days, Aachen (Germany), 13.05.2008 - 16.05.2008.

7.4.2 Poster

DNA-Hybridisierungs-assay basierend auf der Biofunktionalisierung von Nanodrähten. Christian Leiterer, Barbara Seise, Irma Slowik, Gerald Brönstrup, Raphael Niepelt, Karina Weber, Carsten Ronning, Silke Christiansen und Wolfgang Fritzsche. 4. GMM Workshop Mikro-Nano-Integration. Berlin (Germany), 12.11.2012 - 13.11.2012

Integration of nanostructures using AC electrical fields as an approach to low-cost electrical sensing of optical or chemical signals. Christian Leiterer, Gerald Brönstrup, Barbara Seise, Norbert Jahr, Matthias Urban, Cornelia Arnold, Karina Weber, Silke Christiansen, Wolfgang Fritzsche. International symposium in DNA-Nano Sensors, Jena (Germany), 10.05.2012 - 12.05.2012

Approaching the integration problem using DNA superstructures and electrical fields. Christian Leiterer, Andreas Wolff, Andrea Csaki, Wolfgang Fritzsche. 3rd International Meeting on G-Quadruplexes and G-Assembly. Sorento (Italy), 28.06.2011 - 01.07.2011

Scattering properties of single crystalline silicon and gallium-arsenide nanowires. Gerald Brönstrup, Christian Leiterer, Norbert Jahr, Christoph Gutsche, Andrej Lysov,

Ingo Regolin, Werner Prost, Franz-Joseph Tegude, Wolfgang Fritzsche, Silke Christiansen. International symposium in Molecular Plasmonics, Jena (Germany), 19.05.2011 - 21.05.2011

Mikrointegration von nanoskaligen Transducer-Strukturen mittels Dielektrophorese (DEP). Christian Leiterer, Steffen Berg, Antti-Pekka Eskelinen, Andrea Csaki, Matthias Urban, Päivi Törmä, Wolfgang Fritzsche. Deutsches Biosensor Symposium DBS, Heiligenstadt (Germany), 03.04.2011-06.04.2011

Microintegration of micro- and nanoscale objects using dielectrophoresis (DEP). Christian Leiterer, Gerald Brönstrup, Norbert Jahr, Matthias Urban, Cornelia Arnold, Silke Christiansen, Wolfgang Fritzsche. Smart System Integration, Dresden (Germany), 22/23.03.2011

Mikrointegration von Nanostrukturen mittels Dielektrophorese (DEP). Christian Leiterer, Gerald Brönstrup, Norbert Jahr, Matthias Urban, Cornelia Arnold, Silke Christiansen, Wolfgang Fritzsche. 3. GMM-Workshop Mikro-Nano-Integration. Stuttgart (Germany), 03.03.2011 - 04.03.2011

Microintegration of DNA-molecules and nanostructures using dielectrophoresis. Christian Leiterer, Andreas Wolff, Andrea Csaki, Wolfgang Fritzsche. International Symposium in DNA based MicroNano-integration, Jena (Germany), 27.05.2010 – 29.05.2010

Microintegration of plasmonic nanoscale objects using dielectrophoresis for nanophotonic applications. Christian Leiterer, Steffen Berg, Antti-Pekka Eskelinen, Andrea Csaki, Matthias Urban, Päivi Törmä, Wolfgang Fritzsche. International symposium in Molecular Plasmonics, Jena (Germany), 14.05.2009 – 16.05.2009

Literaturverzeichnis

1. Douglas, S. M. et al. Self-assembly of DNA into nanoscale three-dimensional shapes. Nature **459,** 414–418 (2009).
2. Ke, Y., Lindsay, S., Chang, Y., Liu, Y. & Yan, H. Self-Assembled Water-Soluble Nucleic Acid Probe Tiles for Label-Free RNA Hybridization Assays. Science **319,** 180–183 (2008).
3. Voigt, N. V. et al. Single-molecule chemical reactions on DNA origami. Nature Nanotechnology **5,** 200–203 (2010).
4. Hung, A. M. et al. Large-area spatially ordered arrays of gold nanoparticles directed by lithographically confined DNA origami. Nature Nanotechnology **5,** 121–126 (2009).
5. Lund, K. et al. Molecular robots guided by prescriptive landscapes. Nature **465,** 206–210 (2010).
6. Rothemund, P. W. K. Folding DNA to create nanoscale shapes and patterns. Nature **440,** 297–302 (2006).
7. Kuzyk, A. et al. DNA-based self-assembly of chiral plasmonic nanostructures with tailored optical response. Nature **483,** 311–314 (2012).
8. Katz, E. & Willner, I. Integrated Nanoparticle-Biomolecule Hybrid Systems: Synthesis, Properties, and Applications. Angewandte Chemie International Edition **43,** 6042–6108 (2004).
9. EU Komission. Auf dem Weg zu einer europäischen Strategie für Nanotechnologie. (2004). <ftp://ftp.cordis.europa.eu/pub/nanotechnology/docs/nano_com_de_new.pdf>
10. US Goverment. Policy Principles for the U.S. Decision-Making Concerning Regulation and Oversight of Applications of Nanotechnology and Nanomaterials. (2011).
11. Pohl, H. A. The Motion and Precipitation of Suspensoids in Divergent Electric Fields. Journal of Applied Physics **22,** 869–871 (1951).
12. Pohl, H. & Crane, J. Dielectrophoresis of Cells. Biophysical Journal **11,** 711–727 (1971).
13. Pohl, H. A. Dielectrophoresis. Cambridge University Press (1978).
14. Lee, H. J. et al. Simple and rapid preparation of vertically aligned gold nanoparticle arrays and fused nanorods in pores of alumina membrane based on positive dielectrophoresis. Sensors and Actuators B: Chemical **136,** 320–325 (2009).
15. Kumar, S., Yoon, S.-H. & Kim, G.-H. Bridging the nanogap electrodes with gold nanoparticles using dielectrophoresis technique. Current Applied Physics **9,** 101–103 (2009).
16. Kretschmer, R. & Fritzsche, W. Pearl chain formation of nanoparticles in microelectrode gaps by dielectrophoresis. Langmuir **20,** 11797–11801 (2004).
17. Krupke, R. Separation of Metallic from Semiconducting Single-Walled Carbon Nanotubes. Science **301,** 344–347 (2003).

18. Suehiro, J., Zhou, G. & Hara, M. Fabrication of a carbon nanotube-based gas sensor using dielectrophoresis and its application for ammonia detection by impedance spectroscopy. Journal of Physics D: Applied Physics **36,** L109–L114 (2003).

19. Li, J., Zhang, Q., Yang, D. & Tian, J. Fabrication of carbon nanotube field effect transistors by AC dielectrophoresis method. Carbon **42,** 2263–2267 (2004).

20. Suehiro, J. et al. Dielectrophoretic fabrication and characterization of a ZnO nanowire-based UV photosensor. Nanotechnology **17,** 2567–2573 (2006).

21. Lao, C. S. et al. ZnO Nanobelt/Nanowire Schottky Diodes Formed by Dielectrophoresis Alignment across Au Electrodes. Nano Letters **6,** 263–266 (2006).

22. Freer, E. M., Grachev, O. & Stumbo, D. P. High-yield self-limiting single-nanowire assembly with dielectrophoresis. Nature Nanotech (2010). doi:10.1038/nnano.2010.106

23. Raychaudhuri, S., Dayeh, S. A., Wang, D. & Yu, E. T. Precise Semiconductor Nanowire Placement Through Dielectrophoresis. Nano Lett. **9,** 2260–2266 (2009).

24. Washizu, M., Suzuki, S., Kurosawa, O., Nishizaka, T. & Shinohara, T. Molecular dielectrophoresis of biopolymers. IEEE Transactions on Industry Applications **30,** 835–843 (1994).

25. Zheng, L., Brody, J. P. & Burke, P. J. Electronic manipulation of DNA, proteins, and nanoparticles for potential circuit assembly. Biosensors and Bioelectronics **20,** 606–619 (2004).

26. Morgan, H., Green, N. G., Hughes, M. P., Monaghan, W. & Tan, T. C. Large-area travelling-wave dielectrophoresis particle separator. Journal of Micromechanics and Microengineering **7,** 65–70 (1997).

27. Lumsdon, S. O. & Scott, D. M. Assembly of Colloidal Particles into Microwires Using an Alternating Electric Field. Langmuir **21,** 4874–4880 (2005).

28. Hoffman, P. D., Sarangapani, P. S. & Zhu, Y. Dielectrophoresis and AC-Induced Assembly in Binary Colloidal Suspensions. Langmuir **24,** 12164–12171 (2008).

29. Gascoyne, P. R. C. & Vykoukal, J. Particle separation by dielectrophoresis. ELECTROPHORESIS **23,** 1973 (2002).

30. Seo, H. W., Han, C.-S., Hwang, S. O. & Park, J. Dielectrophoretic assembly and characterization of individually suspended Ag, GaN, SnO2 and Ga2O3 nanowires. Nanotechnology **17,** 3388–3393 (2006).

31. Roy, S. & Gao, Z. Nanostructure-based electrical biosensors. Nano Today **4,** 318–334 (2009).

32. Zhang, G.-J., Huang, M. J., Ang, J. J., Liu, E. T. & Desai, K. V. Self-assembled monolayer-assisted silicon nanowire biosensor for detection of protein–DNA interactions in nuclear extracts from breast cancer cell. Biosensors and Bioelectronics **26,** 3233–3239 (2011).

33. Zhang, G.-J. et al. Multiplexed detection of cardiac biomarkers in serum with nanowire arrays using readout ASIC. Biosensors and Bioelectronics **35,** 218–223 (2012).

34. Zhang, G.-J. et al. DNA Sensing by Silicon Nanowire: Charge Layer Distance Dependence. Nano Letters **8,** 1066–1070 (2008).

35. Zhang, G.-J. et al. Highly sensitive measurements of PNA-DNA hybridization using oxide-etched silicon nanowire biosensors. Biosensors and Bioelectronics **23,** 1701–1707 (2008).

36. Zhang, G.-J., Luo, Z. H. H., Huang, M. J., Tay, G. K. I. & Lim, E.-J. A. Morpholino-functionalized silicon nanowire biosensor for sequence-specific label-free detection of DNA. Biosensors and Bioelectronics **25,** 2447–2453 (2010).

37. Chua, J. H., Chee, R.-E., Agarwal, A., Wong, S. M. & Zhang, G.-J. Label-Free Electrical Detection of Cardiac Biomarker with Complementary Metal-Oxide Semiconductor-Compatible Silicon Nanowire Sensor Arrays. Analytical Chemistry **81,** 6266–6271 (2009).

38. Cui, Y., Wei, Q., Park, H. & Lieber, C. M. Nanowire Nanosensors for Highly Sensitive and Selective Detection of Biological and Chemical Species. Science **293,** 1289–1292 (2001).

39. Patolsky, F. Electrical detection of single viruses. Proceedings of the National Academy of Sciences **101,** 14017–14022 (2004).

40. Stern, E. et al. Label-free immunodetection with CMOS-compatible semiconducting nanowires. Nature **445,** 519–522 (2007).

41. Zheng, G., Patolsky, F., Cui, Y., Wang, W. U. & Lieber, C. M. Multiplexed electrical detection of cancer markers with nanowire sensor arrays. Nature Biotechnology **23,** 1294–1301 (2005).

42. Bunimovich, Y. L. et al. Quantitative Real-Time Measurements of DNA Hybridization with Alkylated Nonoxidized Silicon Nanowires in Electrolyte Solution. Journal of the American Chemical Society **128,** 16323–16331 (2006).

43. Gao, Z. et al. Silicon Nanowire Arrays for Label-Free Detection of DNA. Analytical Chemistry **79,** 3291–3297 (2007).

44. Hahm, J. & Lieber, C. M. Direct Ultrasensitive Electrical Detection of DNA and DNA Sequence Variations Using Nanowire Nanosensors. Nano Lett. **4,** 51–54 (2004).

45. Li, Z. et al. Sequence-Specific Label-Free DNA Sensors Based on Silicon Nanowires. Nano Letters **4,** 245–247 (2004).

46. Williams, K. A., Veenhuizen, P. T. M., de la Torre, B. G., Eritja, R. & Dekker, C. Nanotechnology: Carbon nanotubes with DNA recognition. Nature **420,** 761–761 (2002).

47. Star, A. et al. Label-free detection of DNA hybridization using carbon nanotube network field-effect transistors. Proceedings of the National Academy of Sciences of the United States of America **103,** 921–926 (2006).

48. Star, A., Gabriel, J.-C. P., Bradley, K. & Grüner, G. Electronic Detection of Specific Protein Binding Using Nanotube FET Devices. Nano Letters **3,** 459–463 (2003).

49. Boussaad, S., Tao, N. J., Zhang, R., Hopson, T. & Nagahara, L. A. In situ detection of cytochrome c adsorption with single walled carbon nanotube device. Chem. Commun. **0,** 1502–1503 (2003).

50. Artyukhin, A. B. et al. Controlled Electrostatic Gating of Carbon Nanotube FET Devices. Nano Letters **6,** 2080–2085 (2006).

51. Gui, E. L. et al. DNA Sensing by Field-Effect Transistors Based on Networks of Carbon Nanotubes. Journal of the American Chemical Society **129,** 14427–14432 (2007).

52. Chen, R. J. et al. An Investigation of the Mechanisms of Electronic Sensing of Protein Adsorption on Carbon Nanotube Devices. Journal of the American Chemical Society **126,** 1563–1568 (2004).

53. Byon, H. R. & Choi, H. C. Network Single-Walled Carbon Nanotube-Field Effect Transistors (SWNT-FETs) with Increased Schottky Contact Area for Highly Sensitive Biosensor Applications. Journal of the American Chemical Society **128,** 2188–2189 (2006).

54. Tang, X. et al. Carbon Nanotube DNA Sensor and Sensing Mechanism. Nano Letters **6,** 1632–1636 (2006).

55. Jhi, S.-H., Louie, S. & Cohen, M. Electronic Properties of Oxidized Carbon Nanotubes. Physical Review Letters **85,** 1710–1713 (2000).

56. Hecht, D. S. et al. Bioinspired Detection of Light Using a Porphyrin-Sensitized Single-Wall Nanotube Field Effect Transistor. Nano Letters **6,** 2031–2036 (2006).

57. Maroto, A., Balasubramanian, K., Burghard, M. & Kern, K. Functionalized Metallic Carbon Nanotube Devices for pH Sensing. ChemPhysChem **8,** 220–223 (2007).

58. Khondaker, S. I., Luo, K. & Yao, Z. The fabrication of single-electron transistors using dielectrophoretic trapping of individual gold nanoparticles. Nanotechnology **21,** 095204 (2010).

59. Bernard, L., Calame, M., Molen, S. J. van der, Liao, J. & Schönenberger, C. Controlled formation of metallic nanowires via Au nanoparticle ac trapping. Nanotechnology **18,** 235202 (2007).

60. Harrower, C. T. & Oliver, D. R. Electronic transport in dielectrophoretically grown nanowires. Journal of Materials Science **41,** 8166–8172 (2006).

61. Liu, S. & Tang, Z. Nanoparticle assemblies for biological and chemical sensing. Journal of Materials Chemistry **20,** 24 (2010).

62. Musick, M. D., Keating, C. D., Keefe, M. H. & Natan, M. J. Stepwise Construction of Conductive Au Colloid Multilayers from Solution. Chemistry of Materials **9,** 1499–1501 (1997).

63. Abeles, B., Sheng, P., Coutts, M. D. & Arie, Y. Structural and electrical properties of granular metal films. Advances in Physics **24,** 407–461 (1975).

64. Musick, M. D. et al. Metal Films Prepared by Stepwise Assembly. 2. Construction and Characterization of Colloidal Au and Ag Multilayers. Chem. Mater. **12,** 2869–2881 (2000).

65. Snow, A. W. & Wohltjen, H. Size-Induced Metal to Semiconductor Transition in a Stabilized Gold Cluster Ensemble. Chem. Mater. **10,** 947–949 (1998).

66. Wessels, J. M. et al. Optical and electrical properties of three-dimensional interlinked gold nanoparticle assemblies. J. Am. Chem. Soc. **126,** 3349–3356 (2004).

67. Brust, M., Bethell, D., Kiely, C. J. & Schiffrin, D. J. Self-Assembled Gold Nanoparticle Thin Films with Nonmetallic Optical and Electronic Properties. Langmuir **14,** 5425–5429 (1998).

68. Joseph, Y. et al. Self-Assembled Gold Nanoparticle/Alkanedithiol Films: Preparation, Electron Microscopy, XPS-Analysis, Charge Transport, and Vapor-Sensing Properties†. J. Phys. Chem. B **107,** 7406–7413 (2003).

69. Foos, E. E., Snow, A. W., Twigg, M. E. & Ancona, M. G. Thiol-Terminated Di-, Tri-, and Tetraethylene Oxide Functionalized Gold Nanoparticles: A Water-Soluble, Charge-Neutral Cluster. Chem. Mater. **14,** 2401–2408 (2002).

70. Zamborini, F. P. et al. Electron hopping conductivity and vapor sensing properties of flexible network polymer films of metal nanoparticles. J. Am. Chem. Soc. **124,** 8958–8964 (2002).

71. Wohltjen, H. & Snow, A. W. Colloidal Metal−Insulator−Metal Ensemble Chemiresistor Sensor. Anal. Chem. **70,** 2856–2859 (1998).

72. Zhang, H.-L., Evans, S. D., Henderson, J. R., Miles, R. E. & Shen, T.-H. Vapour sensing using surface functionalized gold nanoparticles. Nanotechnology **13,** 439–444 (2002).

73. Evans, S. D., Johnson, S. R., Cheng, Y. L. & Shen, T. Vapour sensing using hybrid organic–inorganic nanostructured materials. Journal of Materials Chemistry **10,** 183–188 (2000).

74. Han, L., Daniel, D. R., Maye, M. M. & Zhong, C.-J. Core−Shell Nanostructured Nanoparticle Films as Chemically Sensitive Interfaces. Anal. Chem. **73,** 4441–4449 (2001).

75. Krasteva, N. et al. Self-Assembled Gold Nanoparticle/Dendrimer Composite Films for Vapor Sensing Applications. Nano Lett. **2,** 551–555 (2002).

76. Krasteva, N., Guse, B., Besnard, I., Yasuda, A. & Vossmeyer, T. Gold nanoparticle/PPI-dendrimer based chemiresistors: Vapor-sensing properties as a function of the dendrimer size. Sensors and Actuators B: Chemical **92,** 137–143 (2003).

77. Vossmeyer, T. et al. Gold Nanoparticle/Polyphenylene Dendrimer Composite Films: Preparation and Vapor-Sensing Properties. Adv. Mater. **14,** 238–242 (2002).

78. Shipway, A. N., Lahav, M., Blonder, R. & Willner, I. Bis-Bipyridinium Cyclophane Receptor−Au Nanoparticle Superstructures for Electrochemical Sensing Applications. Chem. Mater. **11,** 13–15 (1998).

79. Patolsky, F., Gabriel, T. & Willner, I. Controlled electrocatalysis by microperoxidase-11 and Au-nanoparticle superstructures on conductive supports. Journal of Electroanalytical Chemistry **479,** 69–73 (1999).

80. Im, Y. et al. Investigation of a Single Pd Nanowire for Use as a Hydrogen Sensor. Small **2,** 356–358 (2006).

81. Favier, F., Walter, E. C., Zach, M. P., Benter, T. & Penner, R. M. Hydrogen Sensors and Switches from Electrodeposited Palladium Mesowire Arrays. Science **293,** 2227–2231 (2001).

82. Varghese, O. K., Gong, D., Paulose, M., Ong, K. G. & Grimes, C. A. Hydrogen sensing using titania nanotubes. Sensors and Actuators B: Chemical **93,** 338–344 (2003).

83. Yao, K. et al. Individual Bi2S3 Nanowire-Based Room-Temperature H2 Sensor. J. Phys. Chem. C **112,** 8721–8724 (2008).

84. Mubeen, S., Zhang, T., Yoo, B., Deshusses, M. A. & Myung, N. V. Palladium Nanoparticles Decorated Single-Walled Carbon Nanotube Hydrogen Sensor. Journal of Physical Chemistry C **111,** 6321–6327 (2007).

85. Kong, J., Chapline, M. G. & Dai, H. Functionalized Carbon Nanotubes for Molecular Hydrogen Sensors. Adv. Mater. **13,** 1384–1386 (2001).

86. Wang, H. T. et al. Hydrogen-selective sensing at room temperature with ZnO nanorods. Applied Physics Letters **86,** 243503 (2005).

87. Chen, Z. H. et al. Applications of silicon nanowires functionalized with palladium nanoparticles in hydrogen sensors. Nanotechnology **18,** 345502 (2007).

88. Wagner, R. S. & Ellis, W. C. Vapor-liquid-solid mechanism of single crystal growth. Appl. Phys. Lett. **4,** 89 (1964).

89. Wagner, R. S. & Ellis, W. C. VAPOR-LIQUID-SOLID MECHANISM OF SINGLE CRYSTAL GROWTH. Applied Physics Letters **4,** 89 (1964).

90. Wang, J. Highly Polarized Photoluminescence and Photodetection from Single Indium Phosphide Nanowires. Science **293,** 1455–1457 (2001).

91. Brönstrup, G. et al. A precise optical determination of nanoscale diameters of semiconductor nanowires. Nanotechnology **22,** 385201 (2011).

92. Brönstrup, G. et al. Optical Properties of Individual Silicon Nanowires for Photonic Devices. ACS Nano **4,** 7113–7122 (2010).

93. Lysov, A. et al. Spatially resolved photovoltaic performance of axial GaAs nanowire pn-diodes. in 53–54 (IEEE, 2011). doi:10.1109/DRC.2011.5994426

94. Cao, L. et al. Engineering light absorption in semiconductor nanowire devices. Nat Mater **8,** 643–647 (2009).

95. Cao, L., Park, J.-S., Fan, P., Clemens, B. & Brongersma, M. L. Resonant Germanium Nanoantenna Photodetectors. Nano Letters **10,** 1229–1233 (2010).

96. Solanki, A. et al. Geometrical control of photocurrent in active Si nanowire devices. Nano Energy **1,** 714–722 (2012).

97. Cao, L., Fan, P. & Brongersma, M. L. Optical Coupling of Deep-Subwavelength Semiconductor Nanowires. Nano Letters **11,** 1463–1468 (2011).

98. Cao, L., Fan, P., Barnard, E. S., Brown, A. M. & Brongersma, M. L. Tuning the Color of Silicon Nanostructures. Nano Letters **10,** 2649–2654 (2010).

99. Cao, L. et al. Semiconductor Nanowire Optical Antenna Solar Absorbers. Nano Letters **10,** 439–445 (2010).

100. Schuller, J. A. & Brongersma, M. L. General properties of dielectric optical antennas. Optics Express **17,** 24084 (2009).

101. Doerk, G. S., Carraro, C. & Maboudian, R. Single Nanowire Thermal Conductivity Measurements by Raman Thermography. ACS Nano **4,** 4908–4914 (2010).

102. Montazeri, M. et al. Photomodulated Rayleigh Scattering of Single Semiconductor Nanowires: Probing Electronic Band Structure. Nano Letters **11,** 4329–4336 (2011).

103. Ramos, D. et al. Optomechanics with Silicon Nanowires by Harnessing Confined Electromagnetic Modes. Nano Letters **12,** 932–937 (2012).

104. Yu, Y. & Cao, L. Coupled leaky mode theory for light absorption in 2D, 1D, and 0D semiconductor nanostructures. Optics Express **20,** 13847 (2012).

105. Xu, T. et al. Optical absorption of silicon nanowires. Journal of Applied Physics **112,** 033506 (2012).

106. Lopez, F. J. et al. Diameter and Polarization-Dependent Raman Scattering Intensities of Semiconductor Nanowires. Nano Letters **12,** 2266–2271 (2012).

107. Hyun, J. K. & Lauhon, L. J. Spatially resolved plasmonically enhanced photocurrent from Au nanoparticles on a Si nanowire. Nano Lett. **11,** 2731–2734 (2011).

108. Brittman, S., Gao, H., Garnett, E. C. & Yang, P. Absorption of Light in a Single-Nanowire Silicon Solar Cell Decorated with an Octahedral Silver Nanocrystal. Nano Lett. **11,** 5189–5195 (2011).

109. Mie, G. Beiträge zur Optik trüber Medien, speziell kolloidaler Metallösungen. Annalen der Physik **330,** 377–445 (1908).

110. Schmid, H. et al. Doping limits of grown in situ doped silicon nanowires using phosphine. Nano Lett **9,** 173–177 (2009).

Danksagung

An dieser Stelle möchte ich mich bei allen Personen bedanken die mich im Zusammenhang mit meiner Arbeit unterstützt haben.

Besonderer Dank gilt meinen Eltern für die Unterstützung auf meinem gesamten Lebensweg.

Ich danke Dr. Wolfgang Fritzsche für die Betreuung seitens des IPHT, für die Möglichkeit Erfahrungen in einem kreativen wissenschaftlichen Umfeld zu sammeln, das Vertrauen mir verantwortungsvolle Aufgaben zu übertragen und das „immer offene Ohr für mich“ um Probleme unkompliziert zu lösen.

Des Weiteren danke ich Prof. Dr. Jürgen Popp für die Betreuung meiner Arbeit seitens der Universität und für die Möglichkeit, unkompliziert zur Chemisch-Geowissenschaftlichen Fakultät wechseln zu können.

Außerdem möchte ich mich bei allen Wissenschaftlern bedanken, mit denen ich während meiner Promotion direkt an gemeinsamen Projekten zusammengearbeitet habe: Wolfgang Fritzsche, Andrea Csaki, Steffen Berg, Norbert Jahr, Andreas Wolff, David Zopf, Janina Wirth, Erik Wünsche, Thomas Schneider, Steffen Trautmann, Cornelia Arnold, Gerald Brönstrup, Florian Talkenberg, Silke Christiansen, Christoph Gutsche, Muhammad Bashouti, Kasra Sardashati, Vladimir Sivakov, Marina Kulmas, Irma Slowik, Carsten Ronning, Christian-Ulrich Schröder, Uwe Glaser, Ute Neugebauer, Barbara Seise, Karina Weber, Dana Cialla, Thomas Henkel, Matthias Urban, Jens Albert, Mark Kilpinski, Franka Jahn, Regina Treffer, Volker Deckert, Antti-Pekka Eskelinen, Päivi Törmä, Jussi Toppari, Tommi Isoniemi, Michael Heller, Tsukasa Takahashi, Avery Sonnenberg, Youngjun Song, James McCanna, Rachel Grange, Anton Sergejev.

Ich danke auch meinen Büro-Kollegen Ondrej Stranik, Robert Müller, Anett Reichard und allen anderen Mitarbeiten der Gruppen Nanobiophotonik (IPHT), Photonische Nanostrukturen (IPHT), JBCI (IPHT), Mikrofluidik (IPHT), Mikrosystemtechnik (IPHT), Klinisch-Spektroskopische Diagnostik (IPHT), Nanoskopie (IPHT), Reinraum (IPHT), Werkstatt (IPHT), Experimentelle Festkörperphysik (Uni Jena), Heller Group (UCSD), Quantum Dynamics (Aalto) und Nanoscience Group (JYU).

Curriculum Vitae

Name:	Christian Leiterer
Geburtsdatum:	23.01.1984
Geschlecht:	männlich
Geburtsort:	Jena
Staatsangehörigkeit:	deutsch

2009 - 2013	Promotion am Institut für Photonische Technologie, Jena (IPHT)
	Lehrtätigkeit im Physikalisch-Chemischen Praktikum
	Lehrtätigkeit im Praktikum „Spektroskopische Methoden“
	Betreuung von Studenten der FH Jena im Praxissemester / Masterarbeit und Diplomarbeit
	Betreuung von Schülern „Jugend Forscht“
	Gast-Wissenschaftler DAAD Austauschprojekt UC San Diego, USA
	Gast-Wissenschaftler DAAD Austauschprojekt Aalto University Helsinki, Finnland
2008	Abschluss als Diplom-Biochemiker mit dem Thema: DNA-Konstruktion und dielektrophoretische Manipulation von DNA im Mikroelektrodenspalt (IPHT)
2003-2008	Studium der Biochemie an der Friedrich-Schiller-Universität in Jena
	Lehrtätigkeit im Praktikum „Spektroskopische Methoden“
	Wissenschaftliche Hilfskraft am IPHT in Jena
	Wissenschaftliche Hilfskraft in der Landesanstalt für Landwirtschaft in Jena
	Übungsleiter AG Badminton am „Christlichen-Gymnasium“ in Jena
2002 – 2003	Zivildienst
1994 – 2002	Staatliches Gymnasium „Am Anger“ in Jena

	Abschluss mit der Allgemeinen Hochschulreife
1990 – 1994	Grundschule „Heinrich-Heine“ in Jena

Ort, Datum . . . . . .

Unterschrift . . . . . .

Selbständigkeitserklärung

Ich erkläre, dass ich die vorliegende Arbeit selbstständig und unter Verwendung der angegebenen Hilfsmittel, persönlichen Mitteilungen und Quellen angefertigt habe.

Ort, Datum . . . . . .

Unterschrift . . . . . .